REAL-TIME ADAPTIVE CUTTING TOOL FLANK WEAR PREDICTION

By

GUN LEE

A DISSERTATION PRESENTED TO THE GRADUATE SCHOOL
OF THE UNIVERSITY OF FLORIDA IN PARTIAL FULFILLMENT
OF THE REQUIREMENTS FOR THE DEGREE OF
DOCTOR OF PHILOSOPHY

UNIVERSITY OF FLORIDA

2010

To my dear parents, whose continuous love, prayer,
and support made my journey possible

ACKNOWLEDGMENTS

At first, I thank my parents for their support and love. I also thank my advisor, Dr. John K. Schueller, for his kind support and advice during my whole graduate education. I also thank my committee, Dr. Tony L. Schmitz, Dr. Hitomi Greenslet, Dr. Carl D. Crane, and Dr. Jacob Hammer for their support and guidance. Finally, I thank all my colleagues and friends at Machine Tool Research Center (MTRC).

TABLE OF CONTENTS

page

LIST OF TABLES

LIST OF FIGURES

Abstract of Dissertation Presented to the Graduate School
of the University of Florida in Partial Fulfillment of the
Requirements for the Degree of Doctor of Philosophy

REAL-TIME ADAPTIVE CUTTING TOOL FLANK WEAR PREDICTION

By

Gun Lee

December 2010

Chair: John K. Schueller
Major: Mechanical Engineering

In modern manufacturing industry, automation is main stream to create products rapidly and economically. Many researches for automation are also going in the metal cutting industry. Therefore, computer Numerical Controlled (CNC) machines are widely used to achieve this goal while maintaining flexible production. Although the advent of CNC in the cutting industry has given many conveniences and benefits, CNC still has many limits. For example, contemporary CNC machines often cannot anticipate the problems caused by unexpected changes in the workpiece. Consequently, much research has been done to develop techniques to respond to these changes.

For automation in metal cutting, it is very important to predict workpiece and tool condition. In turning operations, unexpected changes in the workpiece material properties can have negative effects on the efficiency of the operation and quality of the product. Variations in workpiece hardness and dimensions can cause variation in cutting forces, which can then lead to accelerated tool wear and even breakage. Such problems can be overcome during CNC operations by measuring the variation in hardness in the workpiece and adjusting the cutting conditions to account for increased forces. However, there are limitations to in-process measurements of material

hardness. Conventional hardness measurement devices require contact with the material being measured, which can be time-consuming and may damage the workpiece. A method to detect variations in workpiece hardness that does not rely on contact could preserve tool life without costing additional time or creating damage in the workpiece. Theoretically, the spindle power required for turning operations in hard materials is higher than that required for soft materials. Therefore, a power sensor provides a novel means of detecting hardness changes in the work material without affecting the cutting process.

Tool condition monitoring is important part for automation in metal cutting and many researches for tool condition monitoring have been done. Currently, many wear models are known. However, there is limitation because metal cutting process is very complex and has various conditions. In this research, flank wear was considered the main wear factor. Flank wear arises due to both adhesive and abrasive wear mechanisms from the intense rubbing action of the two surfaces in contact, i.e., the clearance face of the cutting tool and the newly formed surface of the workpiece. Its rate of increase at the beginning of the tool life is rapid, settling down to a steady state then accelerating rapidly again at the end of tool life. Flank wear leads to a deterioration of surface quality, increased contact area and, consequently, increased heat generation. Flank wear models have been developed for specific workpieces made of a single material in many studies. However, if workpiece material properties (such as hardness) are changed during operation, the existing flank wear models cannot be used, because general flank wear models cannot reflect the real-time workpiece material changes.

Therefore, the flank wear model what is possible to use in cutting of workpiece jointed parts of different materials.

First, the sensor what can detect the workpiece material change was decided. Three different types of sensors (power sensor, ultimate thermometer, and dynamometer) were tested for feasibility of detecting workpiece material changes. In the case of the ultimate thermometer, an infrared sensor was tested, and problems arose due to the difficulty of focusing on the tool edge. The dynamometer was found to be good for detecting the workpiece changes, but installation is difficult and also expensive. The dynamometer also adds unwanted vibrations by increasing the length of tool holder. The power sensor was installed to measure the spindle motor power. The power sensor was found to be the most practical choice for a sensor to detect the workpiece material changes. This is because installation of the sensor is easy compared to the dynamometer and it is also cheaper than the dynamometer.

In this dissertation, the ultimate objective is to demonstrate the real-time flank wear model using a power sensor. This proposed model estimates the flank wear even for a workpiece with varying material properties. To validate proposed model, two different materials was used for cutting test. 8620 alloy steel was as soft metal and P20 tool steel was used as hard metal. Results show that proposed model can be used in cutting of workpiece combined with parts of different materials. However, consistency of tool is very important. In case of low quality tool, flank wear rate was not same when tool was changed. But, the flank wear rate was maintained in sing tool even thought cutting was performed with parts of different materials. Additionally, the study of tool should be performed. The hardness of tool or tool surface patterns may be one of

reason that flank wear rate is not same even though same workpiece is cut with same condition. In the future, this technique can be implemented with adaptive cutting condition rules to make decisions that reduce cutting cost and maintain product quality.

CHAPTER 1
INTRODUCTION

The final goal of manufacturing is to create products rapidly, economically, and with high quality. Computer Numerical Controlled (CNC) machines are widely used in the metal cutting industry to achieve this goal while maintaining flexible production. Although the advent of CNC in the cutting industry has given many conveniences and benefits, CNC still has many limits. For example, contemporary CNC machines often cannot anticipate the problems caused by unexpected changes in the workpiece. Consequently, much research has been done to develop techniques to respond to these changes.

During metal cutting operations, if a tool fails it may damage the tool holder, the workpiece, or the machine elements. Also, as machining progresses and the tool wears out, the surface quality and the dimensional accuracy of the product degrade. Moreover, tool breakage may jeopardize operator safety, or may lead to problem in the manufacturing system.

In turning operations, unexpected changes in the workpiece material properties can have negative effects on the efficiency of the operation and quality of the product. Variations in workpiece hardness and dimensions can cause variation in cutting forces, which can then lead to accelerated tool wear and even breakage. Such problems can be overcome during CNC operations by measuring the variation in hardness in the workpiece and adjusting the cutting conditions to account for increased forces. However, there are limitations to in-process measurements of material hardness. Conventional hardness measurement devices require contact with the material being measured, which can be time-consuming and may damage the workpiece. A method to

detect variations in workpiece hardness that does not rely on contact could preserve tool life without costing additional time or creating damage in the workpiece. Theoretically, the spindle power required for turning operations in hard materials is higher than that required for soft materials. Therefore, a power sensor provides a novel means of detecting hardness changes in the work material without affecting the cutting process.

In this research, flank wear will be considered the main wear factor. Flank wear arises due to both adhesive and abrasive wear mechanisms from the intense rubbing action of the two surfaces in contact, i.e., the clearance face of the cutting tool and the newly formed surface of the workpiece. Its rate of increase at the beginning of the tool life is rapid, settling down to a steady state then accelerating rapidly again at the end of tool life. Flank wear leads to a deterioration of surface quality, increased contact area and, consequently, increased heat generation. Flank wear models have been developed for specific workpieces made of a single material in many studies. However, if workpiece material properties (such as hardness) are changed during operation, the existing flank wear models cannot be used, because general flank wear models cannot reflect the real-time workpiece material changes. In this dissertation, to detect a workpiece material change, three different types of sensors (power sensor, ultimate thermometer, and dynamometer) were tested for feasibility of detecting workpiece material changes. In the case of the ultimate thermometer, an infrared sensor was tested, and problems arose due to the difficulty of focusing on the tool edge. The dynamometer was found to be good for detecting the workpiece changes, but installation is difficult. The dynamometer also adds unwanted vibrations. The power

sensor was found to be the most practical choice for a sensor to detect the workpiece material changes. This is because installation of the sensor is easy compared to the dynamometer and it is also cheaper than the dynamometer. In Chapter 5, the measured data will be presented, and the result will show that the power sensor data trend is the same as that of the dynamometer data.

In this dissertation, the ultimate objective is to demonstrate the real-time flank wear model to detect material change using a power sensor. This proposed model estimates the flank wear even for a workpiece with varying material properties. To validate the proposed model, two different materials which have different hardness were used for cutting tests. Tests showed that tool variability made wear prediction difficult. However, when there was not tool variability, tool wear could be predicted. Therefore, it was concluded that proposed model can be used. In the future, this technique can be implemented with adaptive cutting condition rules to make decisions that reduce cutting cost and maintain product quality. However, the future study of tool, and the sensor will be required. Figure 1-1 shows simplified flow of this research.

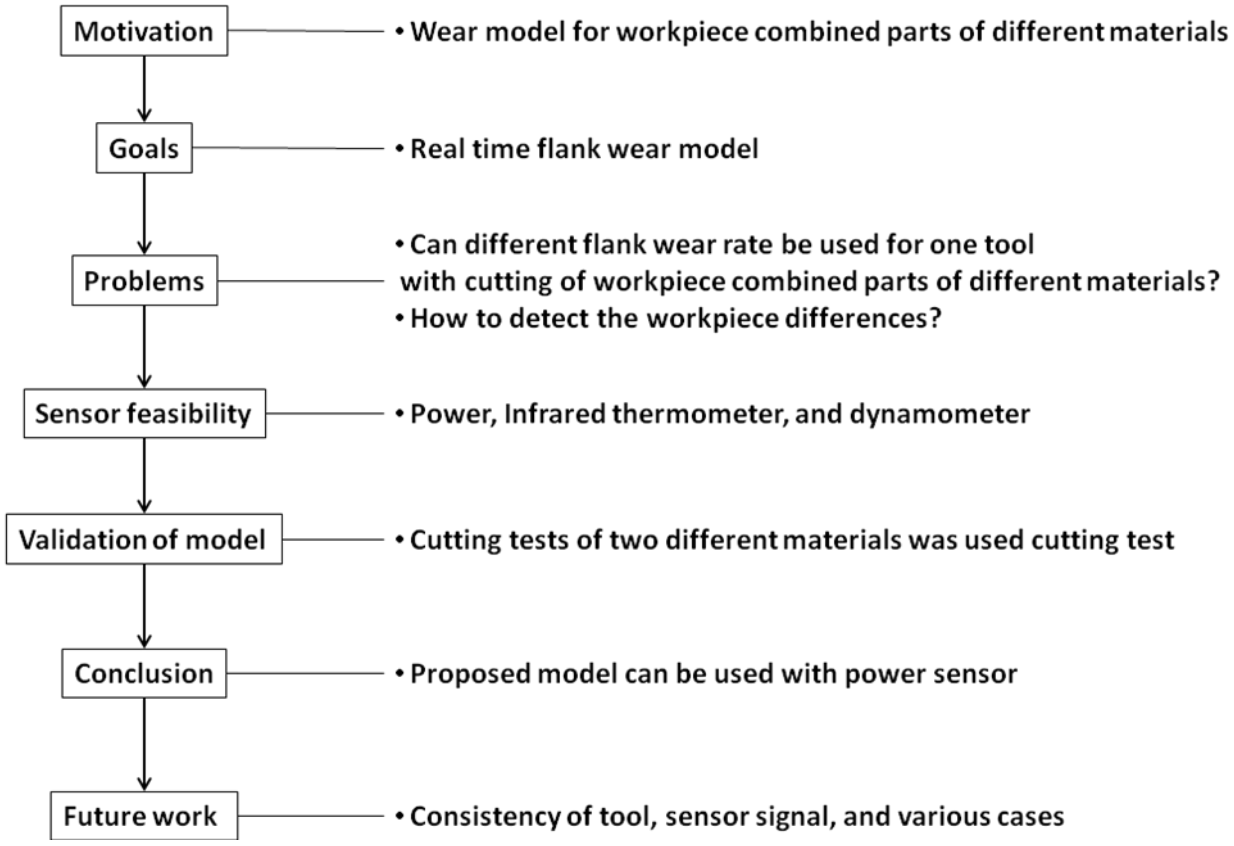

Figure 1-1. Flow of research

CHAPTER 2
PREVIOUS RESEARCH IN TOOL CONDITION MONITORING SYSTEM (TCMS)

Tool condition monitoring (TCM) is recognized to be important in CNC processes since the excessive wear or breakage of tool has to be noticed immediately in an automated manufacturing system to keep the quality and productivity. Much research has been carried out concerning the development of a reliable TCM system. However, none has yet found ubiquitous industrial use (Dimla, 2000 and Silva, 2007). One of the reasons for the lack of industrial application of TCM systems is due to the fact that TCM systems have been developed based mainly on mathematical models, which require huge amounts of empirical data, reducing therefore their adaptation capacity. Another possible hindrance lies in the nature and characteristics of the utilized sensor signals in general, which tend to be stochastic and non-stationary, and therefore difficult to model. There has been much research using acoustic emission (AE), tool dynamometers, motor currents, etc. In this chapter, Tool Condition Monitoring Systems (TCMSs) will be introduced. TCMSs are classified by sensor type (power, cutting force, acoustic emission, temperature, vibration, etc.).

2.1 Need of a Tool Condition Monitoring System

A tool failure such as wear, breakage, chipping, etc., could lead to poor product quality and even damage the machine tool and/or the fixture. Monitoring in a metal cutting process requires monitoring the machine dynamics, the cutting process dynamics, the cutting tools, and the workpiece to ensure optimum performance of the system (Byrne, 1995). A tool condition monitoring system can therefore be viewed as serving as the advanced fault detection system for cutting and tool, to check and safeguard machining process stability, a means by which machining tolerance is

maintained on the workpiece to acceptable limits by providing a compensatory mechanism for tool wear offsets, and a machine tool damage avoidance system (Dilma, 2000). The TCMS may be also required detecting to including excessive power consumption, inaccurate tolerances, serrations, and uneven workpiece surface finish, which eventually could lead to machine tool and/or workpiece damage incurring unnecessary costs. Cook (1980) divided the methods of tool condition monitoring into direct and indirect methods. The direct methods are based on the direct measurement of the geometry of the tool using optical sensors or laser optical sensors (Fan, 1996 and Du, 1993). They can provide accurate measurements of tool conditions but also can be affected by chips, coolant, and various disturbances. In the indirect methods, tool condition is predicted based on various sensor signals such as cutting force, vibration, temperature, acoustic emission, and motor current or power. In this chapter, reviews of power, cutting force, acoustic emission, tool temperature, vibration signature (acceleration signals), and miscellaneous methods such as ultrasonic and optical measurements, workpiece surface finish quality, workpiece dimensions, stress/strain analysis and spindle motor current will be provided.

2.1.1 Electric Motor Current/Power Measurement

Bhattacharyya et al. (2008) proposed a method for continuous on-line estimation of tool wear using spindle motor current and voltage measurement. They applied the method to a face milling operation. They used a multiple linear regression model to estimate tool wear in real-time and obtained accurate predictions of tool wear in both laboratory and industrial experiments.

Lee et al. (2002) developed a TCMS based on spindle motor current. They used the wavelet transform to measured spindle motor current and presented the energy level of tool conditions (new, worn, and bad). The proposed energy level method was measured the wear well. The change was very slight in time domain and it is noticeable in the specific energy level when processed in the wavelet analysis. The wavelet theory has been studied for the detection of tool wear conditions in various processes.

Zhang et al. (1994) measured the spindle motor current of a vertical NC milling machine by using a Hall Effect sensor during cutting. The relationship between the measured motor current and the milling torque was modeled. Computer algorithms were developed to track the waveforms, rate of peak change and the relative eccentricities of the modeled relation. Cutter breakages were more reliably diagnosed with motor current measurements than force/torque measurements.

Constantinides and Bennett (1987) measured the spindle motor power for estimation of wear and the detection of the end of effective tool life for a vertical milling machine. Spectral analysis was used and the effectiveness of using moving average, running-means and cumulative sum of the power spectrum values to estimate wear was evaluated. Between the cumulative sum of the power spectral energies and the total flank wear, there was a strong correlation. Spectral energy fluctuation of the spindle motor power was linearly related to the tool wear rate.

Shaft power, cutting forces, torque and motor current are all related to each other, originating from, and depending entirely on one another. It suffices therefore to measure just one of these parameters as demonstrated by Rangwala and Dornfeld (1987 and 1990). They dropped the electric current in preference to the cutting forces.

2.1.2 Cutting Forces (Dynamic and Static)

The relationship between the cutting force and tool wear (Lister, 1993; Ravindra, 1993; Dimla, 1999; Bayramoglu, 1998; Ko, 1994; Purushothaman, 1994; Tarng, 1994; Dornfeld, 1990; Lee, 1992; Marques, 1991; Kim, 1991; Oraby, 1991; Yao, 1990; Yao, 1992; Ramalingam, 1990; Lee, 1994) has been widely established. However, cutting force may not used in case of small breakage of tool. If small breakage has occurred, this may cause decreasing of the depth of cut. Generally, a smaller depth of cut decreases the cutting force. In practice, application and interpretation of this parameter has been diverse, but concentrated on studying the dynamic characteristic of the cutting force signal and interpreting its relation to tool wear levels. This can largely be attributed to the fact that force becomes important in worn tool conditions as a result of the variations produced due to friction between the cutting tool flank and the workpiece (Ko, 1994 and Dornfeld, 1990).

Existing force-based TCMSs typically operate independently of absolute force magnitude, measuring the relative change of the force that occurs as a new tool wears (Elanayar, 1990 and Gould, 1988) or when it fractures (Choi, 1999). Experiments have shown that the three components of the cutting force (Fig. 3-1) respond differently to the various wear forms occurring on the tool. For example, the feed force is insensitive to crater wear whereas the feed and radial forces may be influenced more than the main cutting force (Lister, 1993 and Gould, 1988).

Dimla (1999 and 2000) developed an on-line tool wear monitoring system for a turning operation using cutting force measurements fused with vibration signatures. A tool post dynamometer was used to measure cutting force. Measurements of flank,

nose and notch wear lengths were made immediately preceding recording the on-line data. Static and dynamic entities of the sampled cutting force were extracted as the mean and oscillatory components respectively (see Fig. 2-1) and analyzed in time and frequency domains from which features sensitive to tool wear were identified. Time domain established the nature and level of static force magnitude change while frequency analysis demonstrated the dynamic force signatures' response to cutting conditions as well as accrued wear levels. The more succinct elements of tool wear as it gradually wore to catastrophic failure were observed better in the frequency domain with certain frequencies correlating very well to the dynamic force changes. Overall, flank and nose wear were better indicators of tool wear than notch wear.

Bayramoglu and Düngel (1998) present a methodical investigation on the use of cutting force ratios in TCM for turning operations. Tests using worn tools were processed in order to examine how the force ratios could be used to monitor tool wear. Results showed that two of the force ratios to be particularly sensitive to the accrued flank wear, thus cutting force ratios could be applied in TCM operations.

Ravindra et al. (1993) proposed a development of mathematical models to describe the wear-time and wear-force relationships for a turning operation. The wear progression was studied and the cutting forces modeled by a multiple regression analysis method. Experiments were designed to obtain data for new and worn tools and the obtained data were used to establish the effect of cutting condition on cutting forces and tool wear. Force models were constructed in terms of speed, feed, and depth of cut using multiple regression analysis. The results showed that an increase in the magnitude of the component of the tri-axial cutting force was related to the wear on the

used insert. From the experiments, a good correlation between flank wear and feed and radial forces was provided.

Lee et al. (1992) developed the TCMS to track the dynamic cutting force based on a personal computer with a Fast Fourier Transform (FFT) card installed inside. The experiments were conducted on a Colchester Mascot 1600 lathe. The cutting forces and wear levels were measured and recorded and analyses of the obtained data showed that the feed and tangential dynamic force components had a good relationship to flank wear trend.

Marques and Mesquita (1991) investigated the relationship between the wear of sintered T15 high-speed-steel cutting tools and the associated cutting forces. The cutting force model was established taking into account the influence of both crater and flank wear. Experimental tests were conducted from during which the forces were measured. The test types conducted consisted of short duration cuts to establish force-wear relationship, and longer duration cuts to observe the progressive influence of wear on the forces. There was good correlation between experimental and theoretical results.

Kim and Lee (1991) presented an analytical model of dynamic cutting forces in orthogonal cutting and verified the proposed model. The dynamic cutting forces were expressed in terms of cutting coefficients that depend on the cutting variables. Good agreement between the theoretical limits of stability and experimental data was shown. Grabec (1988) and Khraisheh et al. (1995) have performed similar modeling of the dynamic cutting force for chatter prediction.

Oraby and Hayhurst (1991) developed mathematical models to describe the wear-time and the wear-force relationships for steady centre lathe turning conditions. Cutting

forces were found to correlate well with wear progress and with tool failure. To establish a universal rather than a case-based example of individual characteristics, a mathematical method to quantitatively formulate the wear-cutting force relation to the cutting speed, feed-rate and depth of cut to achieve repeatability and reliability for practical applications was proposed.

Yao et al. (1990) investigated a comprehensive TCMS which included the measurement of major and minor flank, crater, and nose wear based on the analysis of dynamic cutting forces in oblique machining. Tool wear experiments were performed on a Colchester lathe at varying cutting conditions using only one tool insert and workpiece type. To develop Autoregressive Moving Average Vector (ARMAV) time series models, the force, measured in terms of three orthogonal force components was used. Based on ARMAV, dispersion analysis (DA) was used to extract features sensitive to the rate of various types of wear. The results show that minor flank wear reaches a critical value first in finish-machining, so that optimum cutting conditions or an appropriate tool change strategy must be determined on the basis of minor flank wear. The results also show that the method is a feasible means for on-line tool wear monitoring in finish-machining.

Shi and Ramalingam (1990) performed artificial flank wear tests by measuring cutting force. That feed force to cutting force ratio can be a good indicator of flank wear was shown. This ratio and its derivative can be used to signal tool changes. Experimental results and slip-line field analysis, a new real-time tool condition sensing method using force ratio, was proposed.

Lee et al. (1989) examined the nature and source of the dynamic force frequency spectrum and determined the extent of the correlations between the characteristic peak frequency and flank wear. They found good correlation between the dynamic cutting force and flank wear. The dynamic force decreased rapidly before the entry into the tertiary zone as well as prior to the onset of catastrophic tool failure.

2.1.3 Acoustic Emission (AE)

Acoustic emissions (AE) are commonly defined as transient elastic waves within a material caused by the release of localized stress energy. During metal cutting, the workpiece undergoes considerable plastic deformation associated with the generation of AE. AE is linked to the plastic deformation process during chip formation, due to the interaction between the workpiece and cutting tool (Prickett, 1999). AE is generally found to be more sensitive to tool wear than cutting forces (Blum, 1990). Other sources of AE include phase transformations, friction mechanisms (tool-workpiece contact), and crack formation or extension fracture.

Chen and Li (2007) proposed a technique based on AE signal wavelet analysis for tool condition monitoring. The local characterize of frequency band, which contains the main energy of AE signals, was presented by the wavelet multi-resolution analysis, and the singularity of the signal is represented by wavelet resolution coefficient norm. They showed the advantages of the wavelet multi-scale resolution method in comparison to conventional data process.

Choi et al. (1999) develop a real-time tool-breakage detection system for turning by the sensor fusion of an acoustic emission sensor and a built-in force sensor. A built-in piezoelectric force sensor was used to measure the cutting force without altering the

characteristics of the machine tool dynamics. Two sets of experiments were done using carbide insert tips with one set slotted by wire EDM to accelerate fracture while the second was brazed to the workpiece to induce tool breakage. The recorded data was analyzed through a fast block-averaging algorithm for features and patterns indicative of tool fracture. If tool breakage is occurred, a significant drop of cutting force follows an AE signal burst and this AE signal burst was used as a detecting the force change. In case of signal force drops below the preset threshold, it was considered to be tool breakage. Similar work conducted by Jemielniak and Otman (1998) used a statistical signal-processing algorithm to identify the root mean square (RMS), skew, and kurtosis of the AE signal in the detection of catastrophic tool failure.

Kakade et al. (1994) applied AE analysis on the effect of tool wear and corresponding change in chip-form in face milling by selecting AE parameters namely ring-down count. Rise time was recorded simultaneously with the corresponding flank wear land length measured at fixed intervals. The results concluded that AE may be readily used for in-process monitoring of chip status and consequently tool monitoring.

Zheng et al. (1992) designed a novel intrinsic optical fibre sensor for detection of AE and designed a sensor used in monitoring tool wear. The sensor consisted of two distinct parts: the sensing element and an interferometer. The sensing element principally was used to produce a phase shift in the light transmitted through the optical fiber. The phase shift is generated by stress in an optical fibre due to coupling an AE wave into a backing material. Preliminary drilling and milling operation tests were performed. A commercial AE transducer was used for back-to-back tests and its response in 200 kHz ~ 1 MHz range compared to that from a commercial PZT sensor.

The obtained results were compared and these showed a reasonable degree of agreement.

König et al. (1992) applied AE to detect fracture and/or monitor the condition of small drills. Drilling operations were performed and a ceramic knock detector sensor designed for industrial application was used to measure the AE. Their result showed that at the closing phase of tool life (i.e., tertiary phase of tool wear), the RMS value increased dramatically. The rise, one could argue, was the case of tool breakage. Hence König et al. used this as a prescribed threshold which the RMS for normal operating drills should not exceed. This method however was found to be sensitive to tool chipping.

Blum and Inasaki (1990) performed comprehensive experiments to determine the influence of cutting conditions on the generation of Acoustic Emission (AE) signals during machining S45C steel. During the orthogonal cutting process, AE sensor signals and tool dynamometer signals provided extensive data and theoretical relationships between the energy content of the AE and the plastic work of deformation in the primary and secondary cutting zone was used. A relationship between the AE signals generated and the strain rate was estimated. The influence of flank wear on the generation of AE signals was emphasized. The feasibility of utilizing AE in tool wear sensing was confirmed with force measurement data.

Moriwaki and Tobito (1990) analyzed and measured the AE signals of turning of medium carbon steel with both coated and uncoated tools. They proposed a method to identify the conditions of the tool by AE signals employing a pattern recognition technique. AE RMS values for the recorded AE signal and the wear values (initial,

middle and tertiary stages of tool wear) were graphed on the same scale for comparison. The data was applied to a pattern recognition system and it performed reasonably well.

Roget et al. (1988) investigated the possibility of detecting tool wear using AE experimentally. They used the custom-made AE sensors for turning and milling test cuts. A comparison of the AE and flank wear was carried out and showed a remarkable similarity on both wear-time and AE-time plots. During metal cutting, there are many factors involved. Therefore, they concluded that AE is suited for determining tool wear only in specific and limited conditions.

2.1.4 The Tool Tip/Cutting Edges Temperature

Metal cutting generates a significant amount of heat and the temperature in the cutting zone can change as the tool wear due to changes in the tool geometry and tool's capability to cut. Therefore, the temperature can be used to monitor the tool condition. The high temperatures around the cutting tool edges affects the rate and mode of cutting tool wear, the friction between chip and cutting tool, and also that between the cutting tool and the newly formed surface.

Sarwar et al. (1996) developed a thermal imaging system consisted of a mathematical model of the energy partition during metal cutting for metal cutting applications. Thermal imaging data obtained showed that it was practicable and modifiable to fulfill the requirements of orthogonal cutting. Lin (1995) developed an inverse approach to measure the cutting tool temperature during a milling process for real-time tool/workpiece interface temperature. A least square inverse scheme was applied to solve the unknown boundary at the tool-workpiece interface based on the

surface temperatures measured outside the cutting zone by an infrared (IR) pyrometer. Lin concluded 1) an inverse technique was successfully developed to predict the milling temperature and heat flow by the measured temperature near the milled surface, 2) the mapping model was verified in a flame heating test, and 3) the average tool-chip interface temperature and total heat through the milling area ware influenced by the thermal properties of the workpiece. Radulescu and Kapoor (1994) designed and tested an analytical tool temperature field's prediction model for use during continuous and interrupted cutting. Testing showed that the modeled tool-chip interface temperature agreed well with experimental tests.

Raman et al. (1992) proposed and developed a mathematical model for cutting tool temperature measurement based on the remote thermocouple sensing (RTS) principle. They described the application of the differential quadrature method for modeling the forward thermal behavior of the cutting tool. Initial implementation of the quadrature method verified the suitability of using this technique for RTS.

Stephenson and Ali (1990) summarized the result of studies on tool temperature effects on interrupted metal cutting theoretically and experimentally. Infrared and tool-chip thermocouples were used to measure the cutting temperature during interrupted and turning tests on 2024 aluminum and gray cast iron at speeds up to 18 m/s. Temperatures were generally lower in interrupted cutting than in continuous cutting under the same conditions. Temperatures depended primarily on the length of cutting cycles and secondarily on the length of cooling intervals between cycles. The temperature measurements were found to be lower when the cutting was occasionally interrupted than for continuous cutting under the same cutting conditions. Generally, the

instrument, such as thermocouples, was not easy to install. The use of a non-contact measurement technique such as infrared thermal imaging was the best option. This technique was only capable of temperature measurements that might be considered at best averages rather than the true temperatures, and therefore tended to be dominated by chip images.

Chow and Wright (1988) developed an on-line temperature estimation technique in a turning operation. They used a standard thermocouple which was located at the bottom of the tool insert. The test cuts involved dry machining performed on plain steel tube (AISI 1020) with coated and un-coated controlled contact tool inserts. An increase in the tool wear resulted in an increase in the cutting temperature. The temperature increases were caused primarily by tool wear, which could be used to TCM during metal cutting. Shaw (1988) indicated that the mean tool face temperature was important role relative to the life of a cutting tool. Shaw proposed an approximate solution based on the principle of moving heat source and evaluated the solution.

For on-line TCM by measuring temperature, remote thermocouple sensing appears to be the only worthy way to measure the workpiece-tool temperature since a direct measurement of the tool-tip or rake face temperature distribution cannot be obtained. The temperature measurement of cutting edge is exceptionally difficult due to lack of direct access to the cutting zone. Boothroyd (1975) proposed the use of thermocouple techniques in the workpiece-tool interface, and through such technique, the generated EMF at the junction is considered to be a measure of the mean temperature in that region. Temperature distribution is not taken by using this. Most currently available remote thermocouple sensor instruments can only allow either the

cutting tool or workpiece interface or some other remote area temperature to be measured, and not the tool tip temperature.

2.1.5 Vibration Signatures (Acceleration Signals)

Vibrations are produced by cyclic variations in the dynamic components of the cutting forces (Dilma, 2000). Usually, these vibration motions start as a small chatter responsible for the serrations on the finished surface and chip thickness irregularities. Mechanical vibrations generally result from periodic wave motions. The nature of the vibration signal arising from the metal cutting process is such that it incorporates facets of free, forced, periodic and random types of vibration.

Dimla (1998) presents a detailed investigation of progressive tool wear results obtained during a metal turning operation. The investigation showed that the amount of wear. Its form was dependent more on the main cutting conditions.

El-Wardany et al. (1996) presented a study on monitoring tool wear and failure in drilling using vibration signature analysis techniques. They developed the features in both time and frequency domains. These vibration signature features were sensitive to drill wear and breakage but insensitive to cutting conditions, and sensor location. In the time domain, a monitoring feature was found to be effective for detection of drill breakage. In the frequency domain, a cepstrum ratio from the spectra of the vibrations monitored in both directions was also found effective for detection of breakage. By combining both techniques, it was possible to devise an effective drill monitoring system.

Yao et al. (1991) investigated detection and estimation of groove wear at the minor cutting edge of the tool by using vibration signatures. During turning experiments, a

miniature 3-D accelerometer was used to measure the multivariate vibration signal produced by the turning process. A multivariate time series analysis was performed on the recorded vibration signals. The analysis showed that the thrust cutting vibration was sensitive to the length of groove wear with two peaks: one at a very low frequency <200 Hz and the other at a high frequency ≥ 10 kHz.

Rotberg et al. (1987) presented a tool wear monitoring method based on vibration in face milling. They focused on the milling tool entry and exit conditions. Face milling experiments were conducted and the ensuing flank and crater wear measured. The results indicated that the vibration signal was a suitable indicator of tool wear as it demonstrated considerable change during tool life. Rotberg et al. (1989) focused on tool wear monitoring using vibration as the principal signal. The analysis was performed using two basic models characterized by low frequency and high frequency signal features. Experiments were conducted to validate these models utilizing measured acceleration signal features. The analysis showed the features from the vibration signals could be used in developing a TCMS as it correlated well with tool wear.

Jiang et al. (1987) investigated the frequency composition of the signal and the changes of vibration pattern during tool wear processes and discovered a “micro-breakage stage”. Then a frequency band-energy method in which the problem in frequency domain was changed into that in time domain was proposed. Experimental investigations provided sufficient evidence that the vibration signals were sensitive to tool wear states.

The inter-relationship between vibration signals and the cutting forces determines the dynamic nature of the cutting process, making the employment of these process

parameters attractive in the development of TCMSs (Dimla, 1998). The dynamic behavior on the other hand embodies vibration and certain aspects of the dynamic cutting force. In the real industry, the combination of cutting forces and vibration signals would be necessary.

2.1.6 Miscellaneous Sensors and Methods

Other various sensors are used for tool condition monitoring system. The optical methods, stress/strain measurement, methods based on measuring the workpiece dimension, surface finish quality measurement, and ultrasonic methods have been used for TCMS in metal cutting processes. In this sub-chapter, a review for TCMS using other sensors will be provided.

2.1.6.1 Optical methods

Optical methods for tool condition monitoring system are suitable to evaluate tool wear in a laboratory as a direct measurement system. Most of the image skills are limited to 2D. However, Karthik et al. (1997) developed a 3D measurement system using a pair of stereo imaging cameras. Shiraishi (1988) cited many studies have been made in the laboratory, but commercially available TCMSs based on optic were not available yet. For commercializing of an optic based TCMS, reliability in the actual environment will be required. Currently, industrial application seems at an early stage because of high complexity and costs and low reliability and flexibility. However, vision based tool condition monitoring system will be one of major TCMS according to digital optic development.

Wong et al. (1997) presented an optical method using the scatter pattern of reflected laser light for the monitoring of tool condition in the roughing to near-finishing

range. The images were captured with a digital camera and the recorded images were processed and characterized using the mean and standard deviation of the scatter pattern and the intensity of the optical parameters, and their distribution correlated to the surface roughness. The scatter pattern was formed by a low-power laser beam that was reflected from the surface of the workpiece. The deduced surface roughness in turning operation was then related to the ensuing state of the tool wear. Although to determine tool wear by observing machined surface roughness was very difficult, correlation between tool wear and intensity of the scattered light pattern was good.

Recently, Atli et al. (2006) proposed a computer vision-based approach tool condition monitoring in drilling operation. They used a high-speed CCD camera for capture the images and a Canny edge detector was employed to extract tool features form the acquired images. Detection for the condition of all tests was performed well by using the proposed method.

2.1.6.2 Stress/strain measurements

Noori-Khajavi and Komanduri (1995) used four sensors (thrust, torque, and strains in two orthogonal directions of the machine table) for the study of the correlation of process parameters to drill wear. The measured strain signals were analyzed in both time and frequency domains. Meaningful correlation of the drill wear was obtained in the frequency domain. The area under the x-axis PSD for the strain sensor was found to correlate well to drill wear.

Zhou et al. (1995) proposed a monitoring system using the stresses acting in a cutting edge during a machining process. This provided a more reliable means to monitor and to predict tool spontaneous failure. A TCMS was based on a VME

computer system and real time kernel was designed and implemented with a high speed data acquisition subsystem and a graphic presentation subsystem. They reported that prediction of spontaneous failures were possible by monitoring the risk factor defined as a ratio of the instantaneous stresses.

Lee et al. (1994) presented a three-dimensional loading and measured the loading on the rake face during cutting. From a finite element analysis (FEA), the principal and von Mises stresses in the tool were examined to ascertain the points of highest stress. The principal and von Mises stresses could be used to predict the mode and location of tool failure.

2.1.6.3 Workpiece dimension

El-Gomayel and Bregger (1986) developed a sensing device to measure tool wear indirectly by monitoring the change of the workpiece diameter during turning operations. The workpiece diameter change was measured by electromagnetic sensors. Two electromagnetic sensors on opposite sides of the workpiece gave a voltage output directly related to the gap between the sensor and the workpiece. The experimental data obtained for flank and nose wear were in agreement with the results obtained from the conventional method of measuring the wear by a toolmaker's microscope.

2.1.6.4 Magnetism

Jetley and Gollajesse (1994) proposed the magnetization of tool inserts and then, monitoring the magnetic field flux reduction as TCMS. Magnetized drills were used and implemented in order to validate their methodology. It was possible to accurately predict the end of tool life or fracture “on-line” by observing the magnetic flux, and they

indicated that the system was cost effective with potential for implementation in most metal cutting environments.

2.1.6.5 Ultrasonic methods

Abu-Zahra and Nayfeh (1997) developed a robust method for on-line gradual wear monitoring using normalized ultrasonic signals for tool wear monitoring for turning operations. A consistent calibration mark, cut in the lower corner of the tool nose, was used to generate a calibration echo. Experiments under various cutting conditions showed that the gradual wear measurements can be made tool independent by normalizing the measurements with the calibration mark.

2.1.7 Sensor fusion—synergy of signal integration

The single sensed signal can change with the cutting conditions such as machining parameters, tool wear, etc. Therefore, more than one signal can be used in a complementary way to provide a more robust prediction of one or more machining features. The success of sensor fusion depends on which type of signals is suitable for a given machining outcome, which features are extracted, and in which way they must be complemented (Liang, 2004).

In an early attempt, Lezansky and Rafalowicz (1993) developed the method using multi sensors. They used normal and tangential forces, vibration, acoustic emission, and both diameter and out-of-roundness to characterize the state of a grinding process. The methodology used can be seen as a multisensory rather than a sensor fusion, because the signals were used at the same time but were not complementary to each other.

Bahr et al. (1997) developed a unique multisensory tool monitoring system using machine vision and vibration sensors for turning operations. They used a vibration signal as an on-line monitor to predict tool wear and detect breakage, and they also used machine vision between cuts to quantify the worn tool. In this way, a direct and an indirect technique were complemented and a more accurate tool monitoring system was developed because the machine vision can detect false signals from the vibration sensor.

Azouzi and Guillot (1997) examined the feasibility for an intelligent sensor fusion technique. They presented an exhaustive analysis to determine the most sensitive process parameters (feed, depth of cut, cutting velocity) and signals (AE, forces, vibration) to predict the surface roughness and the final diameter error in machining. Based on experimental data and statistical tools, the feed, the depth of cut, and the radial and feed force components were selected as inputs to a neural network to predict the mentioned machining outcomes. Surface finish was assessed with an error varying from 2 to 25% under different process conditions, while errors ranging between 2 and 20 μm were observed for the prediction of dimensional deviations.

Etekin et al. (2003) studied the signals of force, AE, and spindle quill vibration to predict dimensional accuracy (bore size tolerance) and surface roughness in a CNC milling operation. They used three different material types (6061-T6 aluminum, 7075-T6 aluminum, and ANSI-4140 steel). The RMS of the axial force component and the DC component of the AE signal were the candidate signals to be integrated and predict the quality characteristics of the machined parts using three different workpiece materials.

Recently, Cho et al. (2009) designed the effective multi-sensor-based TCM. The experimental was performed with 4340 steel and multilayer-coated and multi-flute carbide end mill cutter. They used the force, vibration, acoustic emission, and spindle power sensor for the time and frequency domain data. The experimental results showed that the design of TCM based on the feature level fusion can significantly improve the accuracy of the tool condition classification.

Table 2-1. Previous research of tool condition monitoring system

Main Sensor for TCMS	Ref.	Summary
Electric motor current/power measurement	(Bhattacharyya, 2008)	A method for continuous on-line estimation of tool wear using spindle motor current and voltage measurement was proposed.
	(Lee, 2003)	Tool condition monitoring system with wavelet transform was proposed.
	(Zhang, 1994)	A Hall effect sensor to measure the current supplied to the spindle motor drive of a vertical NC miller together with the cutting forces was used.
	(Constantinides, 1987)	Spindle motor power was obtained and the PSD, the moving average, running mean and the accumulative sum power was used.
	(Rangwala, 1987 and 1990)	The electric current in preference to the cutting forces.
Cutting forces (dynamic and static)	(Dimla, 1999 and 2000)	Cutting force measurements fused with vibration signatures.
	(Bayramoglu, 1998)	A systematic investigation on the use of cutting force ratios in TCM for turning operations was presented.
	(Lister, 1993)	The power spectrum of dynamic cutting forces was analyzed.
	(Ravindra, 1993)	A mathematical model for tool wear estimation was developed.
	(Lee, 1992)	Personal computer based fast Fourier transform software to track the dynamic cutting force signal was developed.
	(Marques, 1991)	The relationship between wear of sintered high-speed steel cutting tools and the associated cutting forces was investigated.
	(Kim, 1991)	The modeling of dynamic cutting forces and experimental test data collected and compared with the theoretical model predictions was performed.
	(Oraby, 1991)	A model for tool wear analysis in a turning operation by force characteristics within the different phases of tool wear was developed.
	(Yao, 1992)	The measurement of major and minor flank, crater, and nose wear based on the analysis of dynamic cutting forces was performed.
	(Shi, 1990)	The feed and cutting force components to flank wear length were correlated.
	(Dan, 1990)	An inter-relationship between the tangential, feed and normal components of the dynamic cutting forces has been established.
Acoustic emission (AE)	(Chen, 2007)	A technique based on AE signal wavelet analysis for tool condition monitoring was proposed.
	(Novak,1992)	AE and cutting forces were fused.
	(Jemielniak, 1998)	Statistical signal-processing algorithm was used.
	(Kakade, 1994)	AE parameters (ring-down count, rise time, event duration, frequency and event rate) were selected.

Table 2-1. Continued

Main Sensor for TCMS	Ref.	Summary
Acoustic emission (AE)	(Zheng, 1992)	An intrinsic method for AE sensing based on an optic fibre sensor was presented.
	(König, 1992)	Cutting test to detect fracture and/or monitor the condition of small drills using AE features was performed.
	(Blum, 1990)	Experimental test cuts to determine amongst other things, the influence of flank wear on the generation of AE signals was performed.
	(Moriwaki, 1990)	A method based on AE measurement and analysis for coated tool life estimation was proposed.
	(Roget,1988)	Machining tests from which the sensed AE signals from the cutting operation was carried out.
	(Tansel, 1991)	Substantially little AE was thought to be generated compared to a larger AE accompanying tool breakage and fracture.
	(Lee, 1989)	
The tool tip/cutting edges temperature	(Boothroyd, 1975)	The thermocouple techniques in the workpiece-tool interface and through such technique were proposed.
	(Sarwar, 1996)	A thermal imaging system for metal cutting applications was developed.
	(Lin, 1995)	Inverse approach for real-time tool/workpiece interface temperature was devised.
	(Radulescu, 1994)	An analytical tool temperature field's prediction model for use during continuous and interrupted cutting was designed and tested.
	(Raman, 1992)	A mathematical model for cutting tool temperature measurement based on the remote thermocouple sensing (RTS) principle was proposed and developed.
	(Stephenson, 1990)	Studies on tool temperature effects on interrupted metal cutting were performed and theoretical and experimental results are reported.
	(Chow, 1988)	An on-line method for tool-chip interface temperature measurement in a turning process using a standard thermocouple inserted at the bottom of the tool insert was devised.
	(Shaw, 1988)	An approximate solution based on the principle of moving heat source was proposed and evaluated.
Vibration signatures (acceleration signals)	(Dimla, 1998)	A detailed investigation of progressive tool wear results obtained during a metal turning operation was presented.
	(El-Wardany, 1996)	The use of vibration signature characteristics in on-line drill wear monitoring and breakage was investigated.
	(Yao, 1991)	Detection and estimation of groove wear at the minor cutting edge of the tool by monitoring vibration signatures are investigated.
	(Dan, 1990)	A discrete modeling method called data dependent system to correlate vibration signals to cutting tool wear was employed.
	(Rotberg, 1987)	The emphasis was on the milling tool entry and exit conditions.
	(Rotberg, 1989)	Tool wear monitoring using vibration as the principal signal was focused.

Table 2-1. Continued

Main Sensor for TCMS	Ref.	Summary
Vibration signatures (acceleration signals)	(Jiang, 1987)	A purposely-built test-rig was able to investigate the effects of vibration in the cutting and feed directions on the cutting tool.
Optical methods	(Atli, 2006)	A computer vision-based approach tool condition monitoring in drilling operation was proposed.
	(Karthik, 1997)	a 3D measurement system using a pair of stereo imaging was developed.
	(Kurada, 1997)	A review of the basic principle, instrumentation and various image-processing schemes involved in the development of a vision based TCMS was presented.
	(Oguamanam,1994)	Implementation of optical methods was carried out.
	(Du, 1993) (Cuppini,1986)	
	(Wong, 1997)	A vision-based TCMS using laser scatter pattern of reflected laser ray in the roughing to near-finishing range was devised.
Stress/strain measurements	(Noori-Khajavi, 1995)	Strain sensors of the correlation of process parameters to drill wear was used.
	(Zhou, 1995)	Monitor the stresses acting in a cutting edge during a machining process in order to predict tool spontaneous failure was proposed.
	(Lee, 1994)	FEA and detailed stress analysis of the cutting edges were combined.
Workpiece dimension	(El Gomayel, 1986)	A method for tool wear monitoring based on measurements of workpiece deviation was proposed.
Magnetism	(Jetley, 1994)	The magnetization of tool inserts and then, monitoring the magnetic field flux reduction as the tool wore was proposed.
Ultrasonic methods	(Abu-Zahra, 1997)	A normalized ultrasonic signal based method for in-process tool wear monitoring for turning operations was developed.
Sensor fusion	(Lezanski, 1993)	Normal and tangential forces, vibration, acoustic emission, and both diameter and out-of-roundness to characterize the state of a grinding process were used.
	(Bahr, 1997)	Vibration signal as an on-line technique to predict tool wear and detect breakage, and machine vision between cuts to quantify the worn tool were used.
	(Lou, 1996)	That force is easily affected by the cutting conditions and acoustic emission is interfered by the environmental noise was claimed.
	(Azouzi, 1997)	AE, forces, vibration was used.

Table 2-1. Continued

Main Sensor for TCMS	Ref.	Summary
Sensor fusion	(Etekin, 2003)	The signals of force, AE, and spindle quill vibration to predict dimensional accuracy and surface roughness in a CNC milling operation was used.
	(Cho, 2009)	The effective multisensor-based TCM was designed.

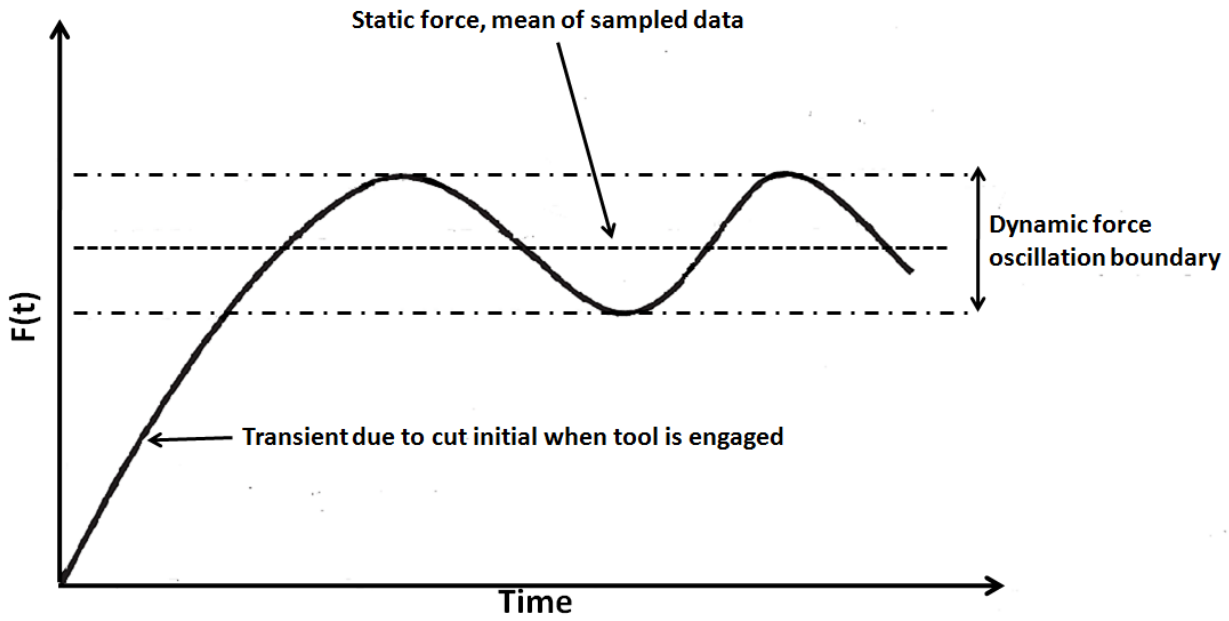

Figure 2-1. Force amplitude vs time (fixed cutting conditions).

CHAPTER 3
FORCE, POWER, FLANK WEAR, AND OPTIMIZED CUTTING CONDITION

In this chapter, the cutting force mechanism of a turning operation, the relation between force and power, the tool wear rate and tool life, the flank wear progress, the optimal cutting conditions (Usui, 1984; Dimla 2000; Tlusty, 2000; Matsumura, 2008), and the proposed real-time flank-wear model will be introduced. The following material in this chapter is extracted from the literature. Large portions are directly taken from Tlusty (2000), Dimla(2000), Usui(1984), and Matsumura (2008).

3.1 The Mechanistic Cutting Force for a Turning Operation

The cutting force acting on the tool is generated by actively engaging part of the cutting edge, which is drawn in Fig. 3-1. It includes the main cutting edge, the nose radius, and a small part of the secondary cutting edge. The direction of the force depends on the ratio of the components of the edge, and on the size of the radius with respect to feed f_r . The force F can be split into components: feed force F_f , which determines the direct load on the feed drive, the radial component F_r , which is decisive for the deflections affecting the accuracy of the machined surface, and the tangential force F_t , which has the direction of the cutting speed v and determines the cutting power $P = F_t v$ which is tangential to the cut surface. The components F_t and F_r may be combined to give the force F , which is normal to the cutting edge.

The tangential cutting force is considered to be approximately directly proportional to the chip area A:

$$F_t = K_s A = K_s bh = K_s a f_r \tag{3-1}$$

where, as shown in Fig. 3-2, b is chip width, h is chip thickness, a is depth of cut, f_r is feed per revolution, and the subscript of the constant K_s means "specific," that is, per unit chip area. Conventionally, the dimensions to use are $F_t(N)$, $b(mm)$, $h(mm)$, $A(mm^2)$, and $K_s(N/mm^2)$.

3.2 Conversion between Cutting Force and Power for a Turning Operation

Generally, the equation between power and torque is

$$P = T\omega \tag{3-2}$$

where T is torque and ω is spindle speed.

The above equation can be rewritten as

$$P = F_t \cdot r \cdot \omega = K_s \cdot a \cdot f_r \cdot r \cdot \omega \tag{3-3}$$

where F_t is tangential cutting force and *r* is workpiece radius.

Therefore, the equation between cutting force and power can be obtained.

$$F_t = \frac{P}{r\omega} \tag{3-4}$$

If power can be measured, cutting force also can be estimated without a force sensor if r and ω are known.

3.3 Wear Rate and Tool Life

Tool wear processes generally occur in combinations of the predominant wear modes, depending upon the cutting conditions, workpiece and tool materials, and the tool insert geometry. For a given cutting tool and workpiece material combination, the tool wear form may depend on the cutting conditions, principally cutting speed *v* and the un-deformed chip thickness *t*, and a combination of the aforementioned wear mechanisms. Ranges of cutting speed where each type of wear is predominant can be

identified by considering the product of these values as *vt*, which is directly proportional to the cutting speed (Shaw, 1984). Sometimes, the tool life can be considerably reduced if the area of cut, the area swept by the cutting tool, is significantly increased (i.e., mainly by increasing the depth of cut). At low cutting speeds, the tool wears predominantly by a rounding-off of the cutting point and subsequently looses sharpness. As the cutting speed increases, the wear-land pattern changes to accommodate the ensuing change with extremely high values leading to plastic flow at the tool point. Craters, on the other hand, depend largely on the cutting temperature, rather than on the cutting speed. The various forms of wear-land pattern and prevailing cutting speed are shown in Fig. 3-3 for a turning operation. The more predominantly occurring forms of cutting tool wear often identified as the principal types of tool wear in metal turning using single-point tools are nose, flank, notch and crater wear. Figure 3-4 shows how these wear features can be measured in a turning process through implementation of appropriate International Standards Organization (ISO) criteria.

Nose wear or edge rounding occurs predominantly through the abrasion wear mechanism on the cutting tool's major edges resulting in an increase in effective negative rake angle. Nose wear can be dependent entirely on the implemented cutting conditions with tool sharpness lost through plastic or elastic deformation. At high cutting speeds, the edge deforms plastically and may result in the loss of the entire nose, as depicted in Figs 3-3(a) and 3-4(b). Edge chipping and cracking occurs during periodic breaks of the built-up edge in interrupted cuts with a brittle tool and thermal fatigue. Catastrophic failure may also occur if the nose is considerably worn or as a result of the

utilization of inappropriate machining conditions and brittle tools such as ceramics (Schey, 1987).

Crater wear results from a combination of high cutting temperatures and high shear stresses creating a crater on the rake face some distance away from the tool edges, quantized by depth and cross-sectional area (Fig. 3-3(c)). Crater wear also arises due to a combination of wear mechanisms: adhesion, abrasion, diffusion or thermal softening, and plastic deformation. Severe depths of crater may trigger catastrophic collapse of the cutting point (see Fig. 3-3(d)).

Flank wear arises due to both adhesive and abrasive wear mechanisms from the intense rubbing action of the two surfaces in contact, i.e., the clearance face of the cutting tool and the newly formed surface of the workpiece. Its rate of increase at the beginning of the tool life is rapid, settling down to a steady state, then accelerating rapidly again at the end of the tool's life. Flank wear leads to a deterioration of surface quality, increased contact area and consequently to increased heat generation (Figs 3-3(b) and 3-4(c)).

A wear notch can form at the depth-of-cut line as the tool rubs against the shoulder of the workpiece (Fig. 3-4(b) and (c)). A wear notch can lead to abrasion by the surface layers, and is accelerated by oxidation or chemical reactions, possibly leading to total tool failure.

Flank wear typically increases with the time of cutting, as shown in Fig. 3-5. At the beginning, Phase I, there is initially a faster increase that is followed by a steady increase in proportion to cutting time, Phase II. When the wear depth reaches a certain size, it will accelerate and may lead to a sudden failure of the edge, Phase III. As an

approximation to actual wear, expressed by the dashed line in the figure, wear can be assumed to be proportional to time according to:

$$FWW = r_w t \tag{3-11}$$

where $r_w = \Delta FWW / \Delta t$ is the rate of wear. A certain value of wear may be chosen as the permissible limit $FWW_{\lim}$. The time at which this limit is reached is called the tool life T.

The wear rate depends, for a given work/tool material combination, on cutting speed v and chip thickness h. Within a practical range of v and h, this relationship is usually expressed in algebraic form:

$$r_w = C_r v^p h^q \tag{3-12}$$

The exponent p on v is rather high, between 2 and 6, indicating the significant influence of v, which is due to its effect on the temperatures of the tool. The exponent q on h is usually between 1.5 and 3 and is due to the influence of h on the load in the tool.

Combining (3-11) and (3-12),

$$FWW = C_r v^p h^q t \tag{3-13}$$

And for $t = T$,

$$FWW_{\lim} = C_r v^p h^q T \tag{3-14}$$

or combining $FWW_{\lim}$ and C_r,

$$v^p h^q T = C^* \tag{3-15}$$

Equation (3-15) is the tool life equation in a form very similar to that chosen by F. W. Taylor in 1905, except that his formulation involved a relationship between v and T

only. Considering that in the turning operation, chip thickness is related, for a given side-cutting-edge angle σ, to feed per revolution f_r,

$$h = f_r \cos\sigma \tag{3-16}$$

Equation (3-17) can be written

$$v^p f_r^{\,q} T = C \tag{3-17}$$

where $C = C^* / (\cos\sigma)^2$.

Equation (3-17) is the usual form of the tool life equation expressing the relationship between cutting speed v, feed f_r, and tool life T, and it is established considering a particular value of the angle σ. However, Eq. (3-15) is more fundamental. It is common to obtain the parameters in Eq. (3-17) experimentally and express them graphically on log-log plot a relationship between two of the three variables involved.

In this dissertation, the flank wear model which will be introduced in chapter 3.6 will be used because the flank wear model in chapter 3.6 is more suitable for real time flank wear update. Equation 3-13 can only estimate the flank wear for one workpiece material. If the workpiece material is changed during the process, calculating the flank wear using Eq. 3-13 is impossible because time (*t*) depends on same workpiece material.

3.4 Cutting Tool Wear Prediction

Since the tool life equation ($VT^n = C$, where T is the tool life, V is the cutting speed and n and C are constants) was discovered by F. W. Taylor, numerous research papers have been published throughout the world for better understanding of cutting tool wear and tool life characteristics. It should be noted that a goal of metal

cutting research is to establish the theories or analytical methods which enable the cutting tool wear and other necessary parameters such as chip formation, cutting force, cutting temperature and surface finish to be predicted quantitatively without any cutting experiment. In order to predict cutting tool life analytically, it is necessary first of all to identify a simple wear characteristic equation for practical use which governs well the actual wear progress under practical cutting conditions. A function of wear rate, normal stress, and temperature, which includes only two material constants, is proposed as the characteristic equation for carbide tools and its appropriative is demonstrated experimentally. Considering a three-dimensional turning operation, there is a need to predict analytically the chip formation and the three components of the cutting force for a given shape of tool edge and given cutting conditions, in order to calculate the normal stress and the temperature on the wear faces of a cutting tool. For this purpose, an energy method which utilizes orthogonal cutting data from machining is introduced and its outline is briefly explained. On the basis of predicted results from the energy method, it is possible to determine the distributions of stresses on the wear faces by introducing some appropriate assumptions. Since the frictional stress on the wear faces and the shear stress on the shear plane of cutting, which are predicted as above, determine the heat sources in the cutting zone, it is possible to calculate the temperature distribution on the wear faces through numerical analysis of the differential equation of heat transfer. The wear characteristic equation mentioned above is then utilized to predict analytically the wear progress (crater wear on the rake face and flank wear on the clearance face of the cutting tool) and the tool life by applying the normal stress and the temperature predicted already for the given cutting conditions.

3.5 Derivation of the Wear Characteristic Equation

Wear due to adhesion and abrasion appears to play the major role in the continuous dry cutting of steels with carbide tools without a built-up edge. It is considered that the adhesion type of wear mechanism would be rate determining, while the abrasion due to hard particles in the matrix of steel such as carbide, silica (SiO_2) and corundum (Al_2O_3) may be complementary because temperatures and normal stress on the tool face are extremely high (Shaw, 1954) and mutual diffusion of constituents between the steel and the tool is well-known to take place (Opitz, 1967) in the practical range of cutting conditions for carbide tools.

Shaw and Dirke (1956) presented an Archard type of equation for adhesive wear:

$$dW' = A_x \frac{c}{b} Z dL \tag{3-18}$$

where dW' is the wear volume for sliding distance dL, A_x the real area of contact, c the height of the postulated plate-like wear particle, b the mean spacing of the asperities and Z the probability of producing a wear particle per asperity encounter (Holm's probability). Regarding A_x in Eq. (3-18) as the area for unit apparent area of contact, Eq. (3-18) may be written as

$$dW = \frac{\sigma_t}{H} \frac{c}{b} Z dL \tag{3-19}$$

where H is the asperity hardness and σ_t is the normal stress on the contact surface. According to Shaw and Dirke (1956), c/b in the above equation may be regarded as being approximately constant owing to the existence of a size effect. Since the asperity hardness H depends more strongly on the bulk properties of the softer of the pair of

mating surfaces than on those of the asperity itself, it may depend on the diffused layer, temperature, strain and strain rate on the chip surface in contact. Neglecting variation in the strain and strain rate in the practical range of cutting conditions for carbide tools, the following equation by analogy with the rate process may be assumed, since material strength and diffusion are similarly affected by temperature:

$$H = A_1 \exp\left(\frac{A_2}{\theta}\right) \tag{3-20}$$

where A_1 and A_2 are constants and θ is the temperature of the chip surface. The probability Z may be considered as that for yielding a weld which is strong enough to produce a wear particle when an asperity encounter takes place. Since such a weld formation is a kind of thermally activated rate process, the probability Z will be expressed by the following equation, if the interlocking time and the flash temperature rise during the encounter are regarded as being almost constant within a given range of cutting conditions:

$$Z = B_1 \exp\left(-\frac{\Delta E}{\lambda\theta}\right) \tag{3-21}$$

where B_1 is a constant, λ is Boltzmann's constant, ΔE is the activation energy and θ is the temperature of the chip surface. Substituting Eqs. (3-20) and (3-21) in Eq. (3-19) and regarding c/b as constant, the following equation can be obtained.

$$\frac{dW}{\sigma_t dL} = C_1 \exp\left(-\frac{\Delta E + \lambda A_2}{\lambda\theta}\right) \tag{3-22}$$

where C_1 is a constant. Although $\Delta E + \lambda A_2$ in the above equation depends on the structure and the element concentration of the diffused layer on the contact surface, it

may be regarded as being approximately constant if the variety of cutting conditions is limited. Then Eq. (3-23) can be obtained.

$$\frac{dW}{\sigma_t dL} = C_1 \exp\left(-\frac{C_2}{\theta}\right) \tag{3-23}$$

which is the same as the equation presented by Trigger and Chao (1956).

If hard abrasive particles are involved at the asperities at various intervals, the average value of Z and H in Eq. (3-19) will be altered and hence the effect of abrasion is expected to appear in C_1 and C_2 of Eq. (3-23). This will be shown later experimentally. Equation (3-23) has been derived by introducing many crude approximations; however, it is simple enough and contains only two characteristic constants to be determined experimentally that it is convenient for practical use. The equation contains not only Boltzmann's canonical distribution as used in the analysis of the diffusion coefficient but also includes some mechanical effects (post-diffusion process) represented by σ_t and dL.

Although the real situation on the wear surface has not been clarified yet, it is still possible to depict another model of tool wear in which the abrasive action of the hard particles in the cut steel is taken as governing the process. Taking the crater wear in the rake face of a carbide tool as an example, it has been believed that the real area of tool-chip contact is close to the apparent area (Finnie, 1956) and viscous flow-like deformation due to thermal softening takes place along the surface layer of the chip in contact with the rake face. In this situation, wear appears to be produced only as a result of plowing of the weak diffused layer on the rake face by the hard particles on the chip surface. Du et al. (1993) feel, however, that the observations of wear particles

(Uehara, 1976) appear to exclude the possibility of this wear model, although it may be worth noting that expression identical to Eq. (3-23) can be obtained if taking the Rabinowicz equation of abrasive wear (Rabinowicz, 1961) and introducing thermal effects similar to those in Eq. (3-20).

3.6 Flank Wear Progress

The cutting force is predicted in the model based on the minimum cutting energy. Figure 3-6 shows the force model in the three-dimensional cutting process. The process is interpreted as a piling up of the orthogonal cuts in the plane containing the cutting velocity and the chip flow velocity. The shear angle ϕ, the friction angle β, the shear stress on the shear plane τ_s, and the tool-chip contact length l_c in the orthogonal cutting can be associated with the cutting velocity V, the uncut chip thickness t_1, and the rake angle α in the following equation:

$$\begin{aligned} \phi &= f(V, t_1, \alpha) \\ \beta &= g(V, t_1, \alpha) \\ \tau &= h(V, t_1, \alpha) \\ l_c &= J(V, t_1, \alpha) \end{aligned} \tag{3-24}$$

The orthogonal cutting data are prepared as a combination of the workpiece material and the cutting tool. If the chip flow direction is assumed, the cutting energy, which is the sum of the shear energy on the shear plane and the friction energy on the rake face, can be calculated with the orthogonal cutting model. The chip flow direction, which is specified by the angle η_c, is determined such that the cutting energy is minimized. Then, the principal, feed, and radial components of the cutting force can be predicted in the chip flow model determined. The shear stress τ_s on the shear plane

and the friction stress τ_t on the rake face can be distributed as shown in Fig. 3-7 (Usui, 1978). The distributions of the normal stress σ_f and the friction stress τ_f are assumed on the flank wear land, where the friction stress is equal to the normal one (Usui, 1984).

The cutting temperature can be calculated via the finite element method (Patankar, 1980). All mechanical work, which includes the plastic work on the shear plane and the friction work on the rake face and the flank wear land, is converted into heat generation based on the stress distributions. The wear rate can be expressed as Eq. (3-23). C_1 and C_2 are the wear characteristic constants given in the combination of the workpiece and the tool. Then the flank wear rate ($\frac{dV_B}{dt}$) can be given by the following equation (Rabinowicz, 1961):

$$\frac{dV_B}{dt} = C_1 \sigma_f \exp\left(-\frac{C_2}{\theta_f}\right) \cdot \left(\frac{1}{\tan\gamma} - \tan\alpha\right) V \qquad (3\text{-}25)$$

where σ_f and θ_f are the normal stress and the temperature on the flank wear land, respectively, and V, α and γ are the cutting speed, the rake angle, and the relief angle, respectively. The temperature distribution can be analyzed by assuming the friction stress τ_f on the flank wear land. The wear rate is then calculated in Eq. (3-25). Because the wear rate is generally constant over the flank wear land, σ_f and τ_f are modified so that the wear rate is the same over the flank wear land. Finally, the stress distribution, the wear rate, and the temperature distribution can be determined. Then the flank wear V_B at the cutting time T can be predicted in the following equation (Matsumura, 1993):

$$V_B(t) = V_{B0} + \int_0^t \left(\frac{dV_B}{dt} \right) dt \tag{3-26}$$

where V_{B0} is the initial wear offset, which is the width of flank wear land at the time *T*=0 in the calculation.

3.7 Real-time Flank Wear Model for a Workpiece Composed of Various Materials

Equation (3-26) can be used in general turning operations only for workpieces with a single material. In other words, the flank wear model of Eq. (3-26) cannot reflect changes in the workpiece material. This is a kind of open loop estimation model and it is limited because all cutting conditions must be known. Therefore, if a workpiece has various materials, the flank wear model should be updated according to these changes. Therefore, this research proposes to extend the model to accumulate changes in material. It is proposed here that the updated flank wear V_B case of updated time $t = t_{updated}$ can be predicted in the following equation:

$$\begin{aligned} V_B\left(t = n \cdot t_{updated}\right) = V_{B0} &+ \int_0^{t_{updated}} \left(\frac{dV_B}{dt} \right)_{material_1} dt + \int_{t_{updated}}^{2 \cdot t_{updated}} \left(\frac{dV_B}{dt} \right)_{material_2} dt \\ &+ \ldots + \int_{(n-1)t_{updated}}^{n \cdot t_{updated}} \left(\frac{dV_B}{dt} \right)_{material_n} dt \\ &= V_{B0} + \sum_{i=1}^{n} \int_{(i-1)t_{updated}}^{i \cdot t_{updated}} \left(\frac{dV_B}{dt} \right)_{material_1} dt \end{aligned} \tag{3-27}$$

At every update time, the flank wear rate $\left(dV_B / dt\right)$ should be changed according to changes of the workpiece properties. In the present research, workpiece material changes will be detected by a power sensor signal.

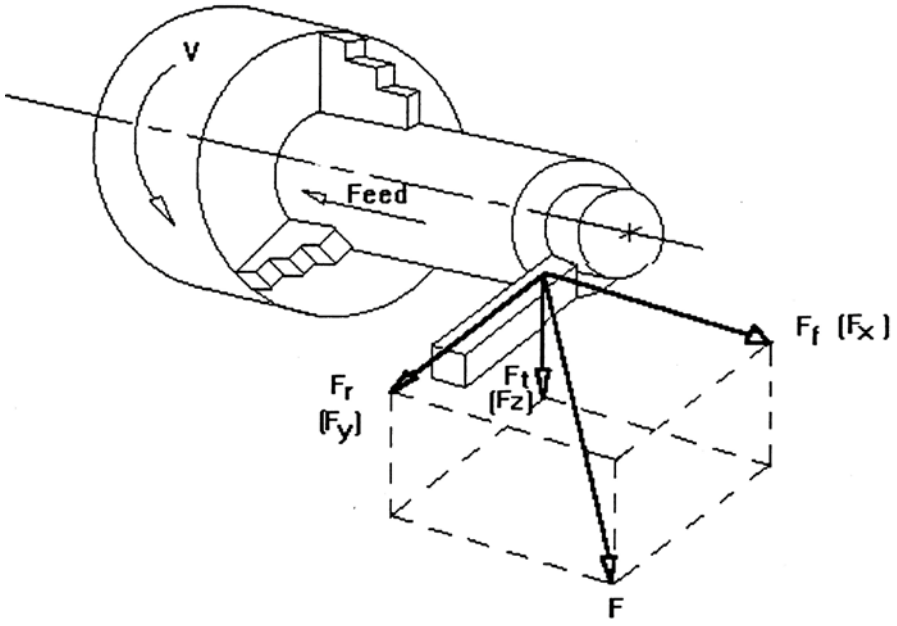

Figure 3-1. The cutting force component in turning operation (Dimla, 2000)

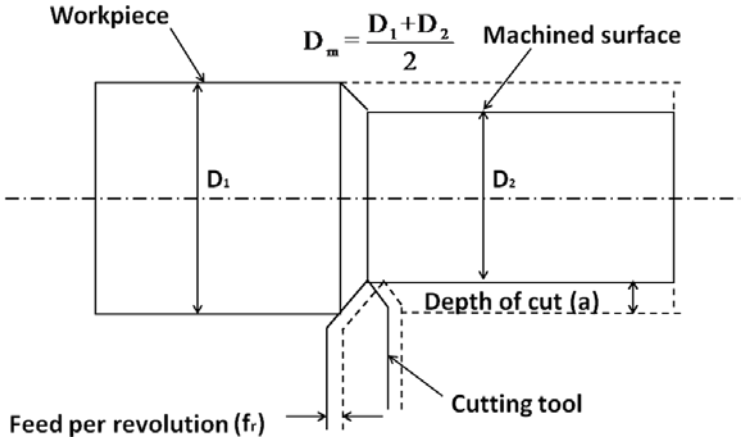

Figure 3-2. Basic turning operation

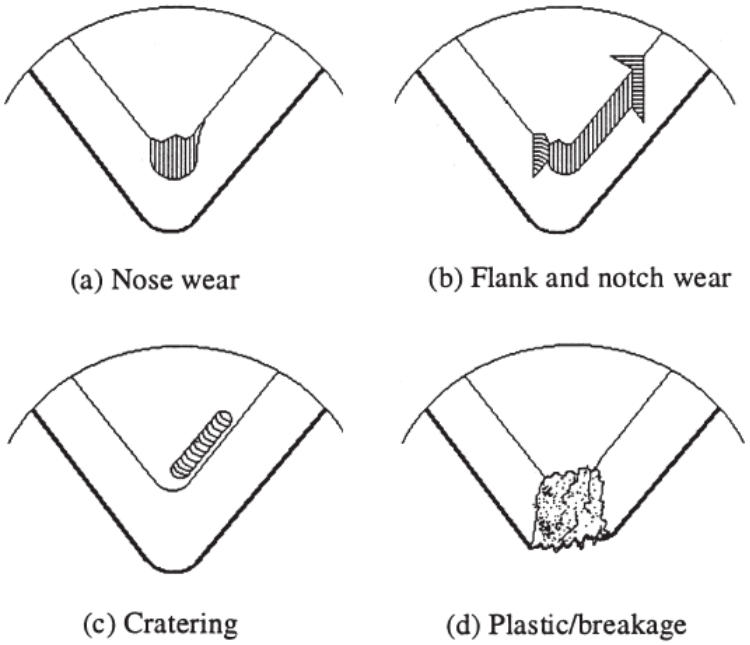

Figure 3-3. Cutting tool wear forms in orthogonal metal cutting (Dimla, 2000)

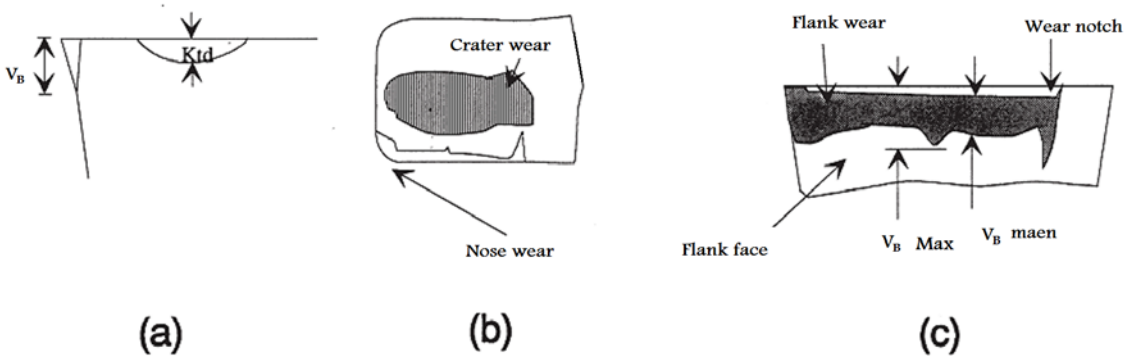

Figure 3-4. Conventional features of turning tool wear measurements (Dimla, 2000)

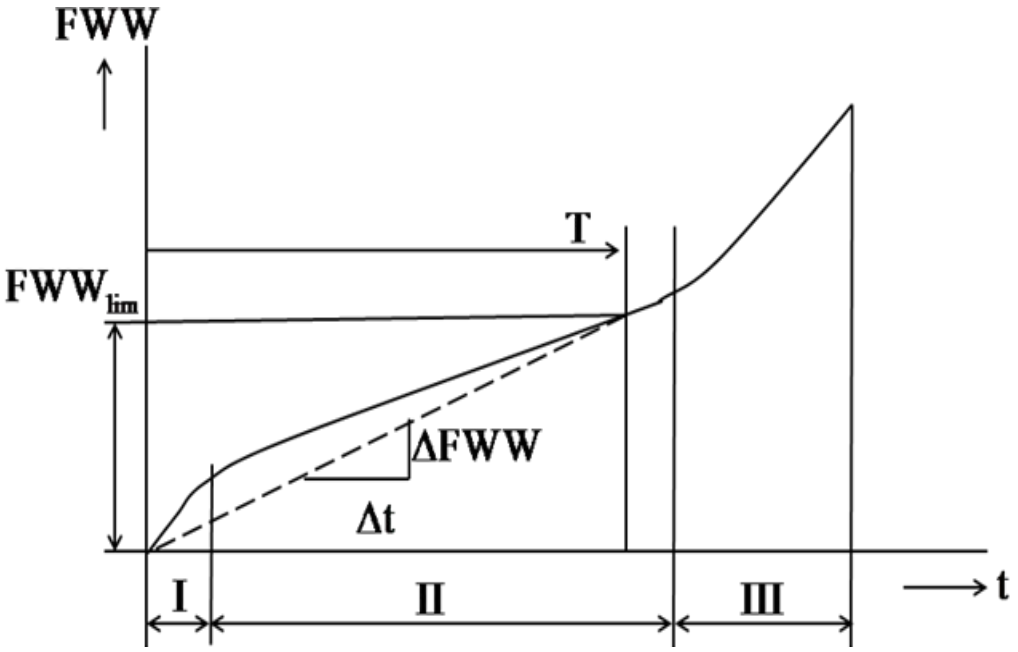

Figure 3-5. Development of flank-wear width with time (redrawn from Tlusty, 2000)

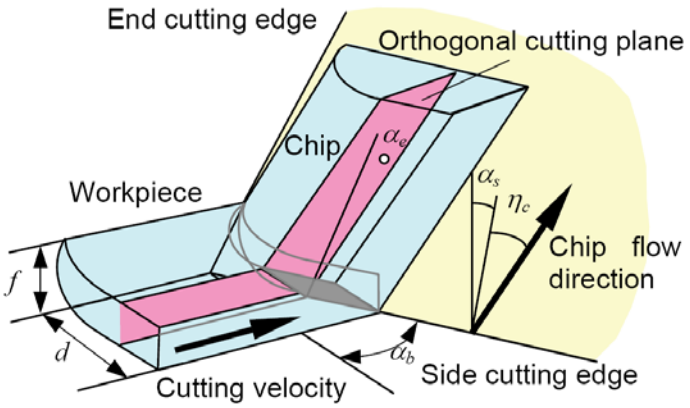

Figure 3-6. Three-dimensional cutting model in turning α_b, α_s, and η_c are back rake angle, side rake angle, and chip flow angle; and f and d are feed rate and depth of cut (Matsumura, 2008)

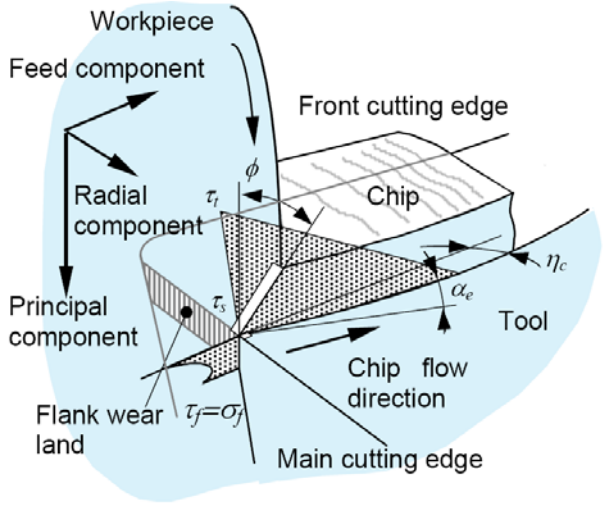

Figure 3-7. Stress distribution on tool face φ, shear angle; τ_t, friction stress on rake face; τ_s, shear stress on shear plane; and τ_f and σ_f are friction stress and normal stress on flank wear land (Matsumura, 2008)

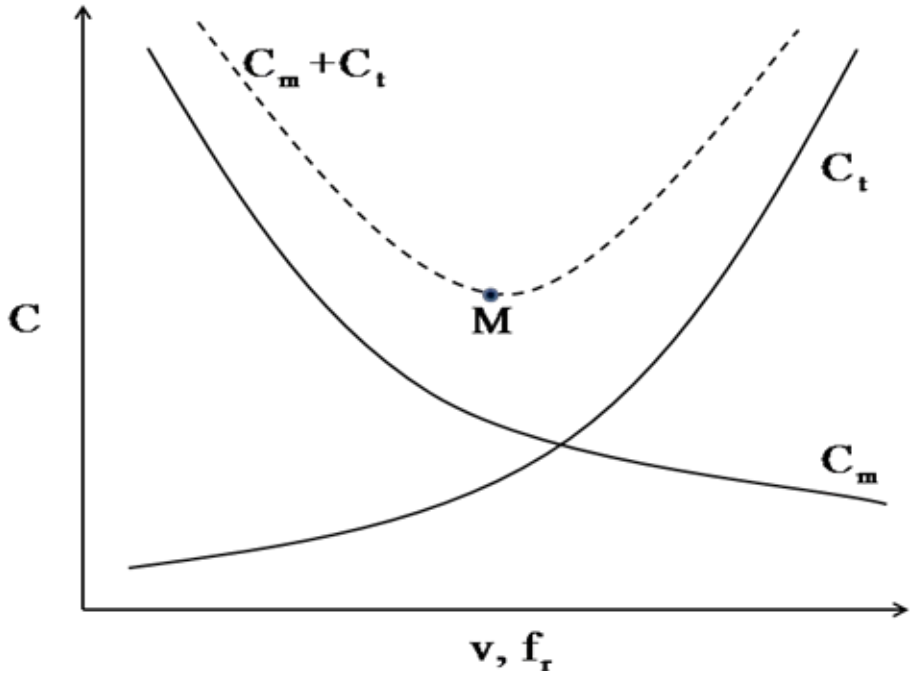

Figure 3-8. Effect of cutting speed (v) and feed (f_r) on the cost per part of components due to machining time and due to tool cost (Tlusty, 2000)

CHAPTER 4
SENSOR FEASIBILITY TEST FOR REAL TIME WORKPIECE MATERIAL DETECTION

This chapter provides the description of feasibility test of sensors for real time workpiece detection. Three sensors were used for feasibility test. First, an infrared sensor was tested by using heating plate. A dynamometer was tested on the Hass SL-10. And a power meter was tested on Hass SL-10 and Okuma LC40 CNC lathes. Lastly, the mini CNC lathe (SyiL C6B) was assembled and the power sensor was tested with various workpieces. In this chapter, the setups, specifications, test conditions, etc., will be described and explained. The test results will be shown in chapter 5.

4.1 Ultimate Thermometer (Infrared Sensor)

In exploring the feasibility of a real time workpiece detection of temperature for compensating tool wear, the ability to measure the temperature of small surface is required. The area for which infrared temperature sensors accurately detect temperature changes linearly with respect to the distance between the sensor's lens and the object of interest. This dependency is characterized by the Distance to Spot diameter ratio or D/S ratio, acquired from the manufacturer. In this test, the Ultimate Thermometer 800043 D/S ratio of 7:1 is verified. Table 4-1 shows the specification of Ultimate thermometer.

A schematic of the experimental setup can be seen in Fig. 4-1. As show, the infrared thermometer hangs with the sensor aimed at a black aluminum cylinder which is heated by a heating plate.

Figure 4-2 is a picture of the actual setup. The aluminum cylinder is subjected by the heating plate to a heating and cooling process giving it a particular heating profile. A heating and cooling cycle is applied to the aluminum cylinder repeatedly as the

thermometer is raised to varying heights. An embedded thermocouple records the temperature of the cylinder while another thermometer records the temperature of the hot plate.

4.2 Cutting Force Measurement on Hass SL-10 Lathe

The cutting force was measured while turning workpieces with step changes in the hardness on a Haas SL-10 CNC lathe. Two workpieces were prepared, i.e., alternating sections of alloyed aluminum and low carbon steel and alternating sections of low carbon steel heat treated to different hardness levels (nominally 20 HRC and 30 HRC). These parts were test for turning operation under different depths of cut *a*, and feed per revolution f_r, values and the three force components were measured using a cutting force dynamometer.

Figure 4-3 shows a schematic of a turning operation and the resultant cutting force F, components. These are the feed force F_f, and radial force F_r, within the plane of the insert cutting face (i.e., the rake face). These forces can be combined to give the normal force F_n, which acts perpendicular to the primary cutting edge. The tangential force, F_t, in the direction of the cutting speed can be combined with the normal force to give the resultant force.

The setup for the heat treated steel workpiece is shown in Fig. 4-4. The cutting force dynamometer (Kistler 9257B) was mounted in the tool turret and the cutting tool holder and insert was clamped to the dynamometer. In this way, the cutting forces were directly recorded by the dynamometer. The force components recorded were $F_f(z)$, $F_t(x)$, and $F_r(y)$.

The insert was mounted on the bottom of the holder according to the photograph provided in Fig. 4-4.

A photograph of the aluminum-steel-aluminum-steel workpiece is provided in Fig. 4-5. The individual sections were approximately 20 mm long.

4.3 Spindle Power Measurements on Hass SL-10 Lathe

The tangential force component F_t, is directly proportional to spindle motor torque, and therefore power. From Eq. 4-1, *T* is torque, r is the workpiece radius, P is the cutting power, and ω is the spindle speed in rad/s. Note that the power depends not only on the cutting force (which is a function of the workpiece hardness), but also on the instantaneous workpiece radius and selected spindle speed.

$$\begin{aligned} T &= F_t r \\ P &= T\omega = F_t r \omega \end{aligned} \tag{4-1}$$

In these tests, a Fast Response PH-13 Power Cell from Load Controls, Inc., was used to monitor the (electrical) spindle power and compared the power levels for segmented workpieces as shown in Fig. 4-5 with cutting forces obtained using the dynamometer setup. The power sensor was wired directly into the Haas SL-10 power cabinet as shown in Fig. 4-6. The addition of the sensor to the machine did not affect the cutting process or the machine functionality. As seen in Fig. 4-6, the three-phase output from the spindle drive was fed through the three inductive sensors (three holes on the left side of the power cell). The same signals were wired to the top right of the unit to measure the reference voltage. Based on this data, an analog voltage is generated which is proportional to the load power consumption. This power signal was

then carried on a BNC cable to the data acquisition system (0-10 V corresponded to 0-15 Hp for this setup).

4.4 Power Measurement on Okuma LC-40 Lathe

A Fast Response PH-13 Power Cell from Load Controls, Inc. was used to monitor the (electrical) machine input power on an Okuma LC-40 lathe. The power cell is designed to sense three phase power. It was used as a standalone transducer with an analog output (0-10 volts). With the installed current chip, this voltage range indicates to 0 to 107 hp. The power cell has three balanced Hall Effect devices, each with a flux concentrator. The Figure 4-7 show the sensor hooked up to the Okuma LC-40 lathe.

A NI USB 6009 I/O board (http://sine.ni.com/nips/cds/view/p/lang/en/nid/14605) in a laptop based data acquisition system and LabView software from National Instruments was used. Specifications of the NI USB 6009 I/O board are given in Table 4-2. Figure 4-8 shows a screen shot of the data measurement program written in LabView. The sampling resolution during gathering was 1 kS/sec.

The spindle power measurement was performed on a Okuma LC-40. The lathe is machining specific parts and the end product shape is shown in Fig. 4-9. There are two facing operations, four roughing turning operations, and finishing facing and turning. For the first and second facing operations, the cutting conditions are 400 rpm spindle speed, 0.016 inch per revolution feed rate and 0.15 inch/pass depth of cut. The first roughing turning operation is simultaneous cut in the OD and ID with 350 rpm spindle speed and 0.02 inch per revolution feed rate. The second roughing turning operation is OD turning with 350 rpm spindle speed, 0.02 inch per revolution feed rate, and 0.2 inch depth of cut from 5.4750 inch diameter to 5.0750 inch diameter. It is followed by a third roughing

turning operation that is OD turning with 350 rpm spindle speed, 0.02 inch per revolution feed rate, and 0.2 inch depth of cut from 5.0750 inch diameter to 4.6750 inch diameter. The last roughing OD turning has cutting conditions as 350 rpm spindle speed, 0.02 inch per revolution feed rate, and 0.1625 inch depth of cut from 4.6750 inch diameter to 4.3500 inch diameter. The finishing operation is the finishing facing and turning with 400 rpm spindle speed, 0.02 inch per revolution feed rate and 0.05 inch depth of cut. Table 4-3 shows the cutting conditions. Figure 4-10 shows a sample of data collection during machining a part with the operations labeled. The power measured from roughing facing operations is labeled 1 and 2. The data from the roughing OD and ID turning operation is 3 in Figure 4-9. The data from roughing OD turning operations is 4, 5, and 6. Lastly, the data from finishing facing and OD-ID turning operation is 7.

4.5 Power Measurement on SyiL CNC Lathe (C6B)

Figure 4-11 shows a picture of the experimental setup, including the SyiL CNC lathe (C6B) and National Instruments USB DAQ board (USB-6009). The Load Control Inc.'s power sensor (UPC) is installed in the input power line of the spindle motor and the data acquisition rate is set to 1 kHz in the LabView program.

Three cylindrical workpieces of diameter of slightly less than 25mm were made for the cutting tests, shown in Fig. 4-12. All workpiece material's original diameter was 1 inch (25.4 mm) and was turned down for reducing the surface effects and exact same diameter. Table 4-4 shows the materials specifications. Workpiece A has four sections of 15mm length, each with a different material: aluminum alloy 6061, hot-rolled 1035 carbon steel, P20 tool steel, and 1018 carbon steel. Workpiece B contains aluminum alloy 6061 and 1018 carbon steel. Workpiece C contains aluminum alloy 6061 and a

stainless steel pin of 3.5 mm diameter to act as a hard spot. Before performing the cutting tests, the Rockwell A hardness values of all materials were measured by Wilson Rockwell hardness tester model 3JR, with three samples per section per workpiece. The average hardness values are shown in Figure 4-12.

The cutting power should be sensitive to cutting conditions such as feedrate, depth of cut, hardness, and workpiece diameter. Spindle speed and feedrate were set to 1000 rpm and 0.1mm/rev, respectively. TCMT32.52 carbide inserts were used in this cutting test.

Table 4-1. Ultimate Thermometer Specification

Type	Range	Resolution	Accuracy (meter only)
Infrared	-20 ~ 400°C -4 ~ 752°F	1°	±3% rdg or ±3°C or ±5°F (which ever is greater)
Note: Accuracy is tested within 23 ± 5°C			
Data Output	RS232 PC serial interface		
D/S	Distance-to-Spot ratio is approximately 7:1.		
IR Wavelength Reg.	6 to 12 micrometer		

Table 4-2. Specifications of the NI USB 6009 I/O board

Feature	USB-6009
AI Resolution	14 bits differential, 13 bits single-ended
Maximum AI Sample Rate, Single Channel*	48 kS/s
Maximum AI Sample Rate, Multiple Channels (Aggregate)*	42 kS/s
DIO Configuration	Open collector or active drive
* Might be system dependent.	

Table 4-3. Cutting conditions for power measurement on Okuma LC-40

Operation	Spindle speed (rpm)	Depth of cut (inch)	Feed rate (inch per revolution)	Produced workpiece diameter (inch)
Facing	400	-	0.016	-
Facing	400	0.15	0.016	-
OD-ID turning	350	0.2	0.02	5.475
OD turning	350	0.2	0.02	5.075
OD turning	350	0.2	0.02	4.675
OD turning	350	0.1625	0.02	4.35
Facing and turning	400	0.05	0.02	-

Table 4-4. Workpiece materials specification (from McMaster-CARR)

Material	Easy-to-Machine Mold-Quality P20 Tool Steel	Multipurpose Aluminum (Alloy 6061)	General-Purpose Low-Carbon Steel	General-Purpose Low-Carbon Steel
Alloy/Low-Carbon Steel type	P20	6061	1018/1018 Carbon Steel	1035/Hot-Rolled 1035
Finish/Coating	Ground	Unpolished (Mill)	Unpolished (Mill)	Zinc-Galvanized
Shape	Rods and Discs	Rods and Discs	Rods and Discs	Rods and Discs
Diameter	1"	1"	1"	1"
Diameter Tolerance	+.045"	±.005"	-.003"	±.009"
Temper/Condition	Hardened, Quenched, Tempered	none	none	none
Hardness	Brinell 262-321	Brinell 95	Brinell 126-167	Rockwell B68
Yield Strength	110,000 PSI	35,000 psi	54,000 to 70,000 psi	30,000 to 44,000 psi

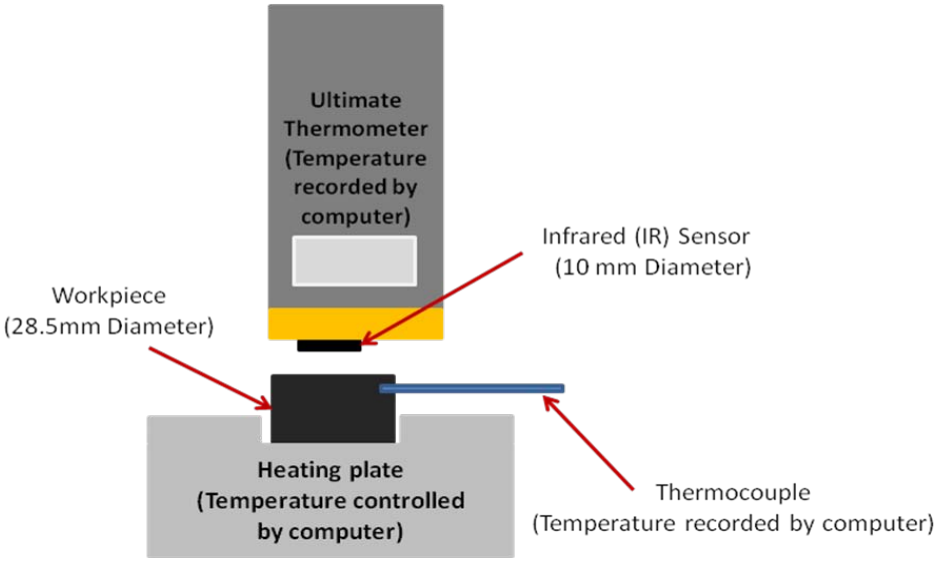

Figure 4-1. Experimental infrared sensor setup schematic

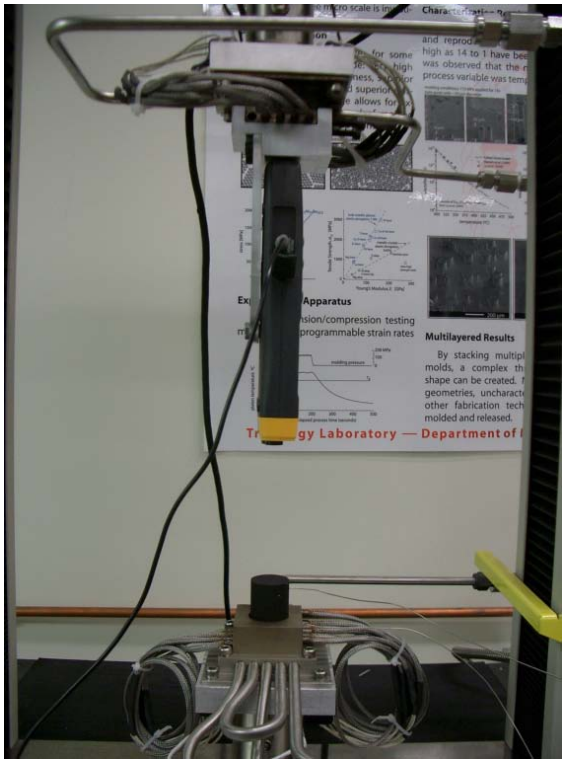

Figure 4-2. Actual setup for infrared sensor test

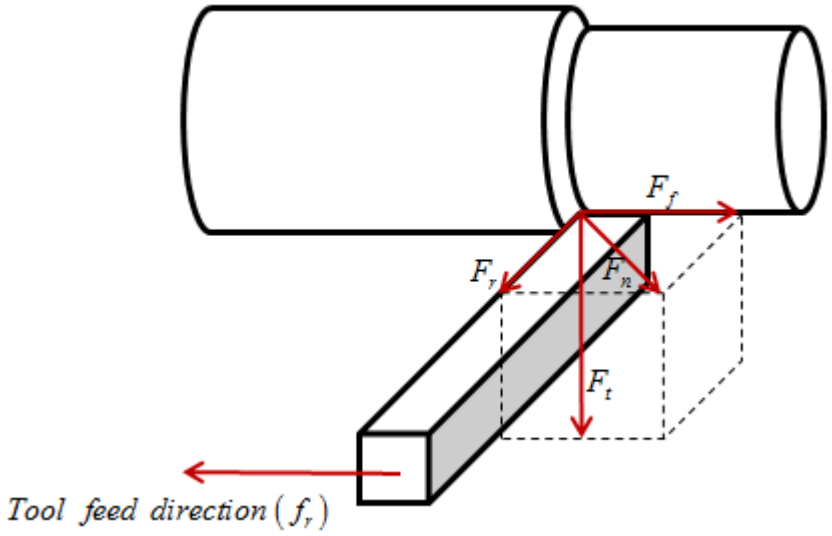

Figure 4-3. Cutting force components measured by dynamometer during cutting tests

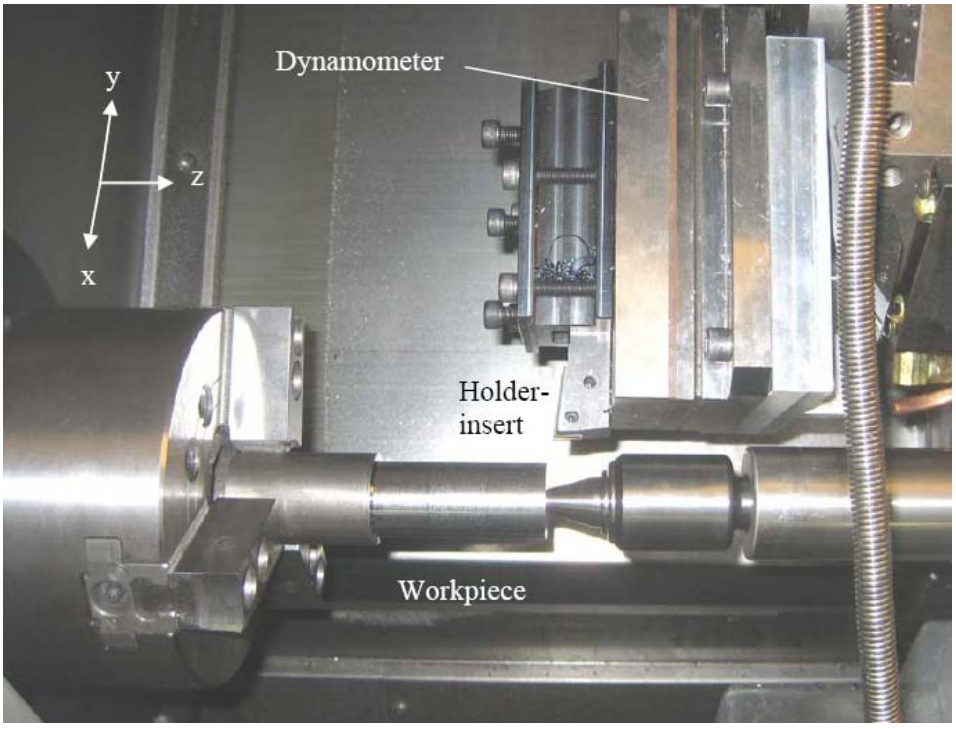

Figure 4-4. Cutting force test setup on Hass SL-10

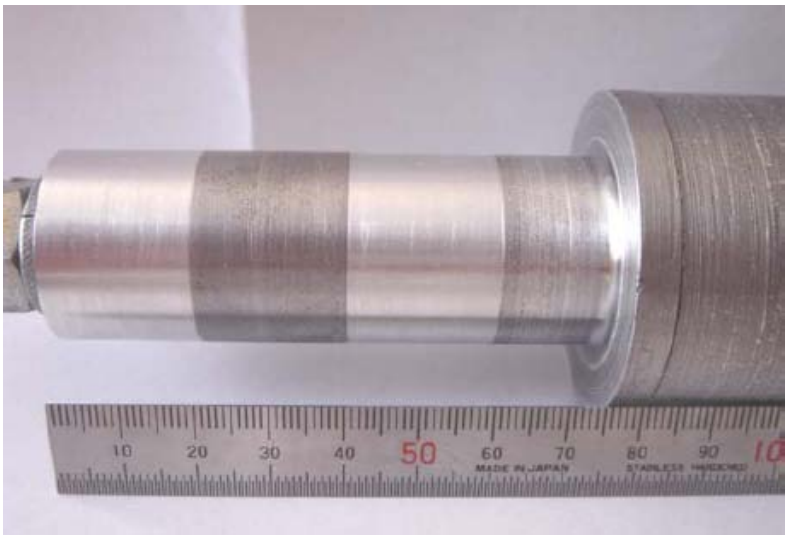

Figure 4-5. Aluminum-steel-aluminum-steel workpiece for Hass SL-10 power and force measurement

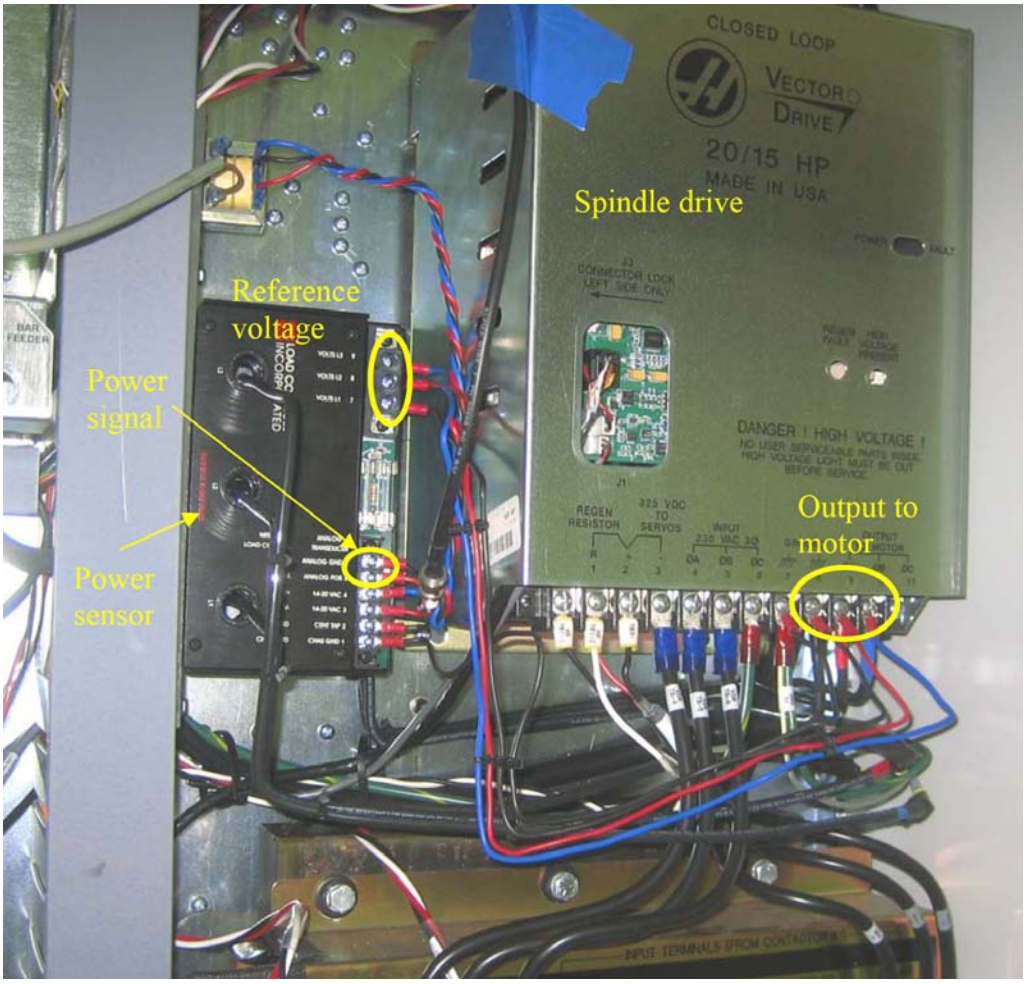

Figure 4-6. Fast Response PH-13 Power Cell mounted in Haas SL-10 power cabinet

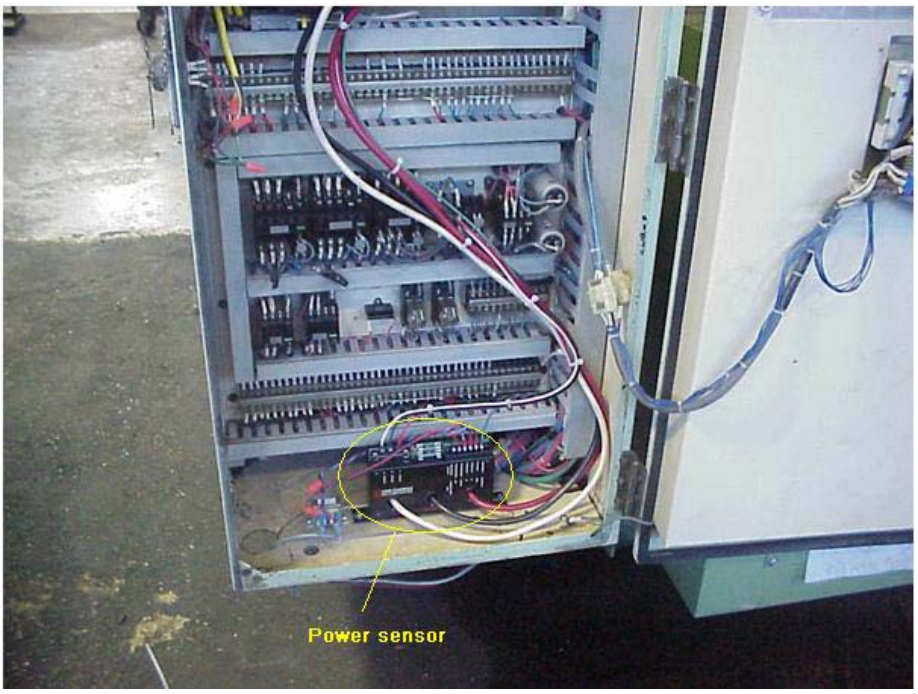

Figure 4-7. Fast Response PH-13 Power Cell mounted in Okuma LC-40 power cabinet

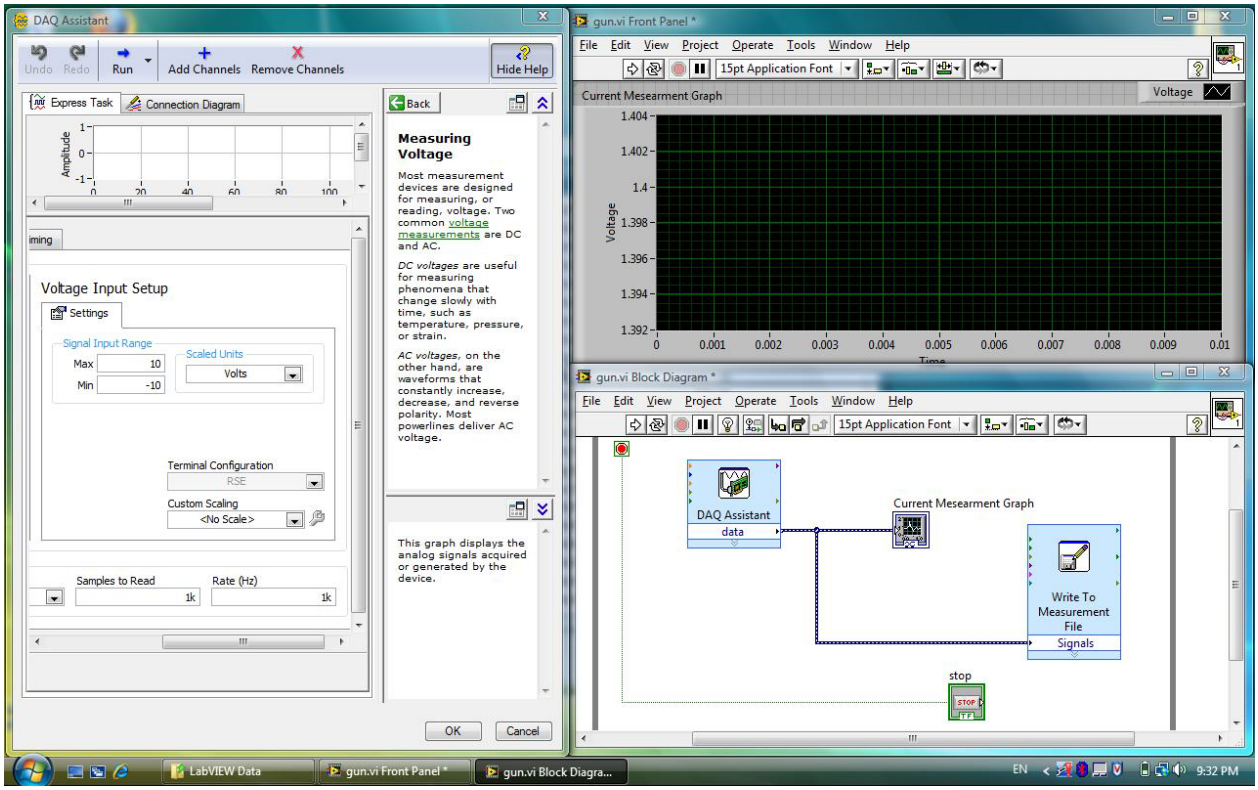

Figure 4-8. Screen shot of data gathering program constructed by LabView for power measurement

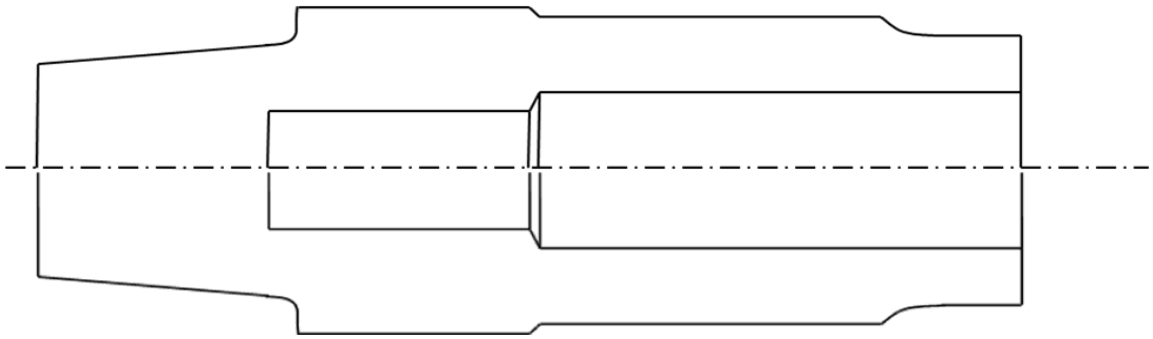

Figure 4-9. Finished pipe joint shape

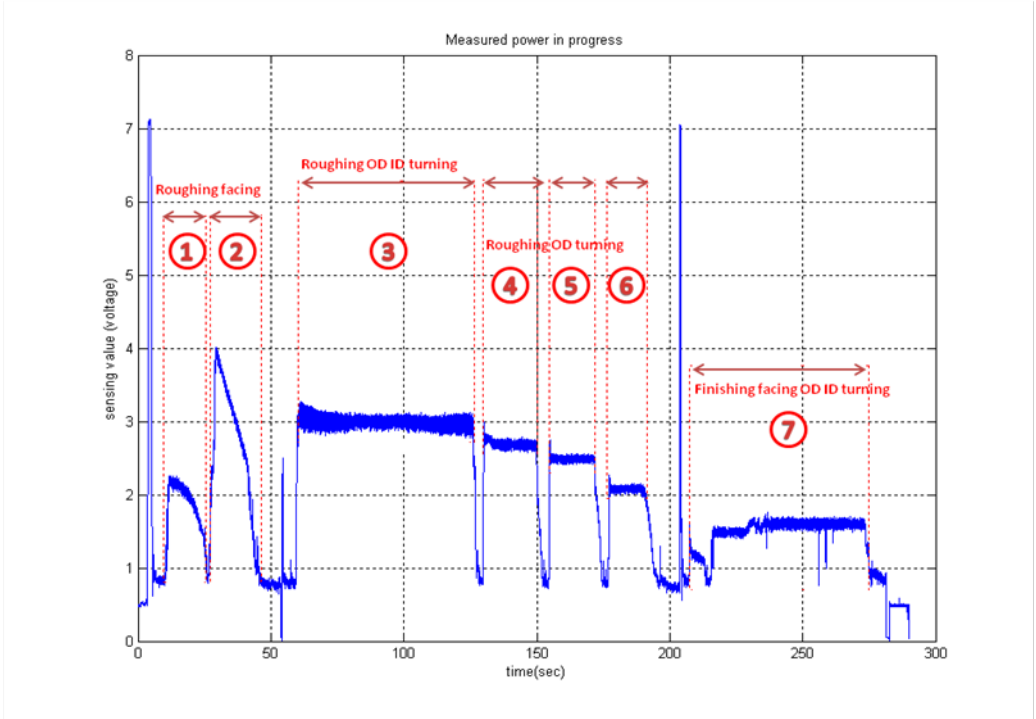

Figure 4-10. Power data while cutting an example part on Okuma LC-40

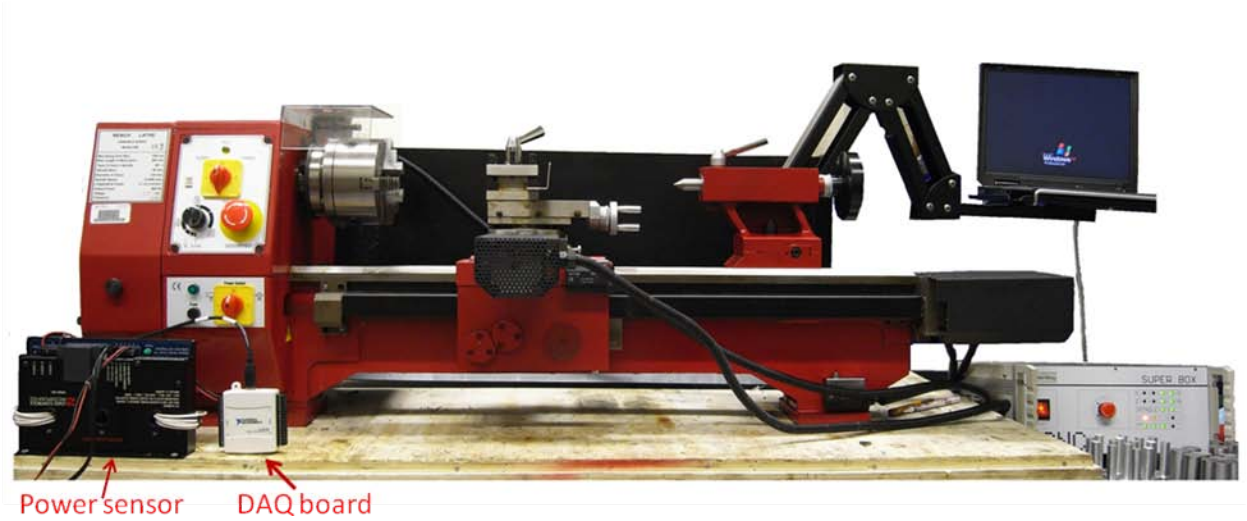

Figure 4-11. SyiL CNC lathe (model C6B), National Instruments USB DAQ board (model USB-6009) and Load Control Inc. power sensor (model UPC)

Figure 4-12. Three different types of workpiece for power measurement test on SyiL CNC lathe

CHAPTER 5
RESULT OF FEASIBILITY TESTS FOR REAL TIME CUTTING POWER DETECTION

5.1 Ultimate Thermometer (Infrared Sensor)

The infrared sensor test was repeated at distances of 50, 100, 150, 200, 250, 300, and 400mm between block and infrared sensor head. The heating plate was heated to 300°C from room temperature, held at for 2 minutes then cooled to room temperature. The thermocouple and Ultimate thermometer readings were recorded. Figure 5-1 shows the result.

Although the behavior of the infrared sensor closely follows that of the thermocouple, there are differences between the readings. The infrared temperature appears to peak after thermocouple does. This delay occurs because the thermocouple is located lower on the aluminum cylinder. The thermocouple encounters the heat “lump” before the infrared sensor does.

The infrared’s highest readings are noticeably higher than the thermocouple readings at small distances. The spatial temperature distribution in the aluminum cylinder is such that the temperature at the center of the top surface reaches a higher peak than the upper sides of the cylinder.

As the distance is increased, the infrared temperature readings tend to become less predictable. The large distance would lead to erroneous results; the intended reading would be affected by the surroundings in view of the infrared sensor. To better prove this inconsistency, a second test was conducted. The heating plate was held at room temperature while the aluminum cylinder was heated separately. The cooling profile from the thermocouple and the infrared sensor were recorded at only two distances, 30mm and 250mm. Figure 5-2 shows these results.

The surrounding temperatures clearly affect the infrared sensor's readings at large distances. And the surface area is at least bigger than sensor head diameter. These results lead us to believe that the Ultimate Thermometer cannot provide good readings for its intended use.

5.2 Power Meter and Dynamometer Test on Hass SL-10

The mean cutting forces for the individual aluminum and steel sections for four different depths of cut/feed per revolution combinations are provided in Table 5-1. For each force component, the ratio is approximately 2:1 for steel (S) versus aluminum (A). The largest force, and highest signal to noise ratio, is seen for the x-direction (F_t).

The same trend was observed for the steel-steel-steel (three different hardness steel) workpiece. However, the force differences were smaller due to the lower hardness difference between the individual sections. Based on these results, cutting force should provide a reasonable signal for real time workpiece detection. However, force measurement is not without its own difficulties.

Force measurements are, in general, actually based on displacement measurements. For example, strain gages are often used to estimate the load on structural members by providing a voltage that is proportional to displacement (within a Wheatstone bridge configuration). To obtain high signal-to-noise ratios, however, a local notch or other feature is typically added to increase the local displacement. In metal cutting, any reduction of the tool-holder assembly stiffness leads to higher potential for chatter and reduced workpiece accuracy. Therefore, adding metrology (force measurement) to monitor workpiece hardness variations to the tool-holder could lead to reduced performance overall. For example, the depth of cut may need to be decreased

to obtain satisfactory cutting conditions once the force sensor is added (i.e., the tool-holder is modified). Measuring the spindle power provides an alternative to force-based process interrogation.

As a first step in the power sensor evaluation, the spindle power as a function of spindle speed (with no cutting load) was measured. Figure 5-4 shows the results of this testing. It is seen that the spindle power increases approximately linearly with spindle speed. Note that this power curve is associated with driving the spindle only and is not a function of the cutting process.

To explore the combined effects of workpiece radius and cutting force on spindle power, multiple cutting tests were completed at three different depths of cut (0.5 mm, 1 mm, and 2 mm) and two feed rates (0.1 mm/rev and 0.2 mm/rev) over a range of workpiece radius values. The spindle speed was 500 rpm in all cases and two different workpieces (aluminum/steel and steel/steel) were used.

Example results for the aluminum/steel workpiece are provided in Figs. 5-5 and 5-6. Figure 5-5 displays the variation in x, y, and z-direction cutting forces, as well as the variation in spindle power with position of the cutting tool along the workpiece. The depth of cut was 1 mm, the feed per revolution was 0.1 mm and the workpiece diameter was 67 mm for the external turning operation. The transition from aluminum to steel to aluminum and back to steel are seen as the step changes in force/power from low to high to low and back to high. The mean values are summarized in Table 5-2. In both the figure and table, it is seen that the power signal mimics the force results with reasonable signal-to-noise ratio (note that no filtering was applied to these signals, except an analog anti-alias filter).

Figure 5-6 shows the cutting forces and spindle power with a depth of cut of 1 mm and feed per revolution of 0.2 mm. The workpiece diameter was 66.5 mm (two workpieces were fabricated from the same bar stock). The same force/power transitions are again observed, but the levels are higher than the values seen in Fig. 5-5 due to the increase in feed with all other conditions remaining approximately constant. Again, the power signal successfully captures the hardness trend without influencing the cutting process.

The influence of radius on power for the aluminum/steel workpiece is demonstrated in Fig. 5-7. For these tests, the depth of cut (0.5 mm) and feed per revolution (0.2 mm/rev) were maintained at constant values as the workpiece radius was reduced with each successive cut. The spindle speed was 500 rpm. The figure shows that the tangential (x-direction) cutting force component remains essentially constant independent of radius (or diameter), while the power demonstrates an approximately linear increase with radius.

A check of the Eq. (4-1) power expression can be performed using the Fig. 5-7 data. For a workpiece diameter of 70 mm (r = 35 mm) and aluminum Ft value of 150 N, the corresponding power should be $P = F_t r\omega = 150\left(\frac{35}{1000}\right)500\left(\frac{2\pi}{60}\right) = 275W$. This agrees reasonably well with the 294 W value shown in the figure (blue solid line). At a diameter of 60 mm (r = 30 mm), the power calculation is $P = F_t r\omega = 150\left(\frac{30}{1000}\right)500\left(\frac{2\pi}{60}\right) = 236W$; the experimental value was 217 W. The overall trend for both the aluminum and steel is a slightly higher slope than is predicted from Eq. (4-1). Additionally, the measured power values to be higher than the calculated values were expected due to the power

consumed in rotating the spindle (Fig. 5-4). These issues could be explored further for the actual tool-material-lathe combination(s) used in practice.

An example result for the steel/steel workpiece is shown in Fig. 5-8. The depth of cut was 1 mm and the feed per revolution was 0.1 mm; the spindle speed was 500 rpm. The change is cutting force (tangential or x-direction) and power between the normalized sections (14.5 and 13.1 Rockwell C hardness values) and hardened section (28.9 Rockwell C) of 4130 steel is apparent. The local deviations in the force/power values in the hardened section is believed to be due to built-up edge that occurred while cutting (no coolant was used in this study).

5.3 Signal Analysis of Okuma LC-40 Power Data

A power sensor was installed to measure machine input power in power cabinet of Okuma LC-40 lathe. Okuma LC-40 is horizontal machine type with an OSP controller. If cutting conditions such as a spindle speed, feed rate, workpiece material, and diameter are the same, a mean value of a power should be same. However, the power is expressed as $P = F_t \cdot \omega \cdot r$, the mean value cannot be used for facing operation because the radius is changed in the cutting progress. Therefore, a maximum value is used for data analysis for facing operation. A standard deviation was also calculated because tool wear and breakage causes more vibration. Total of 1000 samples were used to calculate standard deviation for each operation. Figure 5-9 and Table 5-4 show maximum values of facing operations, mean values of turning operations, and standard deviations of turning operations in one plot. The values for each cutting operation are Figure 5-10 for easy configuration.

There should be a difference between normal and worn tools because tool wear or breakage causes large cutting forces. As shown in equation $P = F_t \cdot r \cdot \omega = K_s \cdot a \cdot f_r \cdot r \cdot \omega$, where F_t is tangential cutting force, r is workpiece radius, ω is spindle speed, K_s is specific cutting force, a is depth of cut, and f_r is feed rate, the power should be larger with a worn tool compared to a normal tool.

As shown in Figure 5-11, after finishing part 5, roughing facing tool 1A was changed. As seen in figure 5-11, before changing the tools, maximum power values were higher than normal.

Generally, tool wear and breakage causes more vibration in cutting. Therefore, the standard variation of power signal was calculated. However, no clear trend was found in this data. Perhaps no trend was found because the machine operator changed tool before serious tool wear or breakage.

If workpiece hardness is lower than normal, the cutting force should be smaller than normal. As shown Figure 5-12, the measured power of parts 6, 7 and 8 from the Aug. 18, 2008 data set (see appendix) is smaller than normal. If cutting conditions and cutting geometry are same and low hardness workpieces are machined, cutting force should be smaller than normal because of $P = K_s \cdot a \cdot f_r \cdot r \cdot \omega$. Small cutting force should cause small spindle power because power is proportioned to cutting force.

In this chapter, the lathe power was measured and analyzed for mean, maximum, standard deviation, and change due to radius change. The possibility to determine the force from the power was checked. If the spindle speed is fixed and the cutting geometry is known, feed rate can be changed to regulate the cutting force. To improve

the productivity of the lathe operations, feed rate should be increased if hardness is low or DOC is smaller than for other parts. Based on the results from this test, the non-invasive, low cost power sensors offered by Load Controls, Inc., offer a feasible option for in-process metrology of turning operations.

Since the cutting power is caused by cutting force, the power under an air cutting was measured. This power isn't caused by the machining process. In this turning operation, non-cutting power value was 0.7008 V (sensor value). When the estimated power was calculated, this value will be subtracted from measured power during cutting. Figure 5-13 shows the measured power during air cutting.

To estimate the power, the data from second, third, and fourth OD turning operations were used because all workpiece radiuses, depths of cut, and spindle speed are known in this period. The second and third OD have same feed rate and spindle speed. And if specific cutting force change due to hardness change is small, workpiece radius change will change power. Therefore, the power change relative to radius change was checked.

Between second and third OD turning operations, workpiece radius is decreased by about 7.6 percent. Estimated power of the third operation by the above equation should be 92.4 percent of second OD turning operation power. The measured power for the third OD turning operation is 90.5 percent of the measured for second OD turning operation.

Another case is the second and forth OD turning operations. In this case, the radius is changed from 2.6375 to 2.2563 inch and depth of cut is changed from 0.2 to 0.1625 inch. According to above equations, the power estimates for the fourth OD

turning should be 69.5 percent of the power for second OD turning operation. The measured power for the forth OD turning was 69.4 percent of the measured power for second OD turning operation.

In turning operations, the power can be expressed using

$$P = F_t \cdot \omega \cdot r + P_{non\ cutting} = K_S \cdot a \cdot f_r \cdot \omega \cdot r + P_{non\ cutting} \quad (5\text{-}1)$$

where F_t is the tangential cutting force, ω is the spindle speed, r is the part radius, $P_{non\ cutting}$ is the non-cutting power, K_S is the specific cutting force, f_r is the feedrate, and a is the depth of cut. Therefore, power with 110% spindle speed override should be bigger than normal spindle speed (100%). Figure 5-14 show power difference of step 2 between normal (100%) and increased (110%) spindle speed. Non cutting power is around 0.68 in this machine. The experimental result is reasonable because cutting power ratio is 1.098. This value should be about 1.1.

5.4 Power Measurement Result on SyiL CNC Lathe (C6B)

Cutting power data (sensor value in voltage) for all workpieces are provided in Figs. 5-15~18. As expected, the average cutting power for harder materials is higher than softer materials. In the case of workpiece B, which had a mixed aluminum and steel region, the cutting power is between that of the aluminum and steel sections separately (see Fig. 5-16). However, the region containing the relatively harder pin (stainless steel) cannot be distinguished by the power measurements in Fig. 5-17. This may be due to the small size of the pin, which only accounted for a maximum of approximately 5% of the workpiece perimeter. In Fig. 5-18, tool breakage occurred when the tool came in contact with the steel pin during a subsequent test. Close inspection reveals a peak corresponding to the instant when the tool was broken.

These results show that the power sensor can detect changes in hardness that last for sufficient duration. Accordingly, the sensor could be used as a sensor in an adaptive real time flank wear scheme.

A simple method to detect variations in the hardness of a workpiece has been implemented in this research by measuring the power of a spindle motor for a turning operation. The power signal successfully captures the hardness trend without influencing the cutting process and requires no additional (external) hardness measurements. However, variations in hardness within a small section are difficult to detect, and may require increased sensitivity of this technique

Table 5-1. Mean cutting force values for aluminum-steel-aluminum-steel workpiece on Hass SL-10

Depth of cut(mm)	Feed per revolution (mm/rev)	Mean of F_x (N)				Mean of F_y (N)				Mean of F_z (N)			
		Al	Steel	Al	Steel	Al	Steel	Al	Steel	Al	Steel	Al	Steel
1	0.1	-160	-318	-167	-341	123	241	109	258	79	166	76	177
2	0.1	-191	-376	-148	-426	133	220	74	217	97	190	78	256
1	0.2	-236	-537	-258	-576	152	329	148	330	120	240	105	275
2	0.2	-443	-1019	-463	-1079	166	341	128	339	278	591	283	623

Table 5-2. Results for a = 1 mm, f_r = 0.1 mm/rev cutting tests using aluminum/steel workpiece at 500 rpm and 67 mm diameter on Hass SL-10

Depth of cut (mm)	Feed per revolution (mm/rev)	Workpiece Diameter (mm)	Mean value of force						Power	
			F_x (N)		F_y (N)		F_z (N)		Al	Steel(W)
			Al	Steel	Al	Steel	Al	Steel	(W)	
1	0.1	67	-178	-415	98	249	99	242	315	762

Table 5-3. Results for a = 1 mm, f_r = 0.2 mm/rev cutting tests using aluminum/steel workpiece at 500 rpm and 66.5 mm diameter on Hass SL-10

Depth of cut (mm)	Feed per revolution (mm/rev)	Workpiece Diameter (mm)	Mean value of force						Power	
			F_x (N)		F_y (N)		F_z (N)		Al	Steel
			Al	Steel	Al	Steel	Al	Steel	(W)	(W)
1	0.2	66.5	-257	-567	138	337	104	246	452	1039

Table 5-4. Maximum values of power during facing operations, mean values and standard deviations of power during turning operations on Okuma LC-40

Part #	First facing Max.	Second facing Max.	First OD-ID turning mean	Second OD turning mean	Third OD turning mean	Fourth OD turning mean	Finishing OD-ID turning mean	First OD-ID turning SD	Second OD turning SD	Third OD turning SD	Fourth OD turning SD	Finishing OD-ID turning SD
1	1.7140	4.2620	3.1697	2.7861	2.5750	2.1432	1.6784	0.0779	0.0273	0.0265	0.0233	0.0356
2	2.2960	4.3670	3.0699	2.6882	2.4894	2.0666	1.6881	0.1476	0.0235	0.0249	0.0277	0.0267
3	1.4080	4.6420	3.0030	2.6371	2.4299	2.0081	1.7122	0.0317	0.0235	0.0191	0.0222	0.0289
4	3.6050	5.0000	3.0659	2.6970	2.4790	2.0653	1.6441	0.0775	0.0263	0.0235	0.0212	0.0239
5	1.9640	5.1050	3.0789	2.6783	2.4923	2.0815	1.5894	0.1072	0.0224	0.0223	0.0237	0.0278
6	2.0720	3.7160	3.0979	2.6239	2.4360	2.0270	1.5197	0.0875	0.0330	0.0243	0.0266	0.0255
7	2.0390	3.6960	3.0996	2.6763	2.4956	2.0791	1.5946	0.1972	0.0463	0.0253	0.0221	0.0444
8	3.1340	3.6940	3.0861	2.6880	2.4997	2.0216	1.5341	0.1896	0.1602	0.0249	0.0238	0.1267
9	2.4880	3.6730	3.0635	2.7077	2.5018	2.0793	1.6410	0.2718	0.0787	0.0280	0.0244	0.0684
10	2.0610	3.7450	3.0976	2.6741	2.5051	2.0174	1.5749	0.1070	0.1956	0.0201	0.0224	0.0298
11	2.0120	3.7750	3.1071	2.6946	2.5133	2.0881	1.6333	0.0767	0.0334	0.0236	0.0231	0.0310
12	2.1530	3.7670	3.1036	2.6809	2.5053	2.0957	1.5889	0.1457	0.0437	0.0195	0.0215	0.0380
13	3.4390	3.7820	3.1177	2.7004	2.5072	2.0917	1.5930	0.0627	0.0248	0.0240	0.0222	0.0227
14	2.9560	3.7870	3.0868	2.7128	2.5166	2.0882	1.6082	0.2383	0.0642	0.0185	0.0210	0.0553
15	1.8260	3.8050	3.1252	2.6907	2.5043	2.0961	1.5946	0.1096	0.0429	0.0215	0.0190	0.0363
16	2.3280	3.8880	3.1384	2.6945	2.5039	2.0970	1.5856	0.1040	0.0190	0.0202	0.0199	0.0281
17	2.3050	3.9650	3.1035	2.7046	2.5130	2.0919	1.5907	0.0823	0.0174	0.0195	0.0215	0.0281
18	1.7980	3.6400	3.1142	2.7016	2.5170	2.1061	1.5863	0.1090	0.0291	0.0185	0.0180	0.0284
19	1.7880	3.5740	3.1464	2.6839	2.5100	2.0933	1.5674	0.0844	0.0224	0.0241	0.0167	0.0296
20	2.2090	3.6940	3.1119	2.7099	2.5131	2.0931	1.5997	0.0673	0.0217	0.0177	0.0146	0.0207
21	1.9080	3.6650	3.0830	2.7003	2.4973	2.0990	1.5636	0.1897	0.1030	0.0274	0.0202	0.0849
22	2.1510	3.7660	3.0941	2.7151	2.5068	2.0958	1.5964	0.1314	0.0303	0.0220	0.0230	0.0283
23	1.8720	3.7520	3.0409	2.7151	2.5130	2.0905	1.5866	0.1796	0.0390	0.0244	0.0212	0.0383
24	2.9970	3.7980	3.0674	2.6979	2.5126	2.0990	1.6017	0.0850	0.0457	0.0231	0.0198	0.0487
25	1.6940	3.8420	3.0879	2.6948	2.5174	2.0970	1.5853	0.0899	0.0228	0.0219	0.0233	0.0241
26	2.0050	3.8020	3.0798	2.6963	2.5072	2.0884	1.5825	0.0957	0.0303	0.0216	0.0218	0.0345
27	1.8390	3.8010	3.0738	2.7063	2.5028	2.0884	1.6011	0.2479	0.0698	0.0251	0.0225	0.0761
28	1.5180	3.8310	3.0713	2.6954	2.5212	2.0835	1.5840	0.1184	0.0554	0.0229	0.0213	0.0473
29	1.3490	3.8720	3.0941	2.6884	2.5185	2.0934	1.5892	0.1262	0.0281	0.0224	0.0234	0.0298
30	1.5560	3.7960	3.0954	2.6998	2.5194	2.0820	1.5974	0.2003	0.0686	0.0331	0.0186	0.0580
31	1.2780	3.8620	3.1278	2.7123	2.5177	2.0965	1.5922	0.1092	0.0378	0.0198	0.0229	0.0299
32	3.1170	3.8450	3.1250	2.7193	2.5191	2.1001	1.5879	0.1606	0.0207	0.0200	0.0252	0.0192
33	2.8030	3.6990	3.0500	2.7143	2.5280	2.1074	1.5873	0.0406	0.0229	0.0229	0.0219	0.0239
34	2.2780	3.8670	3.1340	2.7191	2.5322	2.1130	1.5890	0.0516	0.0307	0.0196	0.0207	0.0317
35	1.6430	3.9340	3.1379	2.7254	2.5155	2.1054	1.5932	0.0571	0.0213	0.0197	0.0184	0.0277
36	1.8360	3.8460	3.1406	2.6913	2.5278	2.1019	1.5592	0.0681	0.0559	0.0217	0.0172	0.0495
37	1.9890	3.8990	3.1362	2.7099	2.5607	2.1067	1.5746	0.0796	0.0232	0.0692	0.0157	0.0294
Mean	2.1587	3.8942	3.0960	2.6957	2.5069	2.0843	1.5949	0.1202	0.0454	0.0238	0.0214	0.0389
S.D.	0.5775	0.3426	0.0314	0.0206	0.0229	0.0258	0.0350	0.0601	0.0382	0.0084	0.0028	0.0216
95% CI	0.1861	0.1104	0.0101	0.0066	0.0074	0.0083	0.0113	0.0194	0.0123	0.0027	0.0009	0.0070

Table 5-5. Predicted power due to radius change and measured power on Okuma LC-40

Operation	Spindle speed (RPM)	Feed rate (IPR)	Depth of cut (inch)	Workpiece radius	Measured power (voltage)	Ratio of workpiece radius	Estimated ratio of power	Experimental ratio of power
Second OD turning	350	0.02	0.2	2.6375	2.6982	1	1	1
Third OD turning	350	0.02	0.2	2.4375	2.5088	0.9242	0.9242	0.9052
Fourth OD turning	350	0.02	0.1625	2.2563	2.0859	0.8555	0.6951	0.6935

Table 5-6. Mean power change by spindle speed change on Okuma LC-40

	100% spindle speed	110% spindle speed	Non cutting power
Mean power	1.8989	2.0184	0.68
Estimated ratio (110%/100%)		1.1	
Experimental result (110%/100%)		1.098	

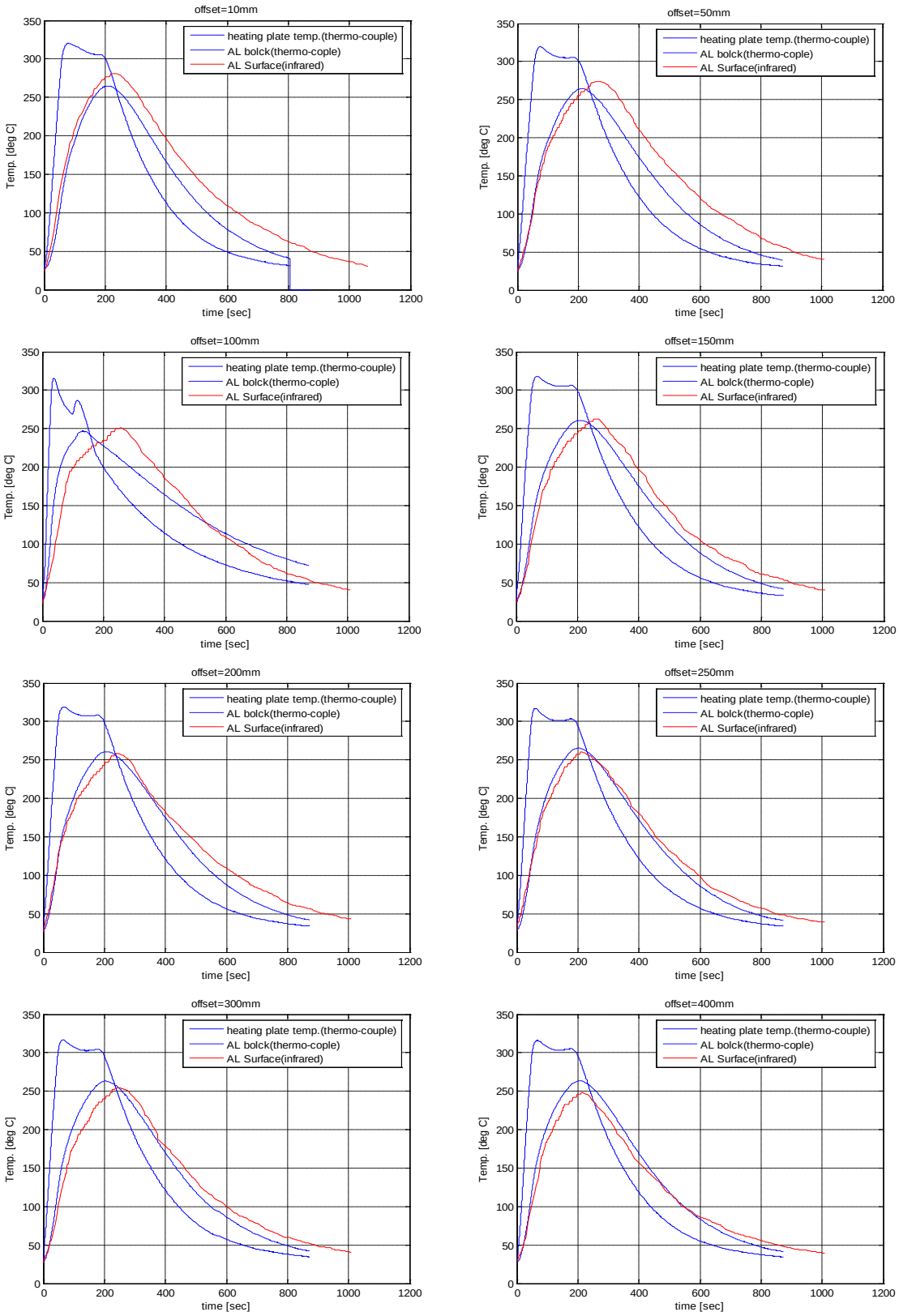

Figure 5-1. Temperature readings from trials for infrared sensor test

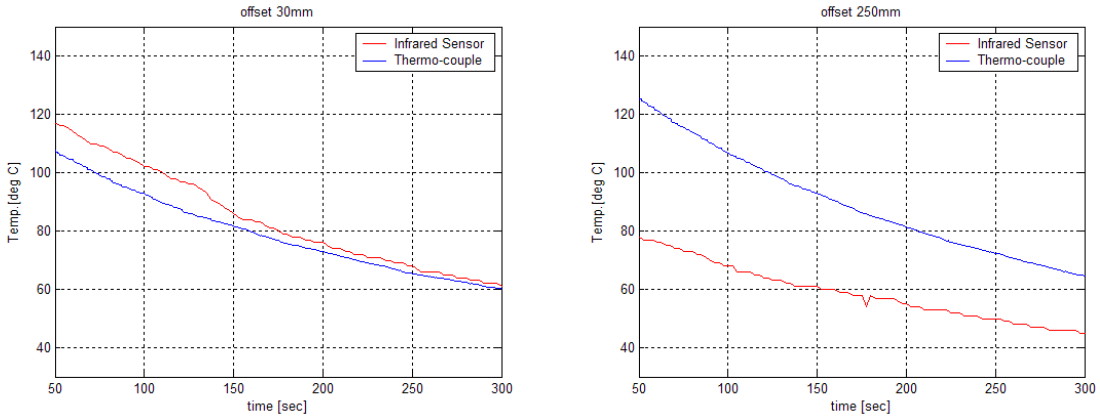

Figure 5-2. Cooling profiles of infrared sensor test

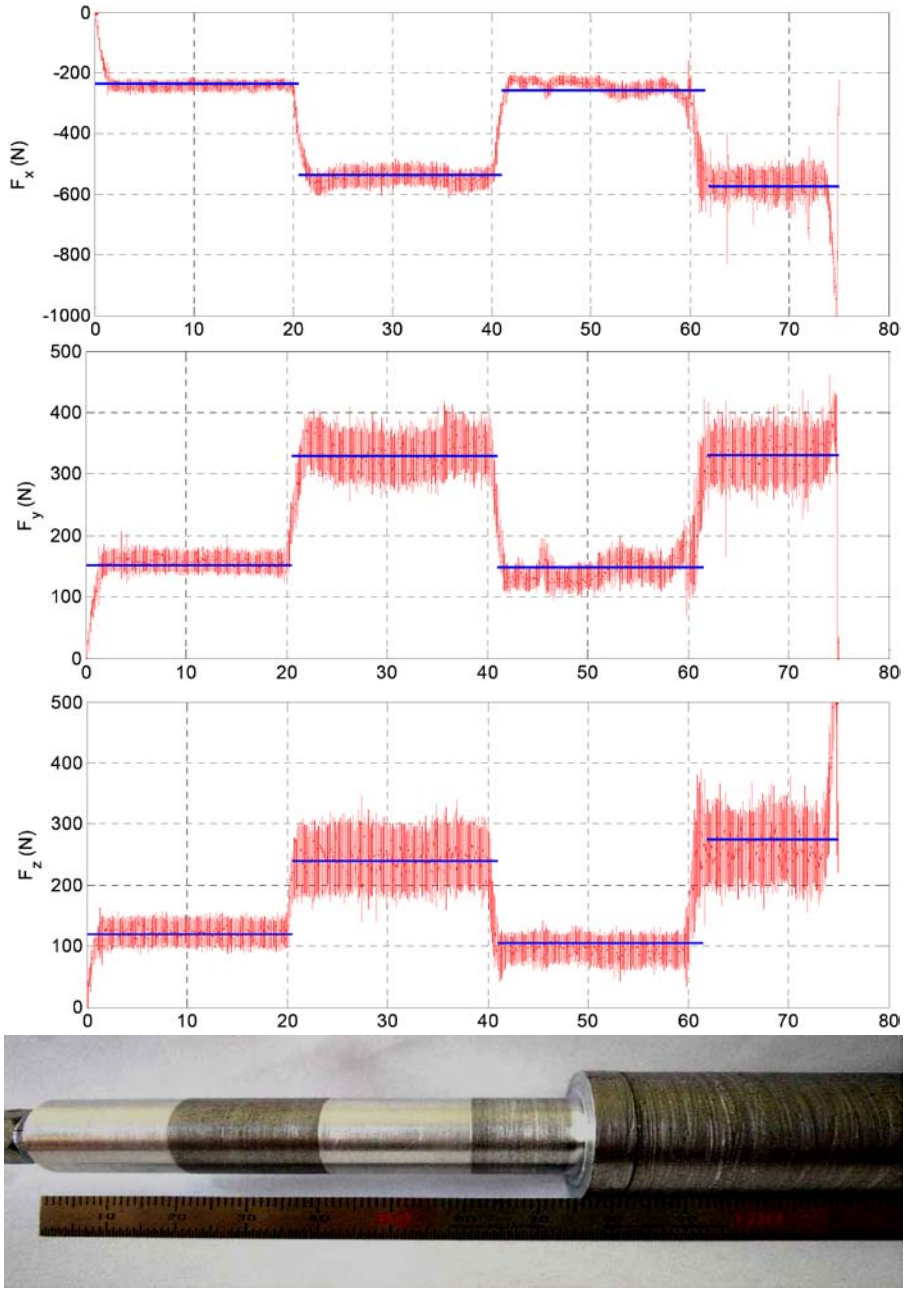

Figure 5-3. Measured cutting force on Hass SL-10 for a = 1 mm and f_r = 0.2 mm/rev(aluminum-steel-aluminum-steel workpiece). A) in x-direction, B) in y-direction, C) in z-direction and D) workpiece

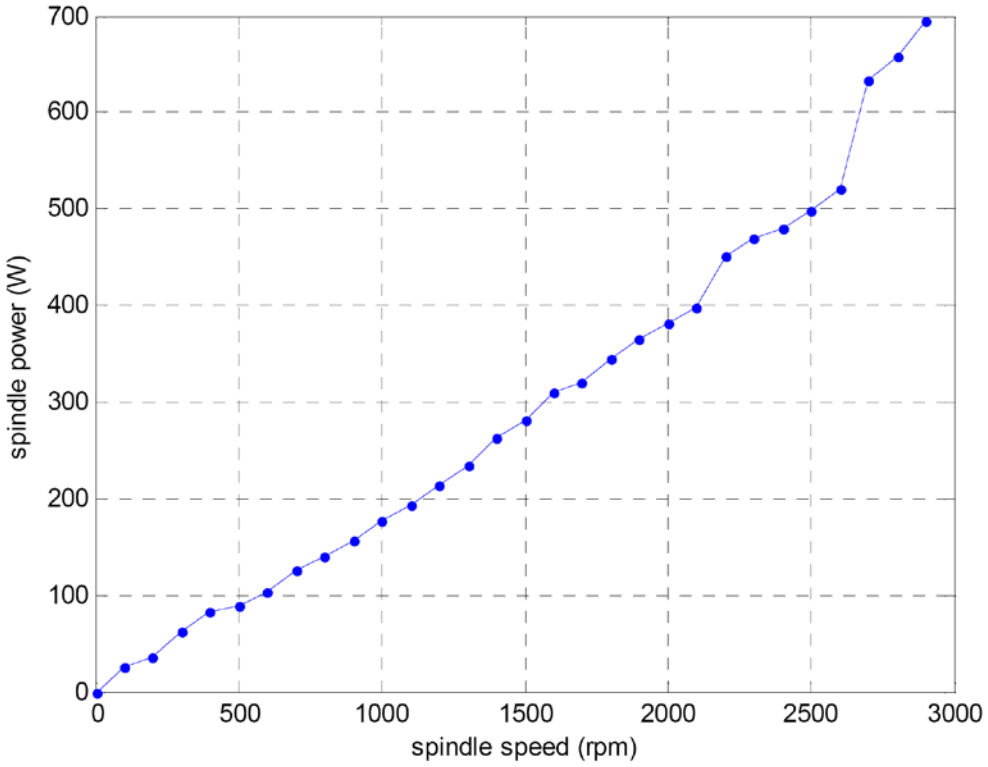

Figure 5-4. Spindle power (no cutting) as a function of spindle speed on Hass SL-10

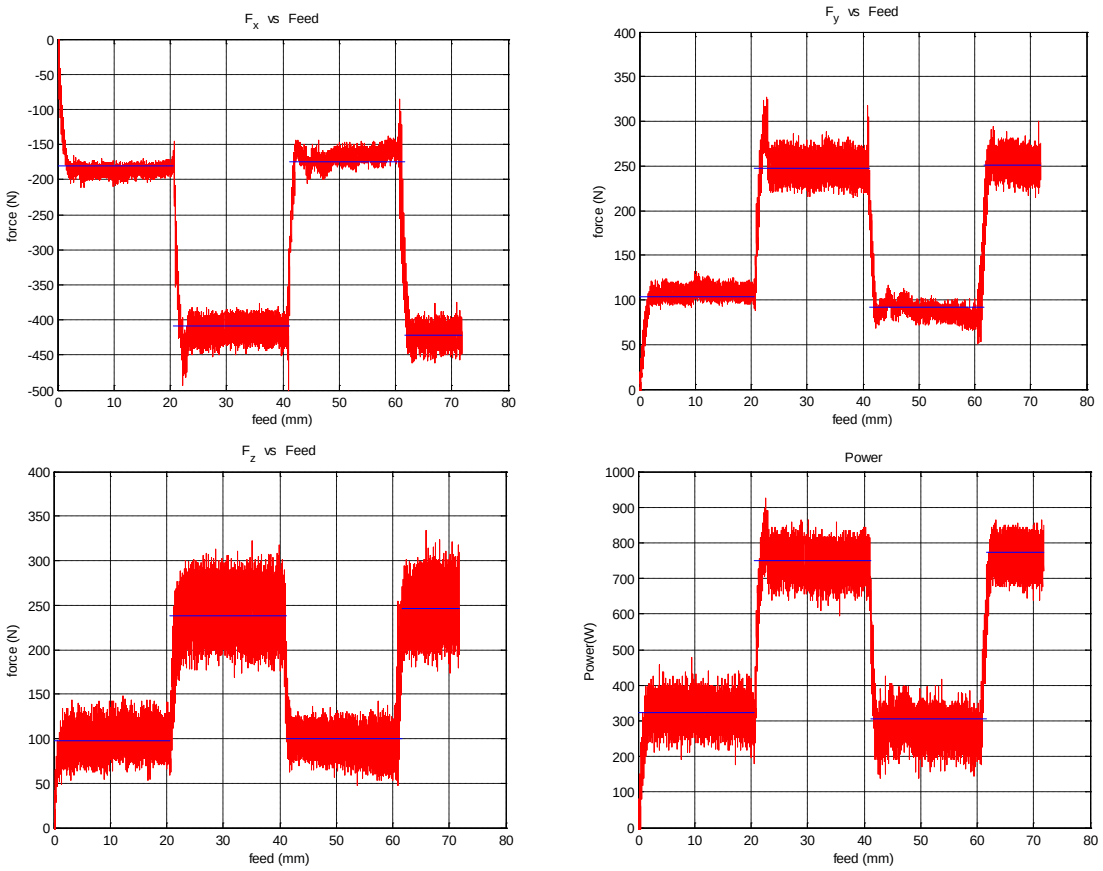

Figure 5-5. Cutting force and spindle power on Hass SL-10 for a = 1 mm and f_r = 0.1 mm/rev using aluminum/steel workpiece at 500 rpm and 67 mm diameter. (Top left) x-direction force (F_t). (Top right) y-direction force (F_r). (Bottom left) z-direction force (F_f). (Bottom right) spindle power.

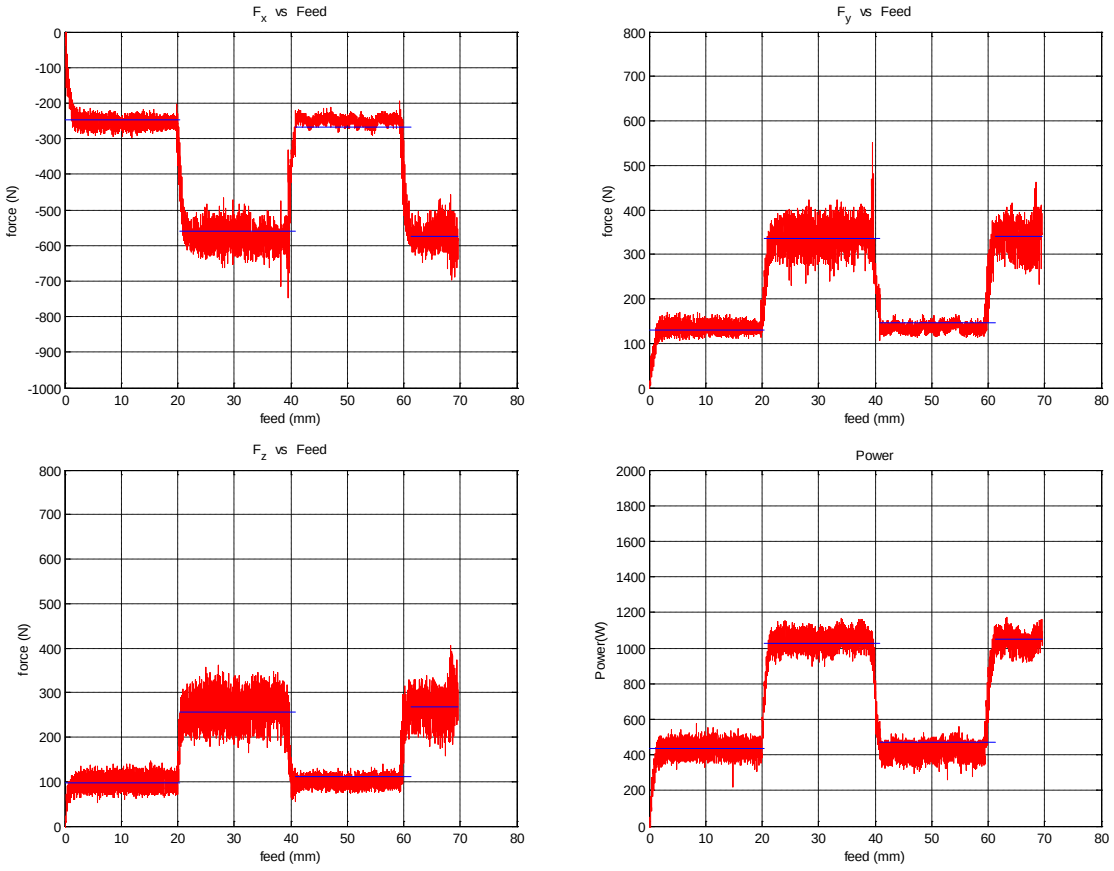

Figure 5-6. Cutting force and spindle power on Hass SL-10 for a = 1 mm and f_r = 0.2 mm/rev using aluminum/steel workpiece at 500 rpm and 66.5 mm diameter. (Top left) x-direction force (F_t). (Top right) y-direction force (F_r). (Bottom left) z-direction force (F_f). (Bottom right) spindle power.

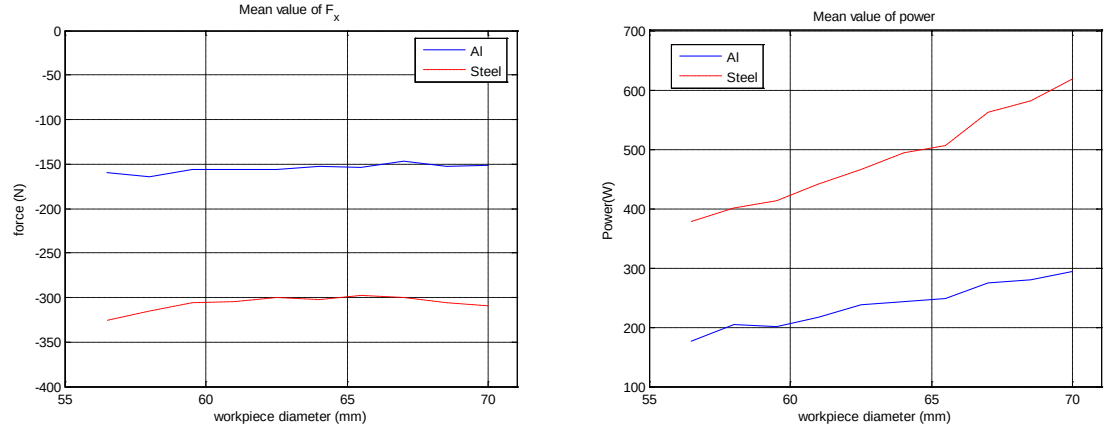

Figure 5-7. Mean x-direction cutting force and spindle power on Hass SL-10 as a function of workpiece diameter for a = 0.5 mm and f_r = 0.2 mm/rev using aluminum/steel workpiece at 500 rpm. (Left) x-direction force (F_t). (Right) spindle power.

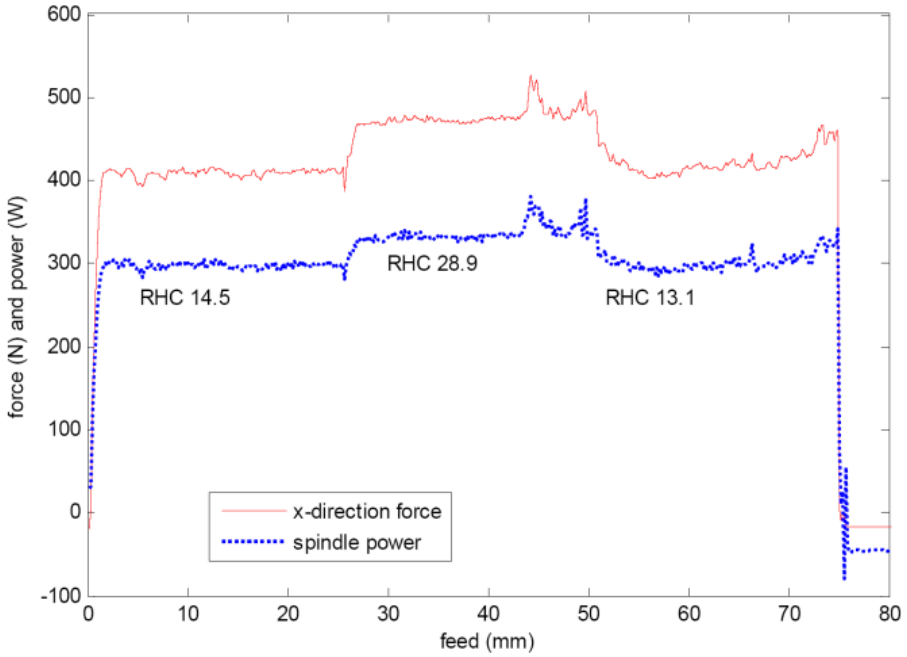

Figure 5-8. Cutting force and spindle power on Hass SL-10 for a=1mm and f_t=0.1 mm/rev using steel/steel at 500rpm

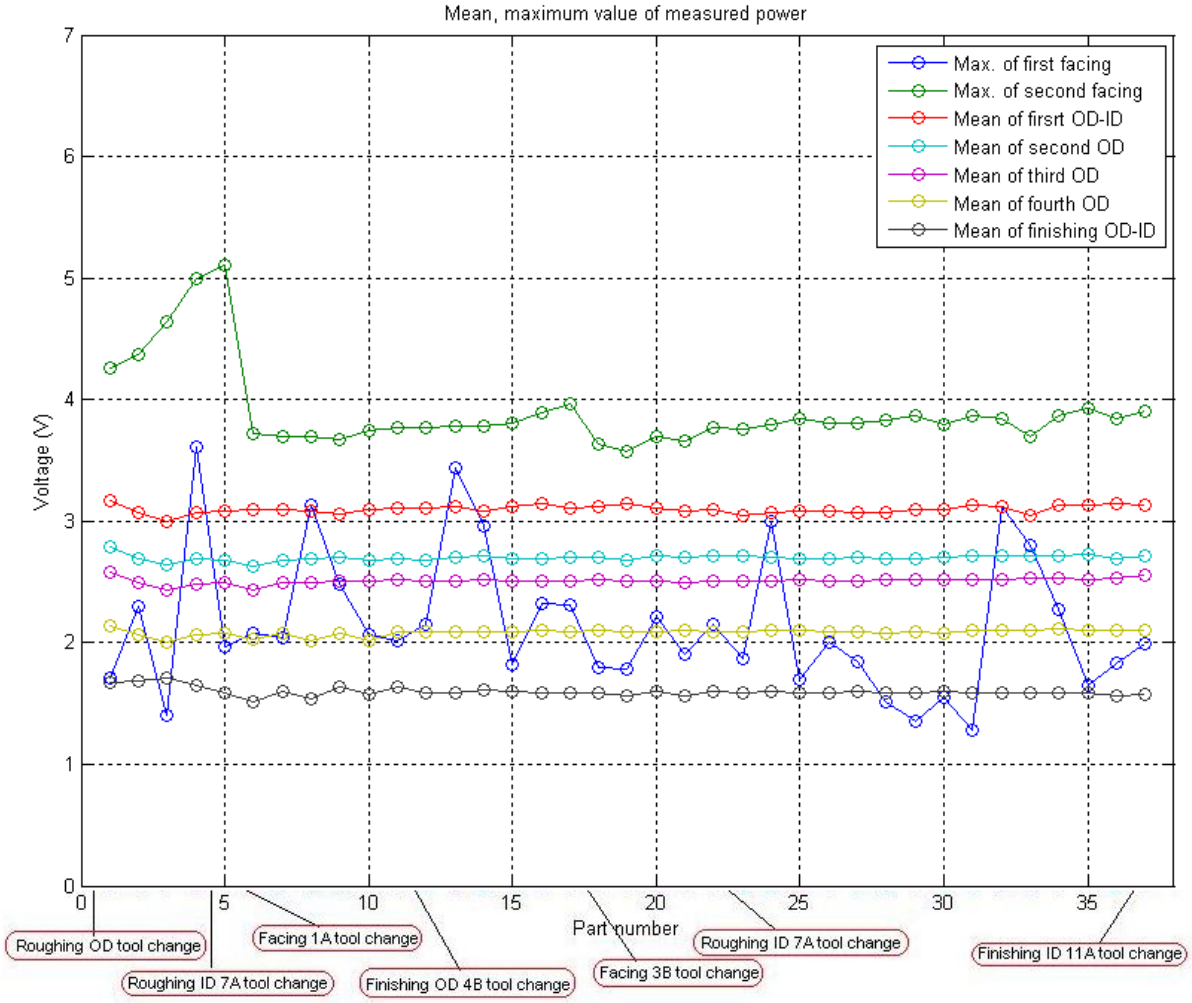
Mean, maximum value of measured power
Max. of first facing
Max. of second facing
Mean of firsrt OD-ID
Mean of second OD
Mean of third OD
Mean of fourth OD
Mean of finishing OD-ID
Voltage (V)
Part number
0
1
2
3
4
5
6
7
0
5
10
15
20
25
30
35
Roughing OD tool change
Roughing ID 7A tool change
Facing 1A tool change
Finishing OD 4B tool change
Facing 3B tool change
Roughing ID 7A tool change
Finishing ID 11A tool change

A)

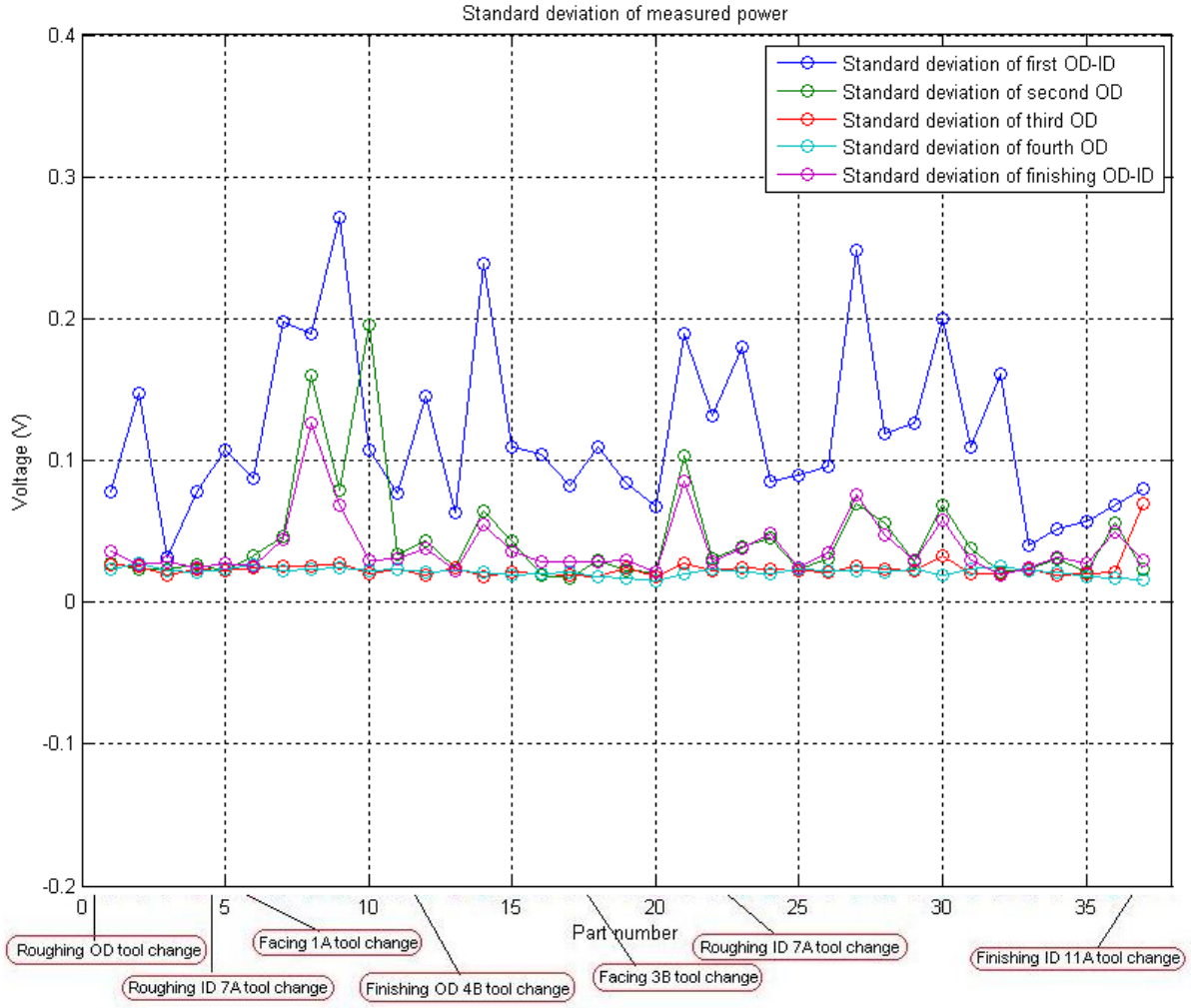

B)

Figure 5-9. A) Maximum values of facing operations, mean values of turning operations B) Standard deviations of turning operations on Okuma LC-40

A)

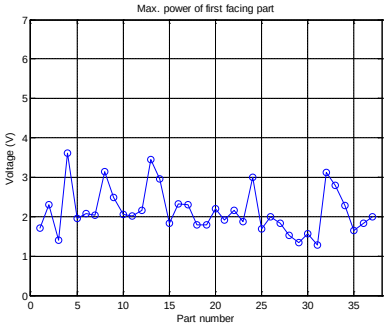
Max. power of first facing part
Voltage (V)
Part number

B)

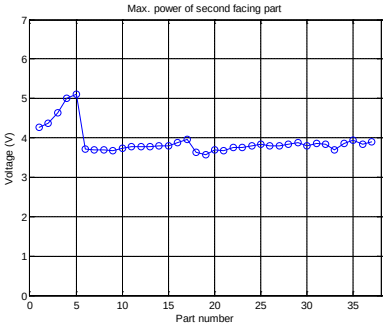
Max. power of second facing part
Voltage (V)
Part number

C)

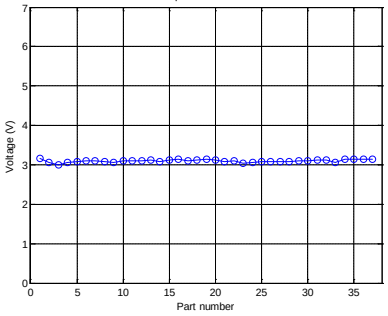
Mean power of first OD-ID
Voltage (V)
Part number

D)

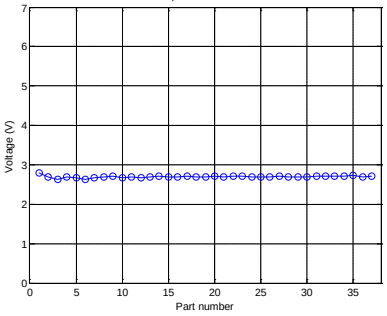
Mean power of second OD
Voltage (V)
Part number

E)

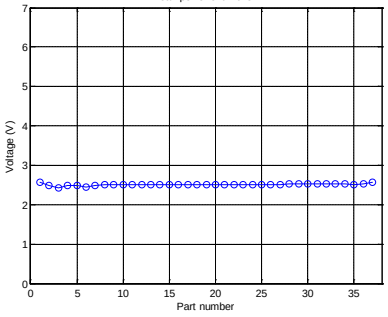
Mean power of third OD
Voltage (V)
Part number

F)

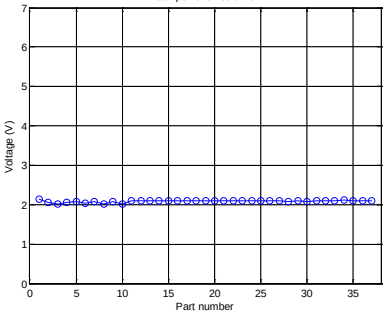
Mean power of fourth OD
Voltage (V)
Part number

G)

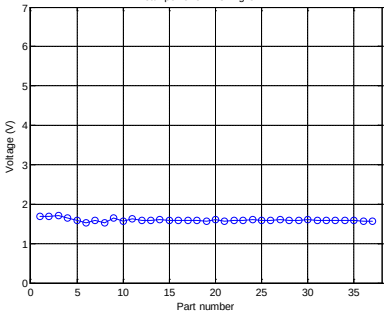
Mean power of finishing OD-ID
Voltage (V)
Part number

H)

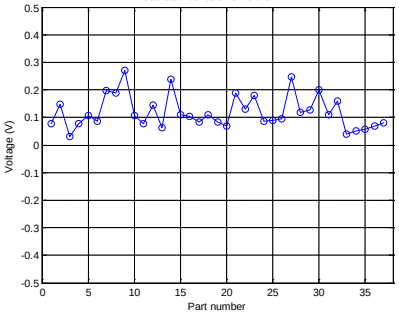
Standard deviation of fisrt OD-ID
Voltage (V)
Part number

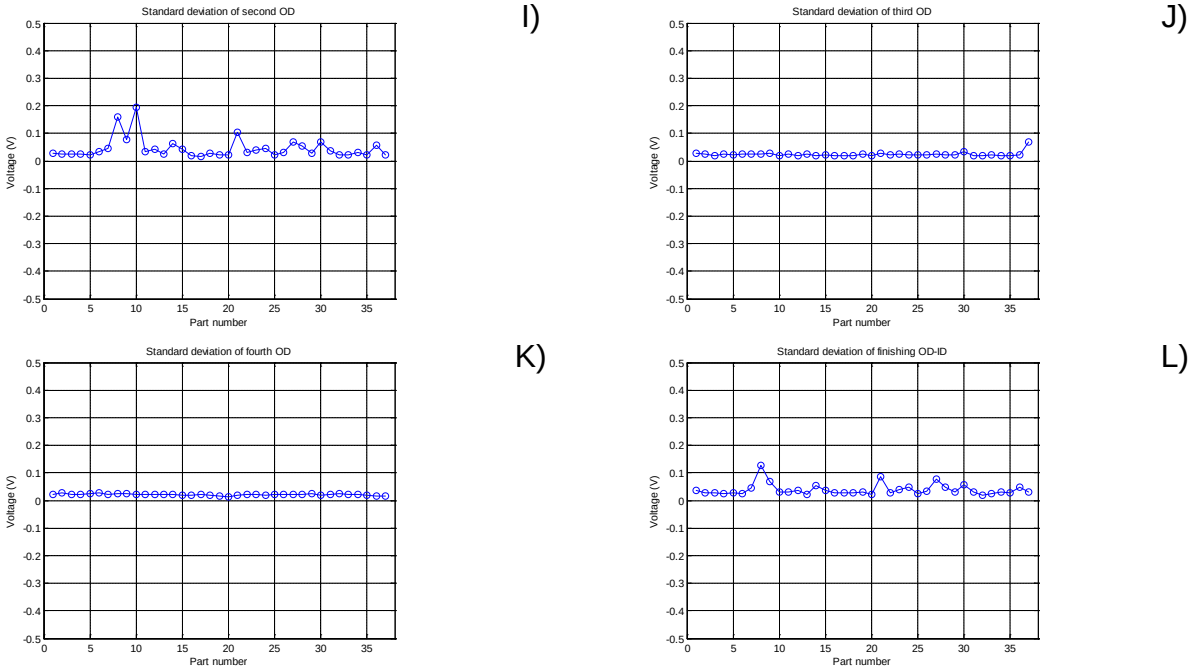

Figure 5-10. A) Max value of first facing, B) Max value of second facing, C) Mean value of first turning (OD and ID are simultaneous cut), D) Mean value of third turning (OD cut), E) Mean value of second turning (OD cut), F) Mean value of fourth turning (OD cut), G) Mean value of finishing turning, H) Standard variation of second turning (OD cut), I) Standard variation of first turning (OD and ID are simultaneous cut), J) Standard variation of third turning (OD cut), K) Standard variation of fourth turning (OD cut), and L) Standard variation of finishing turning on Okuma LC-40

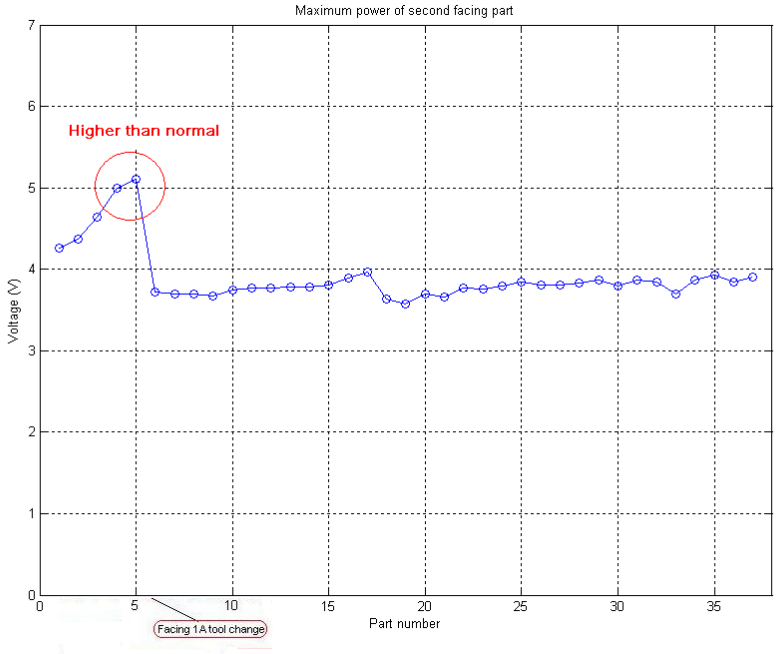

Figure 5-11. Power difference between worn and normal tool in second facing on Okuma LC-40

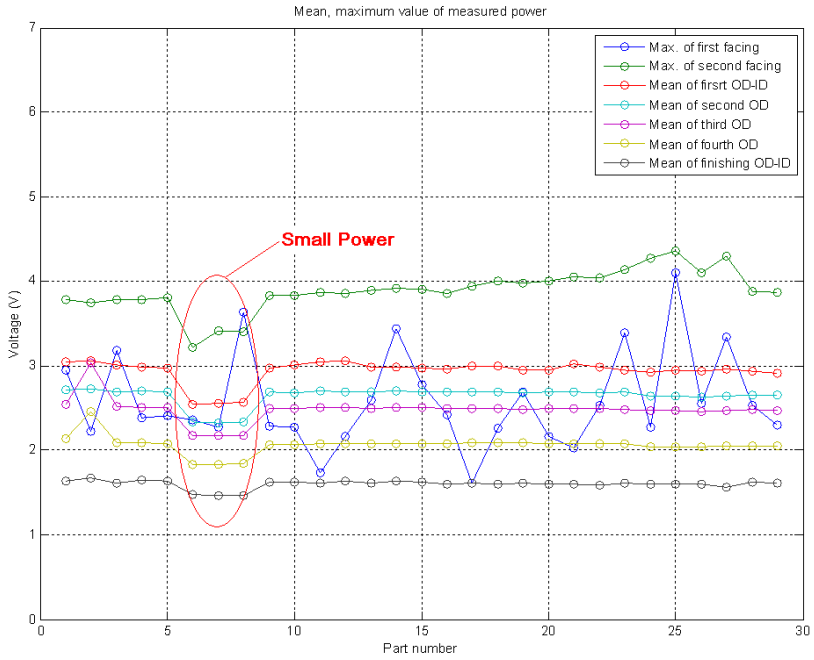

Figure 5-12. Mean and maximum value of measured power on Okuma LC-40

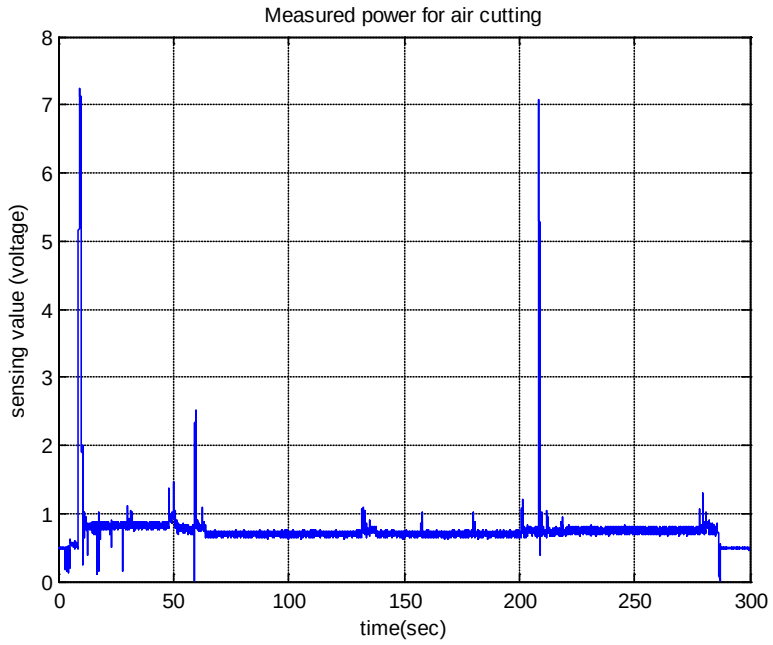

Figure 5-13. Measured power under air cutting on Okuma LC-40

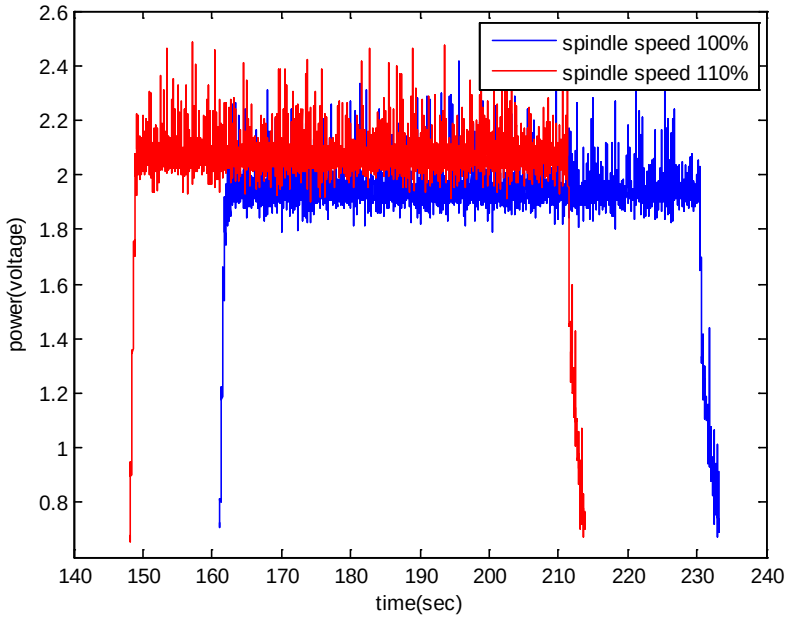

Figure 5-14. Power measurement on Okuma LC-40 under different spindle speed

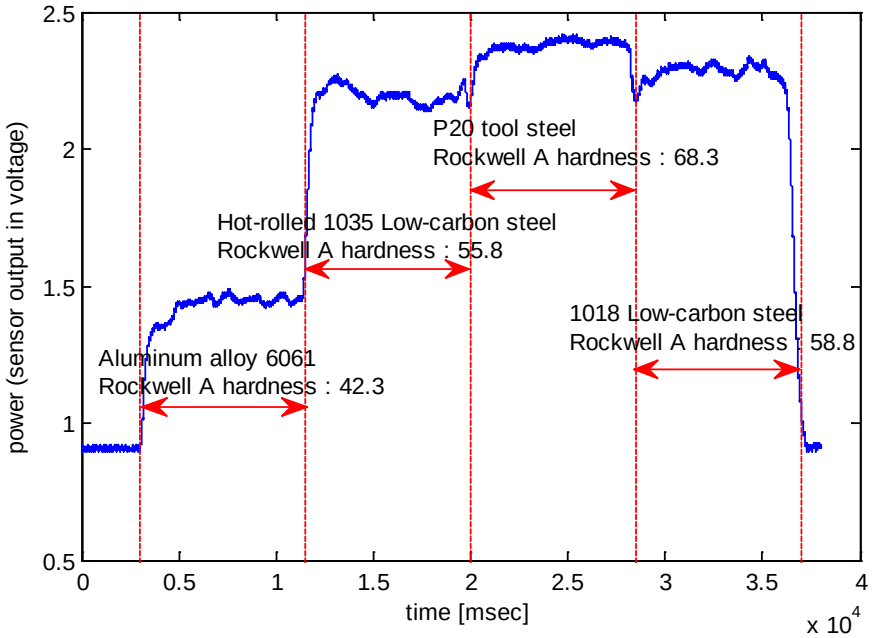

Figure 5-15. Measured cutting power (sensor value in voltage) on SyiL C6B for spindle speed = 1000 rpm, a = 0.5 mm, f_r = 0.1 mm/rev and workpiece diameter = 22 mm (workpiece A)

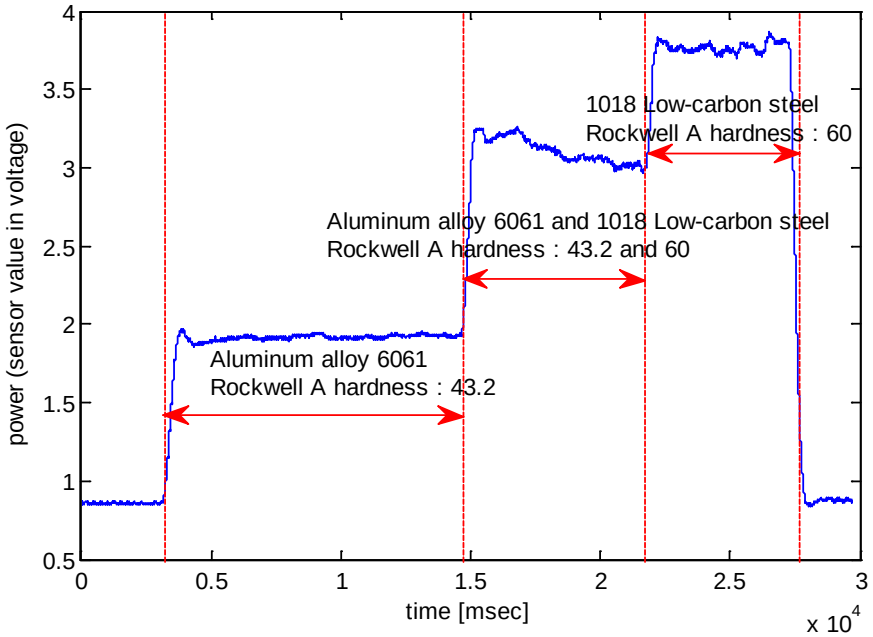

Figure 5-16. Measured cutting power (sensor value in voltage) on SyiL C6B for spindle speed = 1000 rpm, a = 1 mm, f_r = 0.1 mm/rev and workpiece diameter = 23 mm (workpiece B)

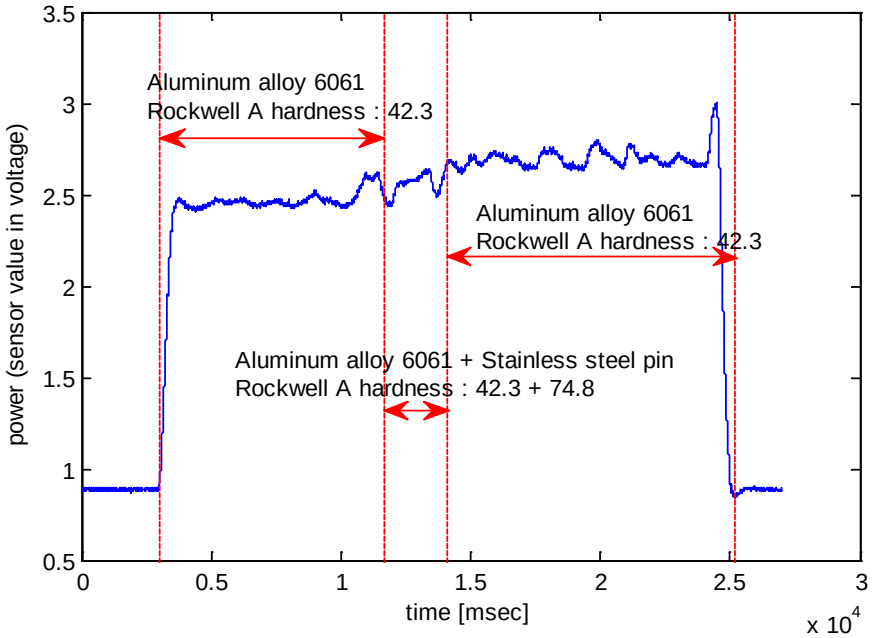

Figure 5-17. Measured cutting power (sensor value in voltage) on SyiL C6B for spindle speed = 1000 rpm, a = 1 mm, f_r = 0.1 mm/rev and workpiece diameter = 24 mm (workpiece C)

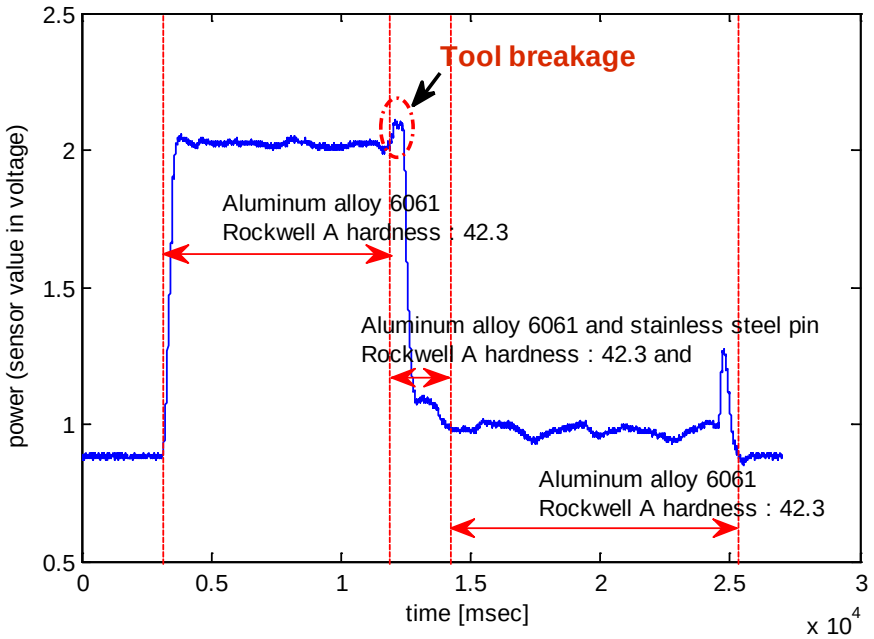

Figure 5-18. Measured cutting power (sensor value in voltage) on SyiL C6B for spindle speed = 1000 rpm, a=1 mm, f_r = 0.1 mm/rev and workpiece diameter = 22 mm (workpiece C)

CHAPTER 6
FLANK WEAR MODEL FOR WORKPIECE COMBINED FROM DIFFERENT HARDNESS MATERIALS

During metal cutting operations, changes in workpiece material properties can cause problems for maintaining the operator's safety, product quality, and machine and tool reliability. Therefore, detecting workpiece material property changes in real-time can be beneficial. In previous chapters, three different types of sensors (power sensor, ultimate thermometer, and dynamometer) were tested for feasibility to detecting workpiece material changes. Based on the results from chapter 5, a power sensor can be used for detect the workpiece material property changes with cost and installation advantages compared to dynamometer. In this research, the noninvasive, low-cost power sensors offer a feasible option for in-process metrology of turning operations.

The final goal of this research is to develop the flank wear model based on power measurement to predict tool wear of tool even though workpiece hardness changes during the process. In this chapter, an adaptive real-time flank wear model will be proposed. How to validate the suggested model will be described. An experimental plan to find flank wear rates of different materials that can be used even if the workpiece has different materials will be described.

6.1 Adaptive Real-Time Flank Wear Model for Workpiece Hardness Changes

The goal is to design the real-time flank wear model using a power sensor in turning operations to improve productivity and reduce tool wear. Generally, flank wear can be determined by using cutting conditions, but if workpiece hardness is variable, and the variation in the hardness cannot be measured, the current flank wear model cannot be predicted accurately without workpiece hardness estimation. There have

been flank wear model research projects studying uniform single material workpieces. In this project, a power sensor will be used to measure the spindle power during cutting of materials with variable hardness. High hardness material cutting should require more power than low hardness material cutting. A power model for workpiece material will be used to detect workpiece material property changes. Based on the power model, flank wear rate should be changed when workpiece material changes in hardness.

The flank wear progression can be predicted accurately using the abrasive wear model with the identified wear characteristic constants and the identified initial wear. Currently, the flank wear model is limited to a workpiece with one material of uniform properties. An adaptive flank wear model will be proposed in this project. Workpiece material properties such as hardness can be predicted by using power sensor. Workpiece material properties will be updated in real time, and the adaptive flank wear model will also be implemented in real time. The adaptive real-time flank wear scheme is shown in Fig. 6-1.

6.2 Experimental Plan

Experiments were designed to obtain the wear rate for two different materials and validate that the proposed real-time adaptive flank wear model is effective.

The flank wear progress can be predicted by Eq. (3-25). In the case of a specific cutting condition, the terms $C_1\sigma_f$, $-\frac{C_2}{\theta_f}$, and $\left(\frac{1}{\tan\gamma}-\tan\alpha\right)V$ are constants. Therefore, the wear rate can be expressed a constant for fixed a cutting condition. The flank wear rate of Eq. (3-25) can be given by the following equation:

$$\frac{dV_B}{dt} = D \text{ (under specific cutting condition)} \tag{6-1}$$

where D is the constant for a specific cutting condition. The experimental plan for obtaining the wear rate was designed in order to calibrate, by an inverse approach, the wear models based on abrasion mechanisms. Two different materials were used for workpieces, one is a soft steel (8620 alloy steel) and the other is hard (P20 tool steel), both with an initial diameter equal to 18.8 mm. The Rockwell hardness A values of both materials were measured with Wilson Hardness tester and will be mentioned in the following chapter. A TCMT32.52 carbide tool was used for almost all tests as the default tool. A TCMT32.52 carbide tool is low quality, low cost, not coated, and wears fast. In this experiment, four different sequence of workpiece materials (soft, hard, half-half, and mainly soft) were used. The workpiece shapes are shown in Fig. 6-2. In cases of soft, hard, half-half, the flank wear was measured every 60 seconds cutting. In case of mainly soft, the flank wear was measured every 84 seconds of soft material cutting and 36 seconds of hard material cutting. The 60 seconds cutting is one pass of 50 mm length of workpiece, 84 seconds cutting is one pass 70 mm length workpiece, and 36 seconds cutting is 30 mm length workpiece cutting under 50 mm/min feedrate. All cutting were continued until total cutting length is 1000 mm or major tool breakage appeared. For this total cutting length, the wear rate can be considered stationary and, therefore, not dependent on the cutting time. Furthermore, in order to increase wear phenomena and temperature, no lubricant was used during the tests.

The wear tests were performed according to the cutting conditions as shown in Table 6-1. The flank wear was measured by a USB-type digital microscope (model: Dino-Lite AM413T). The AM413T digital microscope is designed with a 1.3 megapixel image sensor. The possible magnifications of the microscope range from 10X to 230X.

In this project, a 210X magnification was used for capturing the images. Microscope specifications are shown in Table 6-2.

In this research, cases soft and hard were designed to obtain the wear rate Ds for each material. Cases half-half and mainly soft were performed to validate the proposed real-time adaptive flank wear model. Therefore, four different hardness sequences of workpieces under same cutting conditions were implemented. The workpiece of case soft is 18.8mm diameter cylindrical shape of 8620 alloy steel. The workpiece of case hard is P20 tool steel of the same dimensions. The workpiece of case half-half has the sequence of the same lengths (50 mm for each) of soft and hard materials. The workpiece of case mainly soft is long, soft metal cutting and short, hard metal cutting. For this, a special workpiece was made which includes 70 mm of soft metal combined with 30 mm of hard metal. All cutting test were performed under 1000 rpm spindle speed, 50 mm/min feedrate, 1 mm depth of cut as shown in Table 6-1.

To create the fast flank wear, a low quality non coated carbide tool was used. For repeatability of the flank wear rate, the consistency of tool is very important. In order to reduce the impact of tool differences, additional cases of tests were performed where the three different cases are machined with one insert as “single insert” wear tests. A TCMT32.52 carbide tool has three edges that can be used for cutting. The first edge was used for cutting a soft workpiece. The second edge was used for cutting a hard workpiece and the third edge was used for cutting the half-half workpiece. A C-5 carbide insert from McMaster was used for single insert wear test for the progression of different tool wear. C-5 carbide insert is excellent in heat resistance and wear resistance. In C-5 carbide insert, three different edges of tool were used for cutting three different types of

workpiece sequence (soft, hard, and half-half). These two single insert cutting tests were performed as described table 6-3.

The measured flank wear was compared to the estimated flank wear by proposed adaptive flank wear model (Eq. 3-27). All experiments were performed two or three times for verification of the repeatability.

Table 6-1. Cutting conditions in wear tests

Case	Tool	Workpiece material sequence	Depth of cut	Feedrate	Workpiece diameter	Lubrication
soft	TCMT 32.52 carbide	8620 alloy steel	1 mm	50 mm/min	18.8 mm	Dry
hard		P20 tool steel				
halt-half		50 mm 8620 alloy steel and 50 mm P20 tool steel				
mainly soft		70 mm 8620 alloy steel and 30 mm P20 tool steel				

Table 6-2. Digital microscope specification

Model	AM413T-Dino-Lite Pro
Basic Specifications	
Interface	USB2.0
Product Resolution	1.3M pixels. (SXGA)
Magnification Rate	10x~50x-230x
Sensor	Color CMOS
Frame rate	up to 30fps
Image Format	jpg, bmp, avi
Microtouch	Yes
LED Switchable (via DinoCapture)	Yes
Measurement Function (via DinoCapture)	Yes
Calibration Function (via DinoCapture)	Yes
Software	Windows Vista, XP, 2000, or Windows Server 2003 MAC OS (Microtouch function no supported)
Unit Weight	90(g)
Units Dimension	10cm (H) x 3.2cm (D)

Table 6-3. Cutting conditions in single insert tests

Tool	Edge	Workpiece material sequence	Depth of cut	Feedrate	Workpiece diameter	Lubrication
TCMT32.52 carbide	1	8620 alloy steel	1 mm	50 mm/min	18.8 mm	Dry
	2	P20 tool steel				
	3	50 mm 8620 alloy steel and 50 mm P20 tool steel				
C-5 carbide	1	8620 alloy steel				
	2	P20 tool steel				
	3	50 mm 8620 alloy steel and 50 mm P20 tool steel				

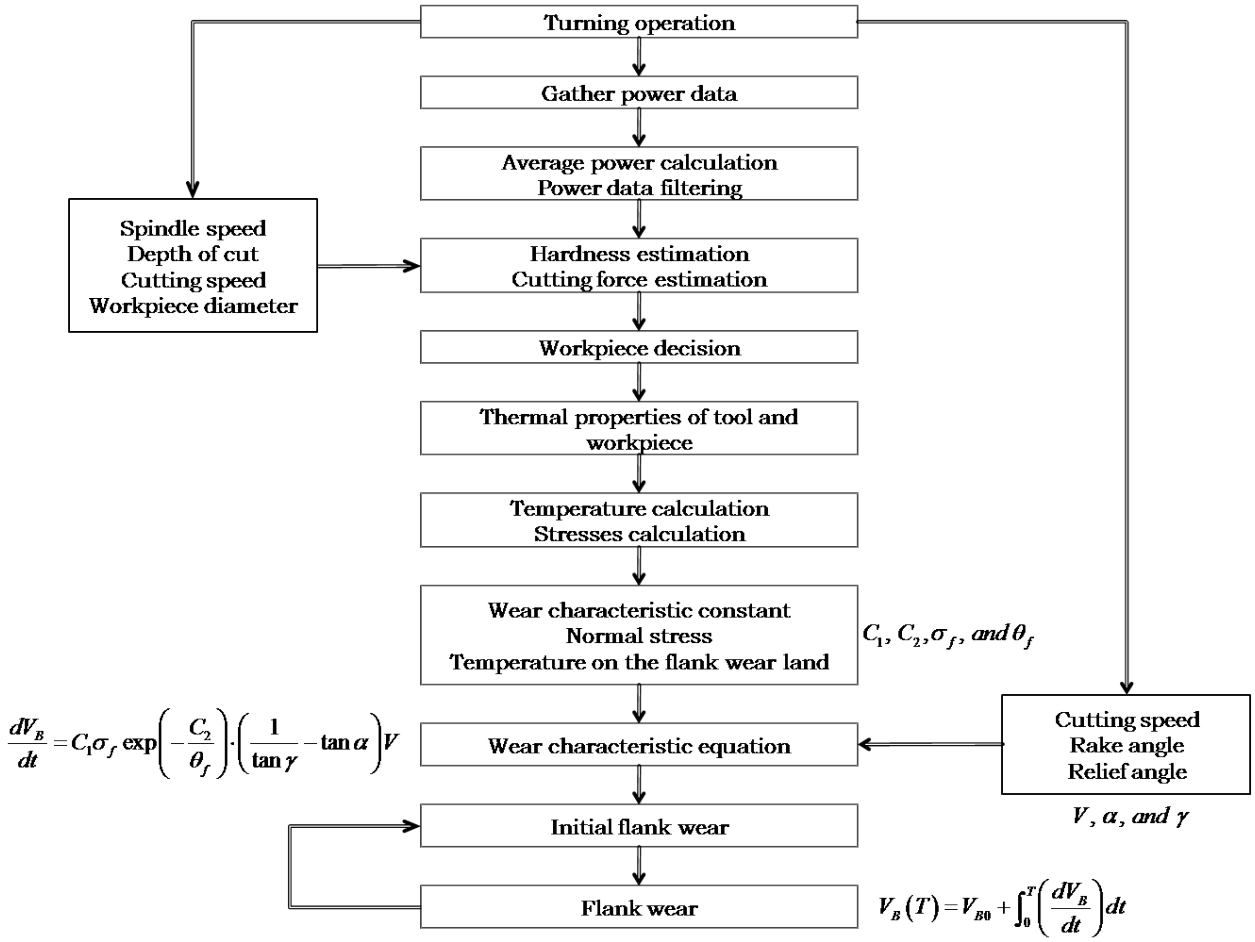

Figure 6-1. Real time flank wear estimation model scheme

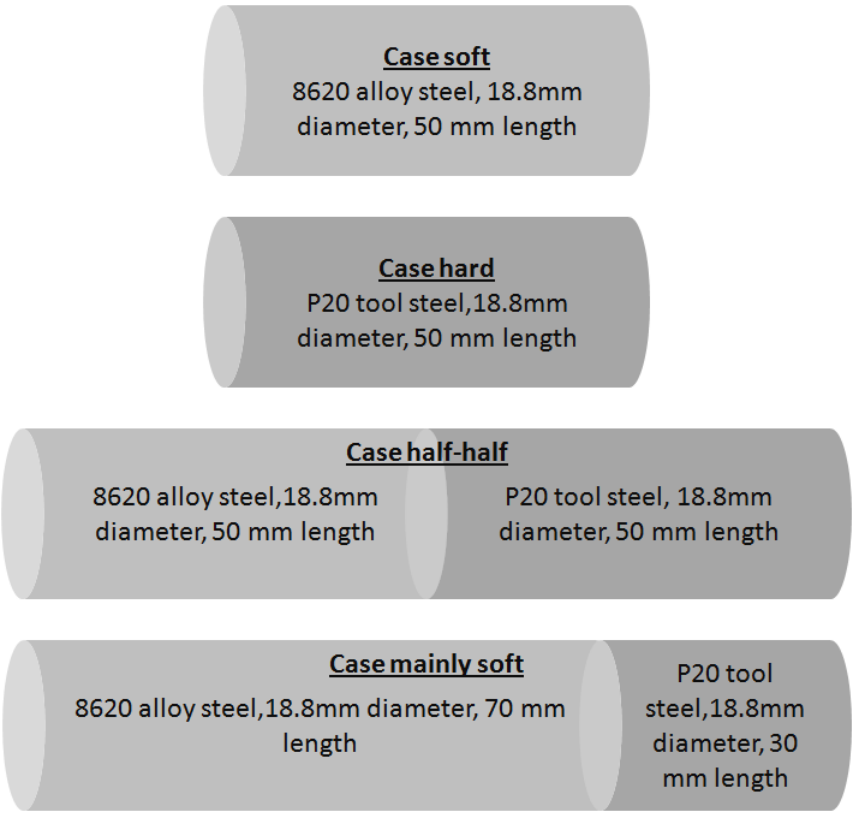

Figure 6-2. Workpiece shapes for validation

CHAPTER 7
RESULT OF FLANK WEAR MODEL FOR WORKPIECE COMBINED WITH TWO DIFFERENT HARDNESS MATERIALS

In previous chapter 6, the experimental plan to test the flank wear model for workpieces consisting of different hardness materials was described. In chapter 7, the experimental cutting test result will be presented the possibilities of the proposed flank wear rate model discussed. The proposed flank wear rate model will be demonstrated with power sensor what was tested in chapter 5.

7.1 Hardness Measurement of 8620 Alloy Steel and P20 and Flank Wear Images

A Wilson Rockwell hardness tester model 3JR was used to measure the workpiece hardness using the Rockwell A scale. Figure 7-1 shows the Rockwell hardness tester and specifications of the tester are shown in Table 7-1. Two different materials were used in the cutting tests. One is the 8620 alloy steel as the soft metal and another is the P20 tool steel as the hard metal. Chemistry data of these two materials are shown in table 7-2. To confirm the material hardness difference, the Rockwell hardness A values of 8620 alloy steel parts (122 parts) and P20 tool steel parts (77 parts) were measured and these values are shown in Fig. 7-2. The mean value of Rockwell hardness A of 8620 alloy steel is 42.44 and the mean value of Rockwell hardness A of P20 is 53.23. The standard deviations were 1.87 and 2.10 respectively. Figure 7-3 shows the box plots with whiskers of both materials. As shown in Fig. 7-3, the 8620 alloy steel and P20 tool steel materials have significantly different Rockwell hardness A value.

To measure the flank wear, images were captured by using the USB portable microscope with 210X magnification. The program Dino Capture provided with the Dino-

Lite was used for capturing and measurement the length of flank wear. Figure 7-4 shows flank wear images of case soft. Each image was taken after 50 mm cutting of workpiece.

7.2 Flank Wear Measurement

All cutting experiments were performed under cutting conditions of 50 mm/min feedrate, 1mm depth of cut, and 1000 rpm spindle speed (equivalent to a cutting speed of 55.92 m/min). All workpieces were 18.8 mm diameter cylindrical shape. During the cutting, the power was measured by using the power sensor. The original diameter was recorded and the machined diameter was recorded to check the dimension of product. Case hard is P20 tool steel cutting. After every 50 mm cutting, an image of the flank wear surface was taken by USB portable microscope. Case hard was repeated 3 times. Figure 7-5 shows the flank wear versus cutting length. As shown in Fig. 7-5, after break-in period, the flank wear has constant wear rate in case hard 1 and 2. But in case hard 3, the break-in period is longer than the other cases.

The cutting of the case soft was under same cutting conditions the as case hard. After every 50 mm cutting, an image of the flank wear surface was taken by USB portable microscope. All cutting conditions and measurement were same as case hard. The only difference was that workpiece material was not P20 tool steel, but 8620 alloy steel as soft metal. Figure 7-6 shows the flank wear versus cutting length of three case soft cutting experiments. As shown in Fig. 7-6, after break-in period, all flank wear has constant wear rate. In theory, the wear rate should be same if all cutting conditions are the same. As seen in Fig. 7-6, case soft 1 and 2 had almost the same slope, but the

case soft 3 had a different slope. Tool differences may be one of the reasons why the wear rates are different.

The cutting conditions of the case half-half were the same as the previous cases. But workpiece consisted of the two different materials, a combination of 8620 alloy steel and P20. After 50 mm of 8620 alloy steel cutting, 50 mm cutting of P20 was cut. This cutting sequence was repeated until cutting was stopped. Figure 7-7 shows the flank wear of case half-half. The slope of flank wear for hard metal cutting should be higher than the slope of flank wear for soft metal cutting. As seen in Fig. 7-7, the slope of the period of P20 tool steel cutting (red color background) is higher than the slope of the period of 8620 alloy steel cutting (white color background).

The cutting conditions of the case mainly soft were the same as the previous cases. But the workpieces consisted of 70 mm of 8620 alloy steel and 30 mm P20 tool steel. This cutting sequence was repeated. Figure 7-8 shows the flank wear of case mainly soft. The slope of flank wear for hard metal cutting should be higher than the slope of flank wear for soft metal cutting. As seen in Fig. 7-8, the slope of the period of P20 tool steel cutting is higher (red color background) than the slope of the period of 8620 alloy steel cutting (white color background).

In the case single tool, three different cutting tests were performed with only one insert. All tool edges were used in three different types of cutting. The first edge was used for 8620 alloy steel cutting (case soft), the second edge was used for P20 tool steel cutting (case hard), and the third edge was used for combined workpiece of 8620 alloy steel and P20 tool steel cutting (case half-half). Figure 7-9 shows the flank wear of the three different tool edges when using a TCMT32.52 carbide tool. Bottom of Fig. 7-9

shows the flank wear of case half-half. Red color background is P20 tool steel cutting. Figure 7-10 shows the flank wear of the three different tool edges when cutting with C-5 carbide tool. Bottom of Fig. 7-10 shows the flank wear of case half-half. The red color background is P20 tool steel cutting. As shown in Figures 7-8 and 9, each flank wear rate if workpiece is combined of 8620 alloy steel and P20 tool steel is almost same as workpiece is one material.

7.2 Flank Wear Rate between 8620 Alloy Steel and P20

If cutting conditions are the same, the flank wear rate should be constant in constant wear rate zone (phase II in Fig. 3-5) between break-in period and rapid wear to failure. Figure 7-11 shows that flank wear rate versus Rockwell A hardness from the case soft and hard data. Bad data was eliminated using Chauvenet's criterion (Huggins 1975). The critical boundary for rejection of data must be specified by the researcher prior to conducting the experiment. The approach recommended herein is to accept as valid all data values, X_i, which fall between the critical limits X_l and X_u such that:

$$P\{X_l < X_i < X_u\} = 1 - \frac{1}{kN} \tag{7-1}$$

where N is sample number and k is a constant specified by researcher. A common approach, known as Chauvenet's criterion, is to let k equal 2. Table 7-3 shows the probability levels and the range of acceptable data. As mentioned previously, the tool difference may impact the flank wear rate. In the research reported in this dissertation, a TCMT32.52 carbide was used mainly. A TCMT32.52 is low cost and uncoated tool. Figure 7-12 shows the flank wear surface of two different new inserts. As shown in Fig. 7-12, the consistency of tool is very poor in the pattern of surface. In statistics, analysis

of variance (ANOVA) is a collection of statistical models, and their associated procedures, in which the observed variance in a particular variable is partitioned into components due to different sources of variation. To check the effects of tool and hardness, ANOVA was performed on the data of all tool edges, hardness, and flank wear rate. Fact 1 is tool edge number and fact 2 is workpiece materials (8620 alloy steel or P20 tool steel). As seen in Fig. 7-13, fact 1 (tool edge number) has the probability of F-value of 0.001%, enough to conclude statistical significance. But workpiece effect is not big (the probability of F-value of 17.2%). Predictive Analytics Soft Ware (PASW) from SPSS Inc. was used for analyzing the data.To reduce the dominating effect of tool over workpiece the case single tool will be analyzed next.

When a workpiece combines different materials, the cutting period for each material should have specific own flank wear rate. The flank wear rate in intervals of 8620 alloy steel was compared with the flank wear rate in intervals of P20. As to be predicted, the flank wear rate of hard material is higher than soft material. As shown in Fig. 7-15~18, flank wear rate of soft material cutting section is lower than flank wear rate of hard material cutting section. Correlation coefficient r values also show that flank wear rate is increased as the hardness increases even though workpiece materials are periodically changed. Figure 7-14 shows the one way ANOVA for case half-half. The fact is workpiece material. As shown in Fig. 7-14, flank wear rates of 8620 alloy steel and P20 tool steel are different (the probability of F-value of 0%) if the tool is not changed.

Theoretically, the flank wear rate should only depend upon the material hardness and the wear during case half-half and mainly soft should be same as flank wear rate

during the corresponding case hard and case soft. According to the results of the cutting tests, the flank wear rate was constant under same tool, but flank wear rate has different constants with different tools. This result may be caused by inconsistent tool quality. The case single tool was designed to reduce the impact caused by tool difference. Figure 7-19 and 20 show flank wear rates, which are the empty circle symbol as the flank wear rate if only 8620 alloy steel is cut, the empty triangle symbol as flank wear rate if only the P20 tool steel is cut, the solid circle symbol as flank wear rate of 8620 alloy steel section of case half-half (combined 50 mm length 8620 alloy steel and 50 mm length P20 tool steel), and solid triangle symbol is flank wear rate of P20 tool steel section of case half-half. From the result of case single tool, the flank wear rates are maintained when workpiece was a combination of two different materials.

7.3 Flank Wear Estimation Using Power

If tools are perfectly same with same cutting conditions, flank wear rate should be same in the stable wear increasing range. Previously, each flank wear rate of different materials has the same in same material with one insert. To minimize the effect of tool, the case single tool was performed. In case single tool, the flank wear rates in case soft and hard were maintained same as the rates case half-half. A power sensor was used for detecting material changes. Figure 7-21 shows an example of cutting power (sensor value) during 8620 alloy steel cutting of case single tool cutting. The average power value of stable cutting range was recorded and compared to hardness and flank wear rate. Figure 7-22 shows the hardness versus flank wear rate (case single tool C-5). The relationship between hardness and flank wear rate is linear as shown in Fig. 7-22. As shown in Fig. 7- 23, the relationship between hardness and average cutting power is

also linear. Therefore, the average cutting power can be used for detecting the material property changes instead of hardness measurement (see Fig. 7-24). In case of single tool C-5, estimated flank wear rates can be calculated by

$$\mathrm{FWR} = 0.39 \times \mathrm{AP} - 0.2 \tag{7-2}$$

where $\mathrm{FWR}\ (mm/m\ \text{cutting length})$ is estimated flank wear rate and $\mathrm{AP}\ (\text{sensor value})$ is average cutting power which is from case soft and hard of single tool C-5. Figure 7- 25 shows the relationship between average power and flank wear rate.

Flank wear estimation for fixed cutting conditions as everything is same except the workpiece materials will be following steps:

Step 1: Power measurement and average power calculation for specific time (for example 1 sec)

Step 2: Flank wear rate decision from average power

Step 3: Flank wear estimation from multiple by cutting length and flank wear rate

Step 4: Update the flank wear and repeat the process step 1~4 again

During cutting of two different materials as case single tool, flank wear can be estimated by summation of each workpiece section with flank wear rate decided using power value as shown in Fig. 7-26.

Figure 7-27 shows the difference between flank wear captured by microscope and estimated flank wear from Eq. (7-2). Figure 7-28 shows the difference of flank wear rate (mm/m cutting length) during 50 mm cutting length between flank wear captured by microscope and estimated flank wear from Eq. (7-2). Initial length of estimated flank wear was the same as flank wear after first 50 mm length cut. Since flank wear is update from initial point, the difference between flank wear and estimated flank wear

can be increased after long cutting length. If initial flank wear can be update after specific cutting length, it is possible to estimate flank wear accurately without many times of flank wear measurement.

Table 7-1. Specification of Wilson Rockwell hardness tester model 3JR

Tests Rockwell Scales	A,B,C,D,E,F,G,H,K,L,M,P,R,S & V
Maximum Vertical Gap	8"
Throat Depth	5-1/4"
Overall Dimensions	13" x 20" x 28" Tall

Table 7-2. Chemistry data of P20 tool steel and 8620 alloy steel

	P20 tool steel	8620 ALLOY STEEL
Carbon	0.28 - 0.4	0.18 - 0.23
Chromium	1.4 - 2	0.4 - 0.6
Iron	Balance	Balance
Manganese	0.6 - 1	0.7 - 0.9
Molybdenum	0.3 - 0.55	0.15 - 0.25
Phosphorus	0.03 max	0.035 max
Silicon	0.2 - 0.8	0.15 - 0.35
Sulphur	0.03 max	0.04 max
Nickel		0.4 - 0.7

Table 7-3. Probability levels and the range of acceptable data of flank wear rates of case hard and soft (Chauvenet's criterion)

	N	probability point $1-\frac{1}{2N}$	t	mean $\overline{X}$	Standard deviation	range of acceptable data $\overline{X} \pm t \cdot s$	
case hard 1	9	0.94	2.1892	0.6953	0.1345	[0.4008	0.9898]
case hard 2	3	0.83	2.1045	0.9573	0.1947	[0.5477	1.3670]
case hard 3	8	0.94	2.2409	1.1415	1.5074	[-2.2364	4.5194]
case soft 1	12	0.96	2.3282	0.4482	0.2408	[-0.1125	1.0088]
case soft 2	18	0.97	2.3681	0.3192	0.1327	[0.0049	0.6335]
case soft 3	22	0.98	2.5176	0.1373	0.0692	[-0.0370	0.3116]

Figure 7-1. Wilson Rockwell hardness tester model 3JR

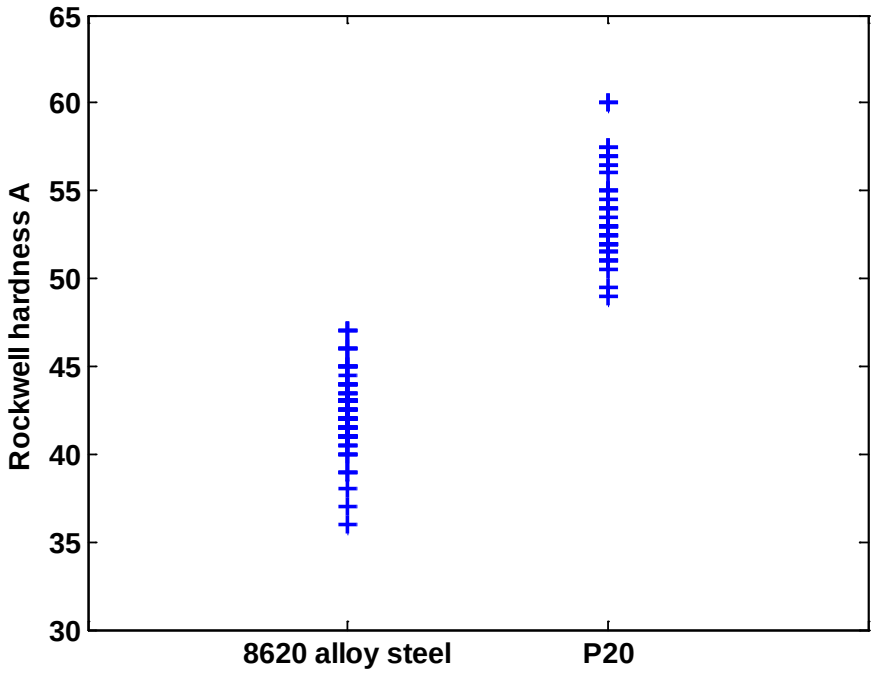

Figure 7-2. Rockwell hardness A of 8620 alloy steel and P20 tool steel workpieces

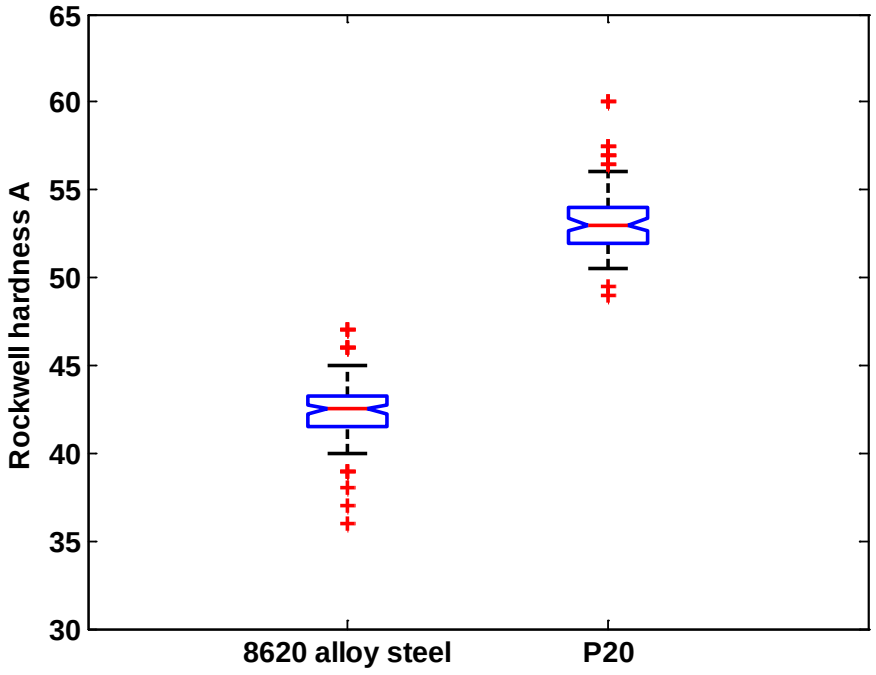

Figure 7-3. Box plots of Rockwell hardness A with whisker of 8620 alloy steel and P20 tool steel workpieces

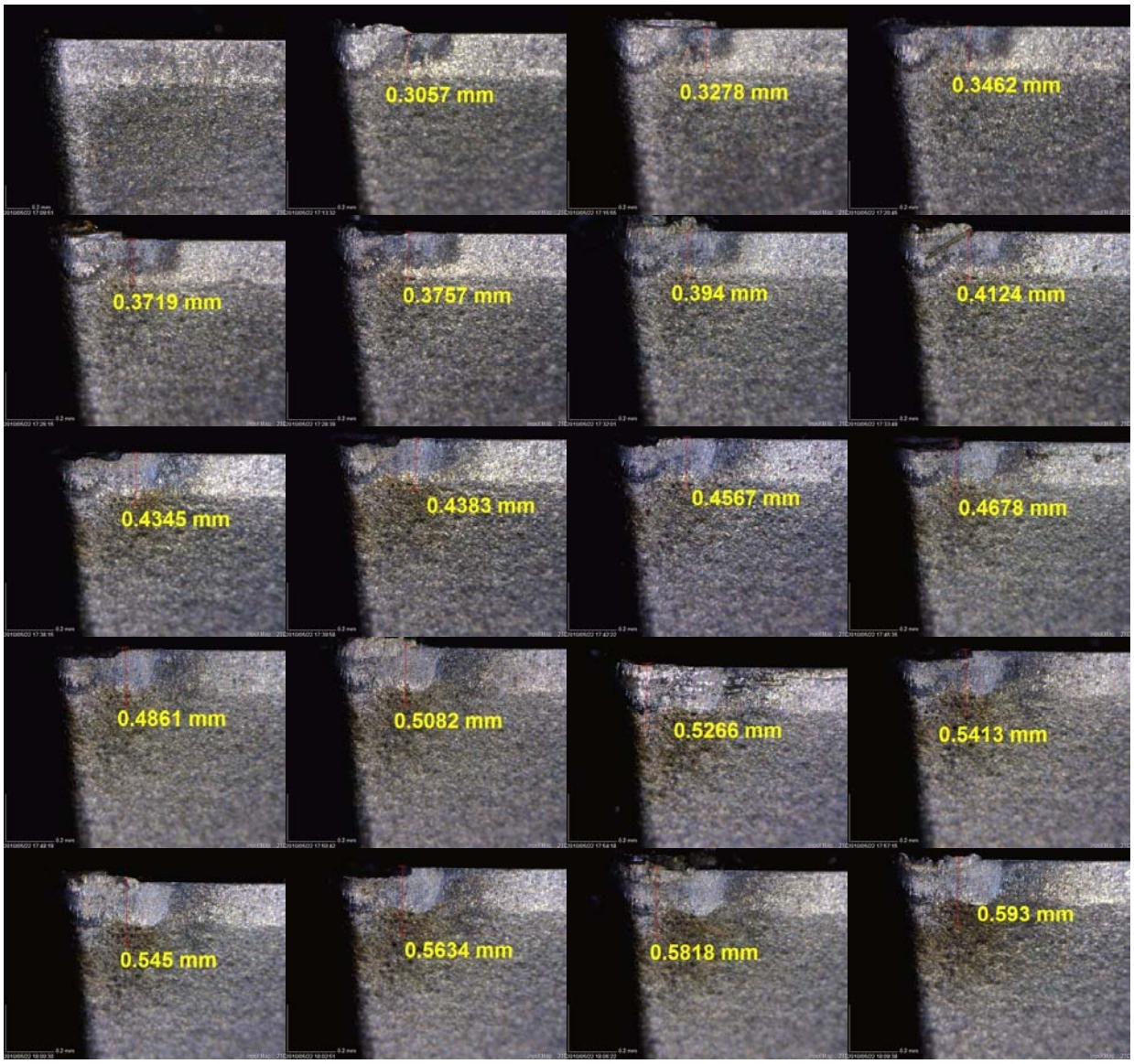

Figure 7-4. Flank wear images of case soft second cutting test by microcope

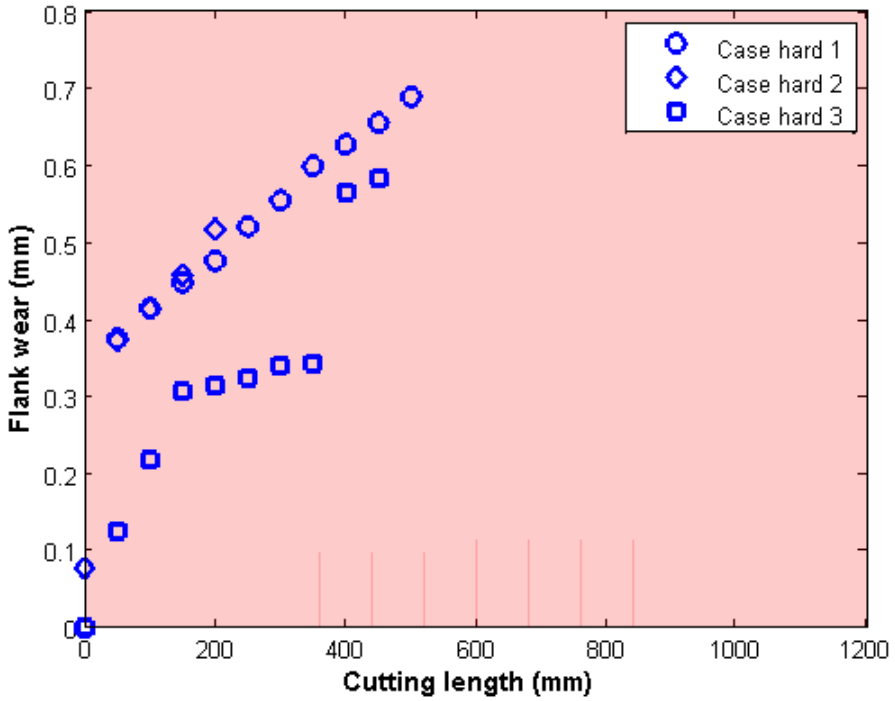

Figure 7-5. Flank wear of case hard

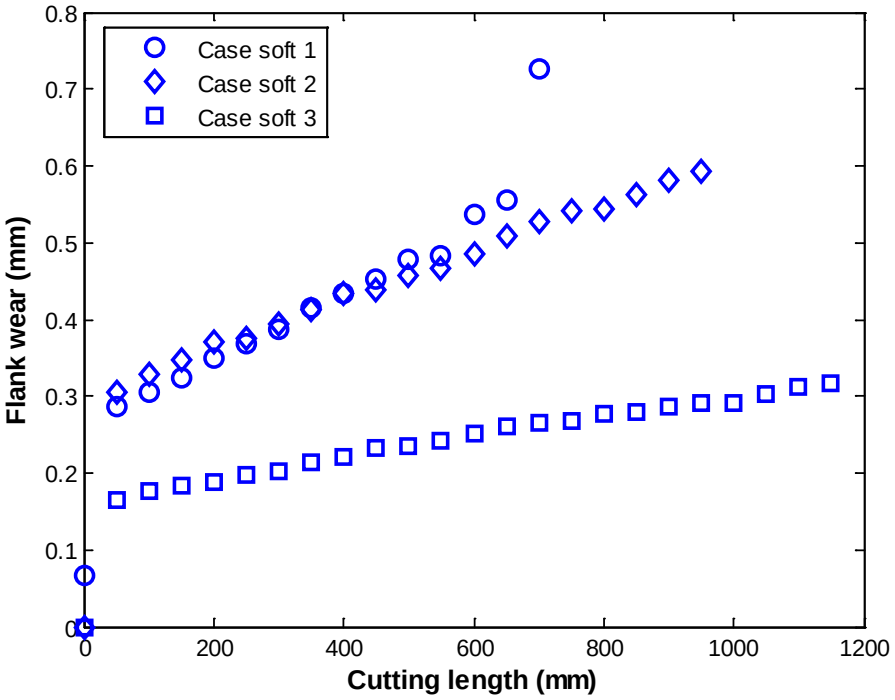

Figure 7-6. Flank wear of case soft

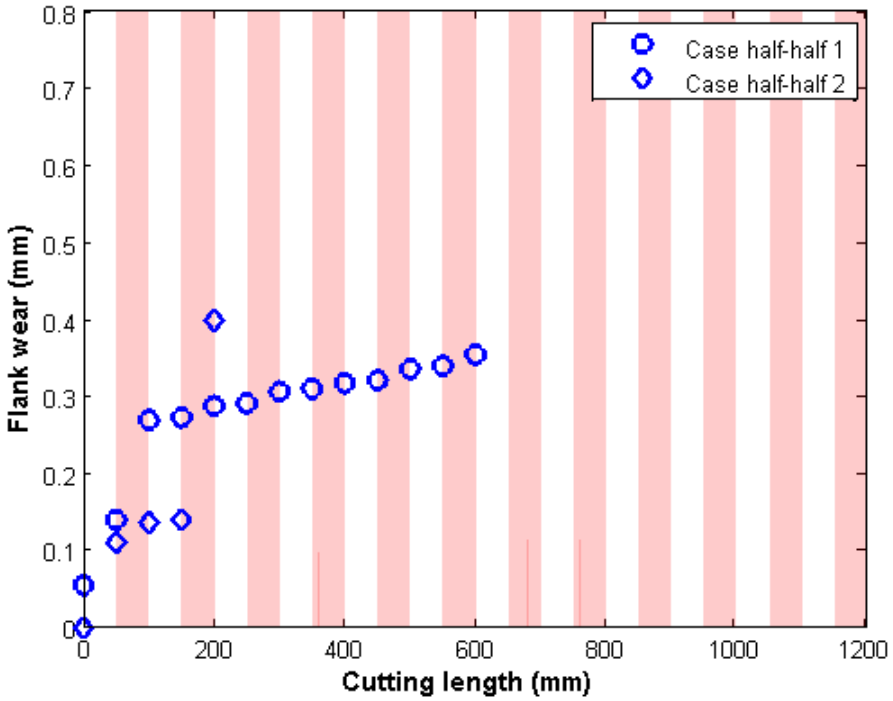

Figure 7-7. Flank wear of case half-half

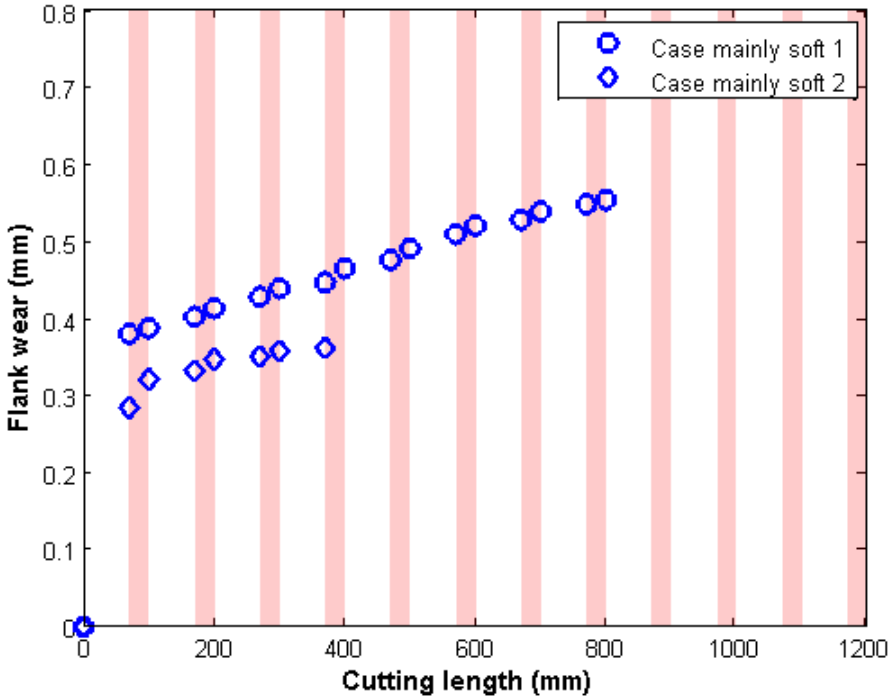

Figure 7-8. Flank wear of case mainly soft

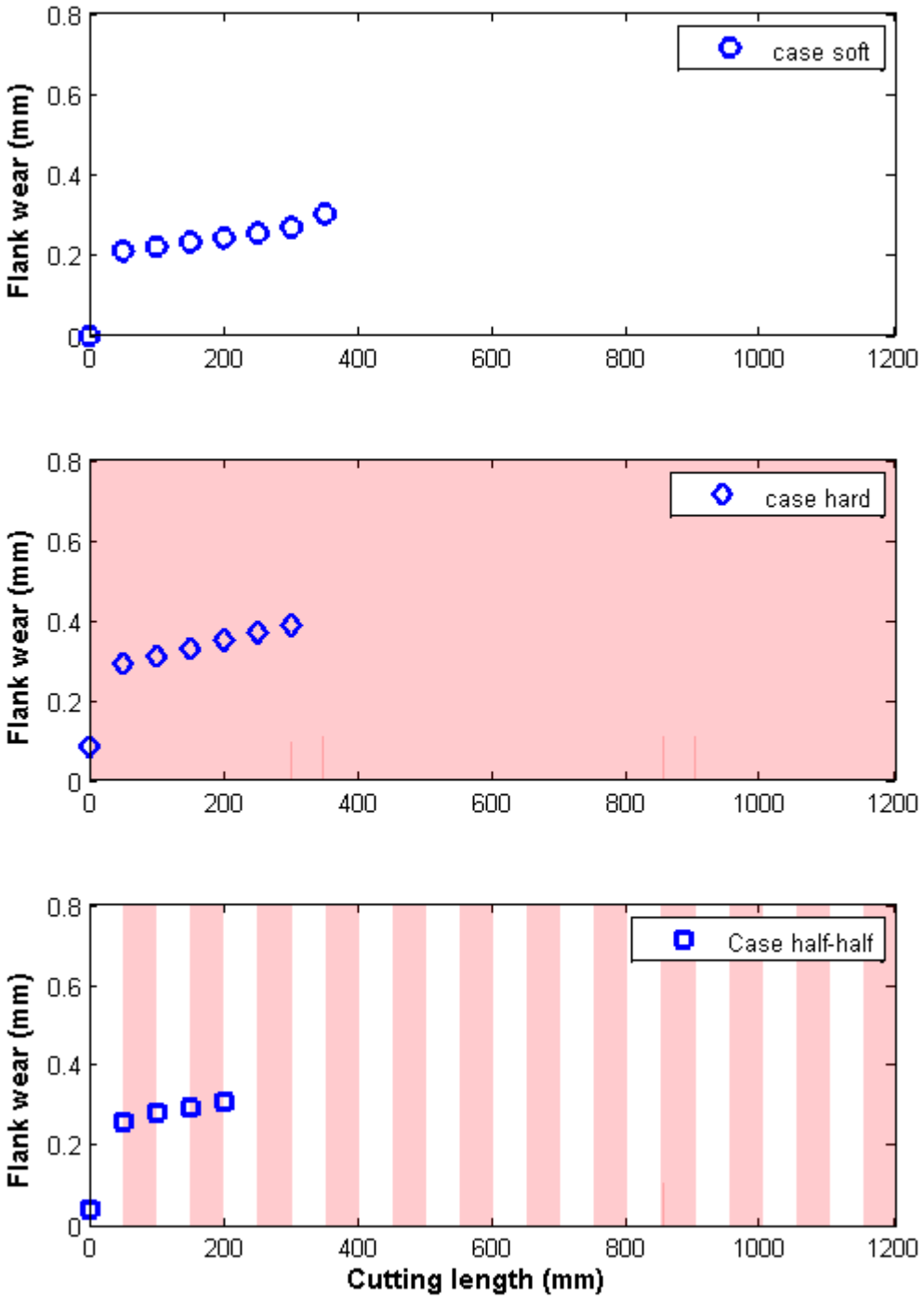

Figure 7-9. Flank wear of case single tool (TCMT32.52 carbide)

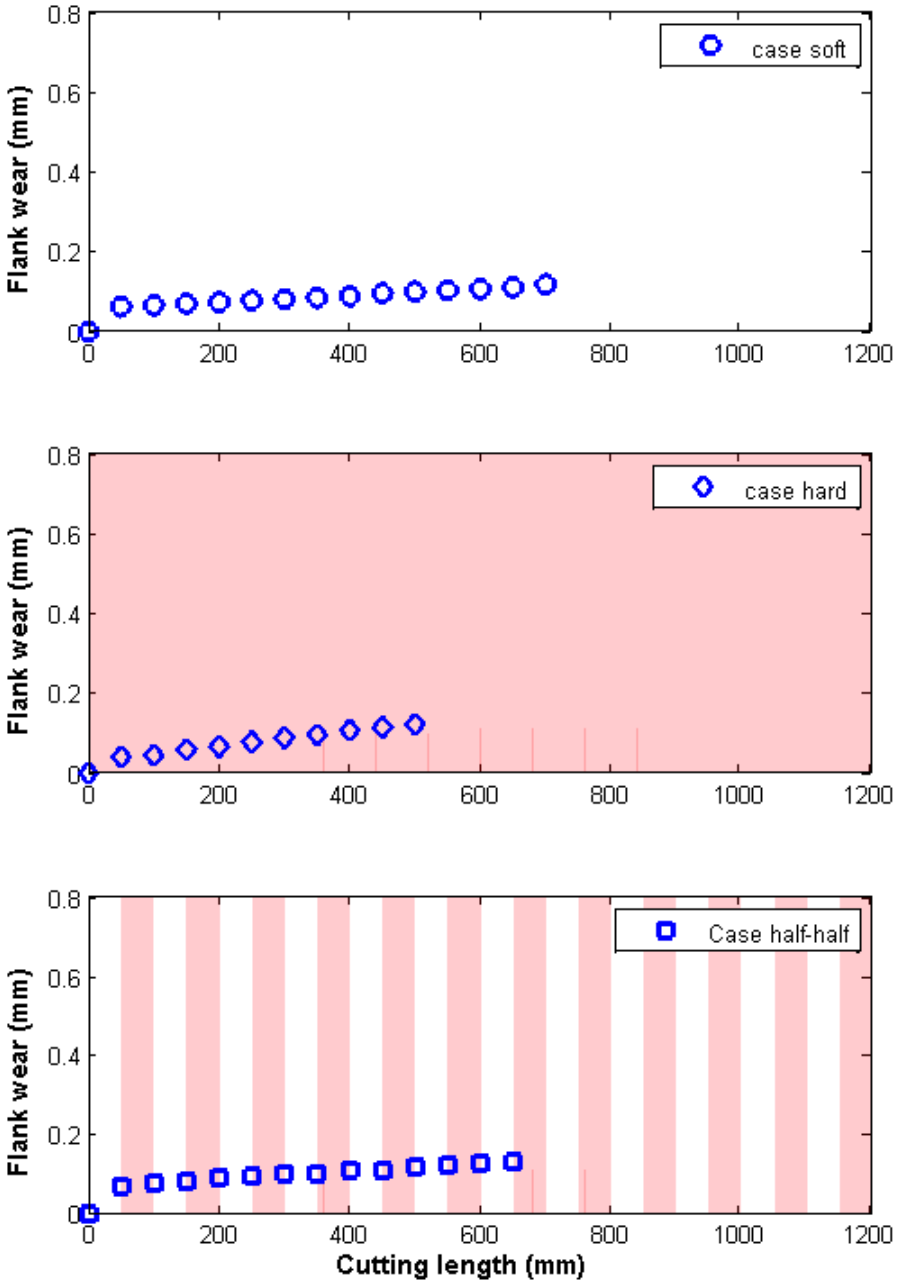

Figure 7-10. Flank wear of case single tool (C-5 carbide)

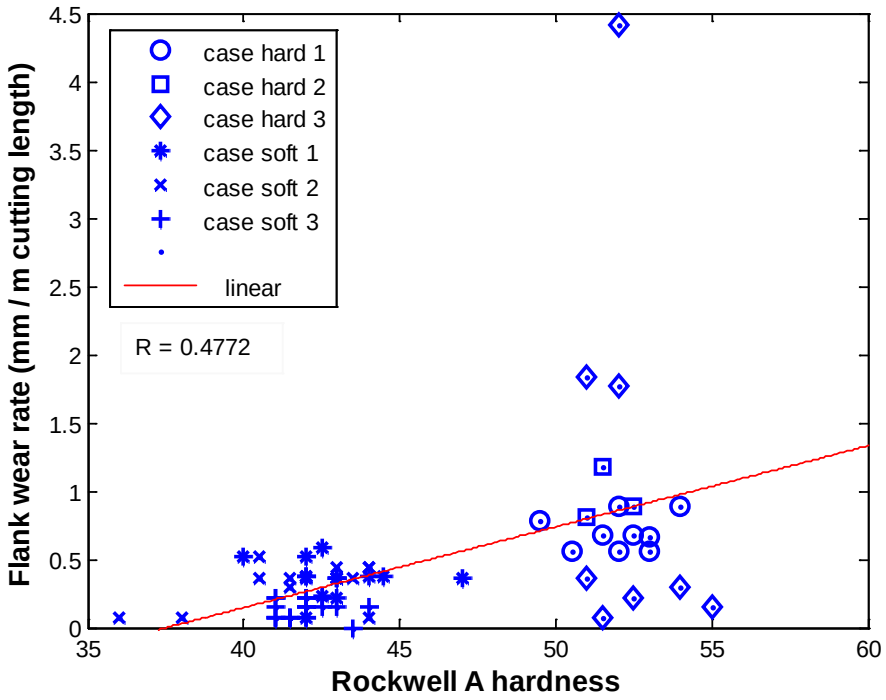

Figure 7-11. Flank wear rate versus Rockwell hardness A

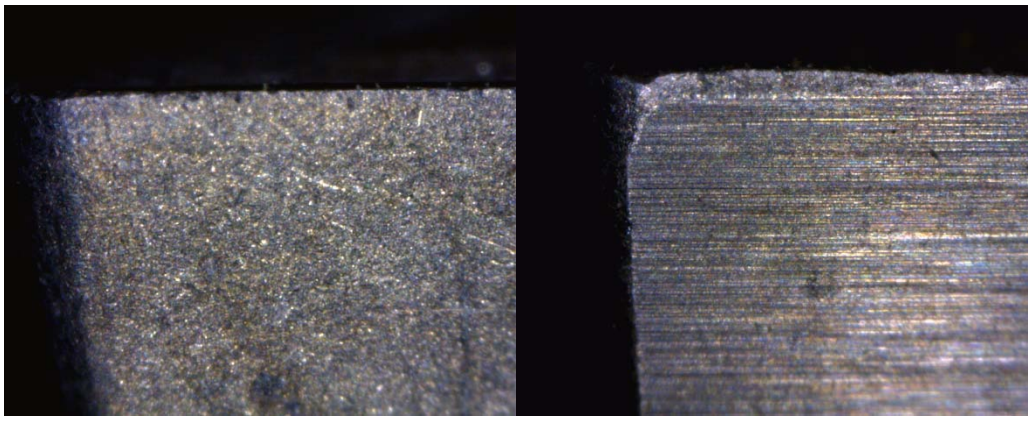

Figure 7-12. Flank wear surface of two different new inserts

Tests of Between-Subjects Effects

Dependent Variable:Flank wear rate

Source	Type III Sum of Squares	df	Mean Square	F	Sig.
Corrected Model	.032[a]	21	.002	2.649	.000
Intercept	.033	1	.033	56.168	.000
Tool	.024	15	.002	2.766	.001
Workpiece	.001	1	.001	1.889	.172
Tool * Workpiece	.002	5	.000	.566	.726
Error	.075	129	.001		
Total	.154	151			
Corrected Total	.107	150			

a. R Squared = .301 (Adjusted R Squared = .188)

Figure 7-13. ANOVA screen shot case soft, case hard, case half-half, and case mainly soft

Tests of Between-Subjects Effects

Dependent Variable:Flank wear rate

Source	Type III Sum of Squares	df	Mean Square	F	Sig.
Corrected Model	.000[a]	1	.000	41.084	.000
Intercept	.001	1	.001	130.391	.000
Workpiece	.000	1	.000	41.084	.000
Error	4.412E-5	8	5.515E-6		
Total	.001	10			
Corrected Total	.000	9			

a. R Squared = .837 (Adjusted R Squared = .817)

Figure 7-14. One way ANOVA screen shot for case half-half (case half-half 1)

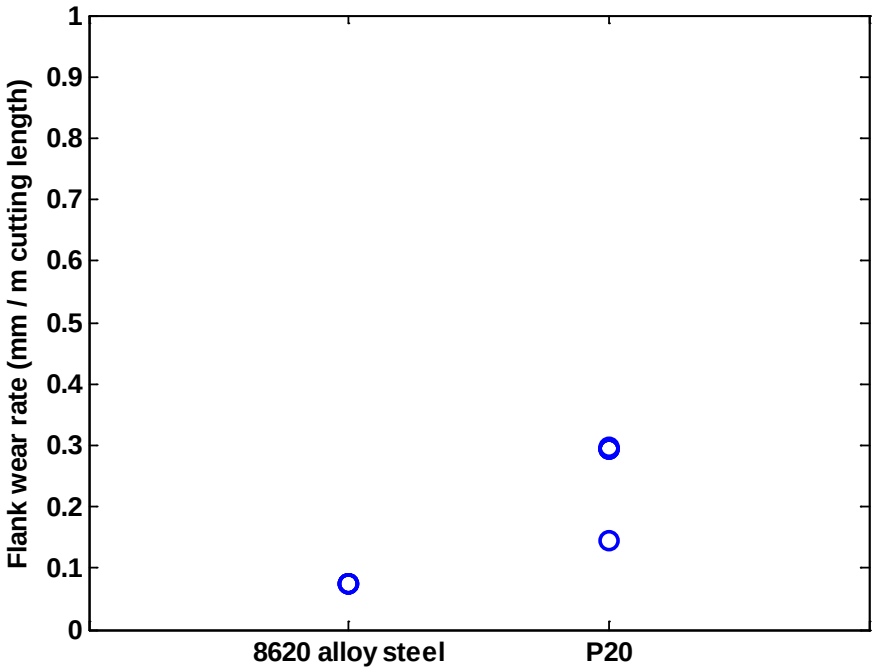

Figure 7-15. Flank wear rate versus workpiece materials (case half-half 1, Correlation coefficient r = 0.9149)

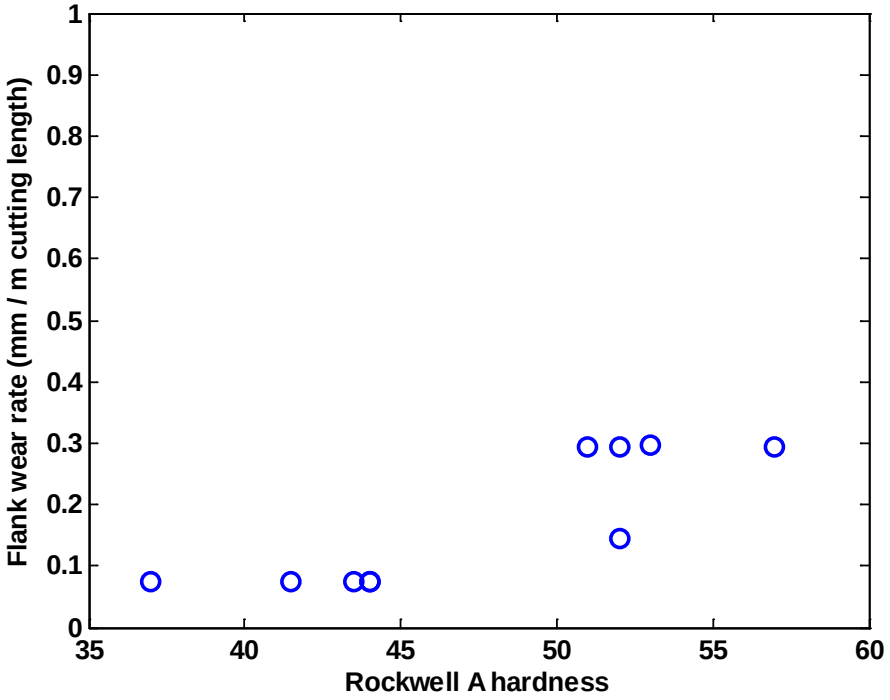

Figure 7-16. Flank wear rate versus Rockwell hardness A (case half-half 1, Correlation coefficient r = 0.8622)

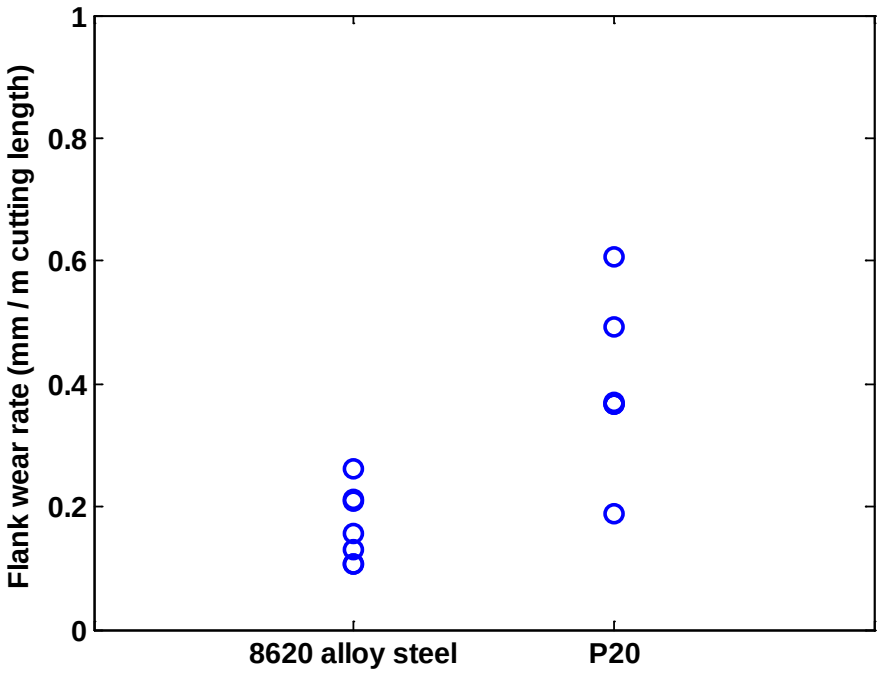

Figure 7-17. Flank wear rate versus workpiece materials (case mainly soft 1, Correlation coefficient r = 0.7706)

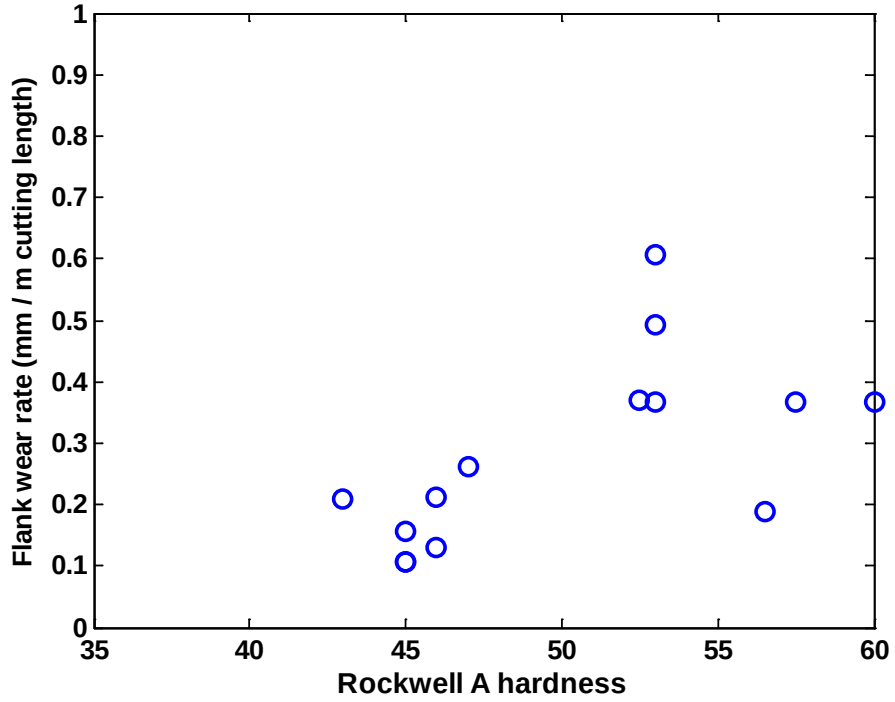

Figure 7-18. Flank wear rate versus Rockwell hardness A (case mainly soft 1, Correlation coefficient r = 0.6249)

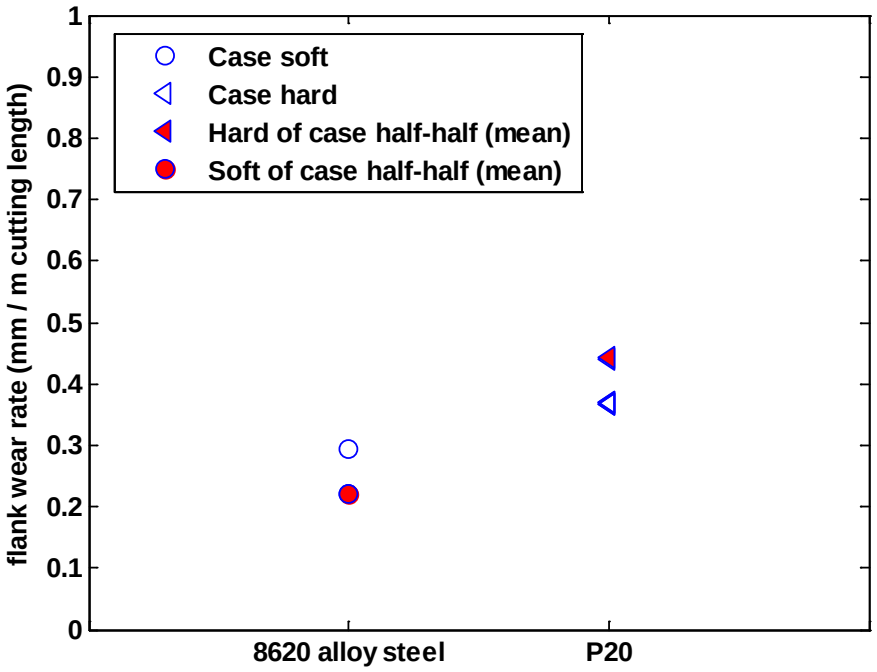

Figure 7-19. Flank wear rate versus workpiece materials (case single tool TCMT32.52 carbide)

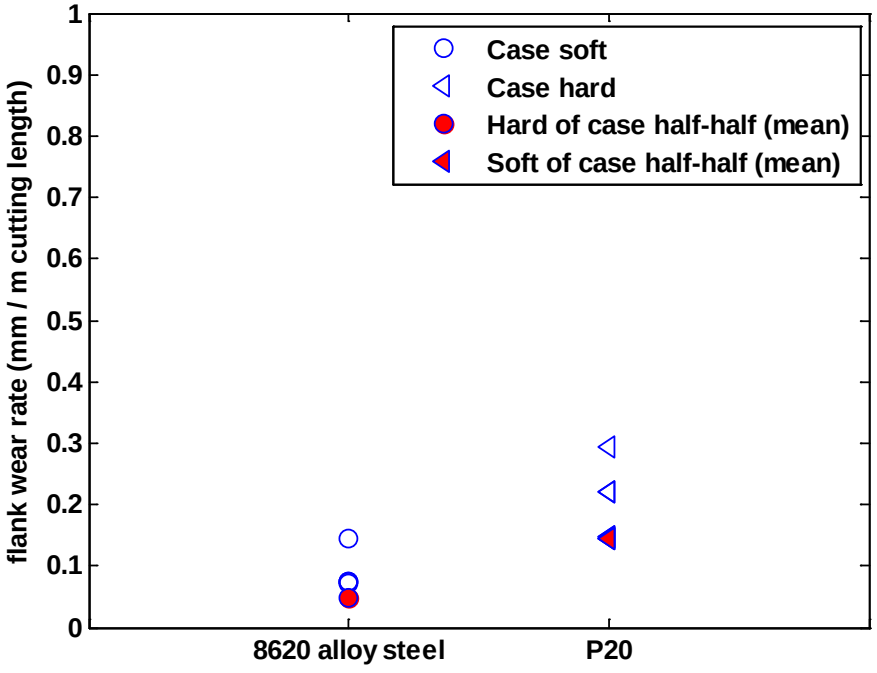

Figure 7-20. Flank wear rate versus workpiece materials (case single tool C-5 carbide)

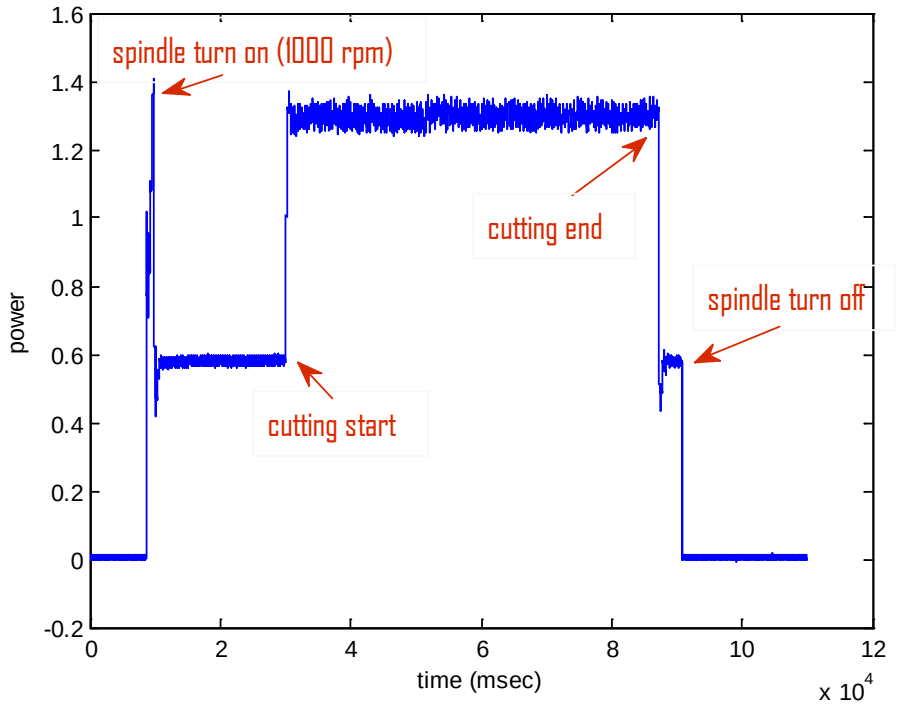

Figure 7-21. Power measurement of 8620 alloy steel cut

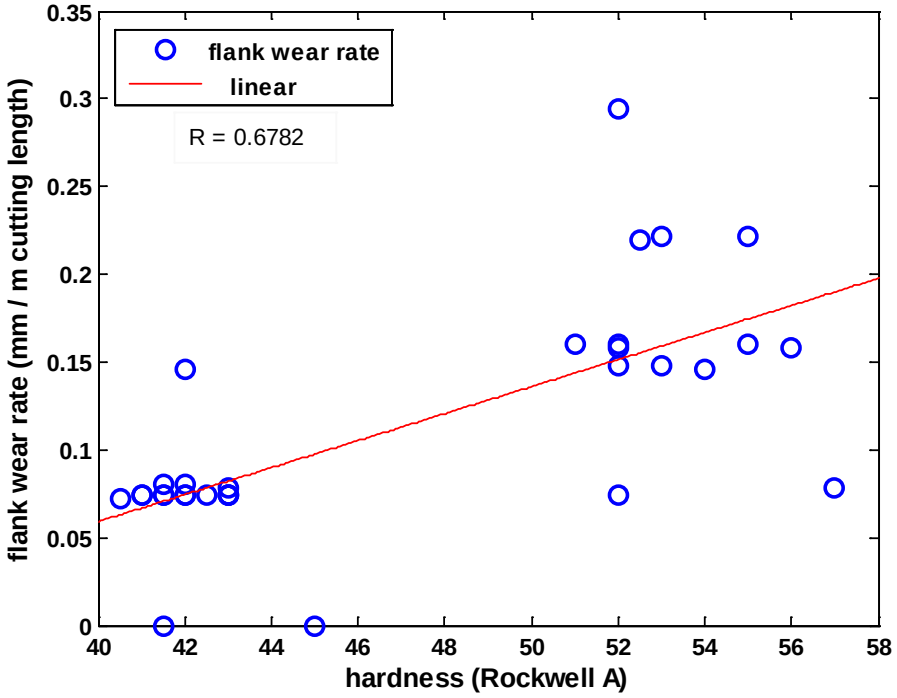

Figure 7-22. Hardness vs flank wear rate (case single tool C-5)

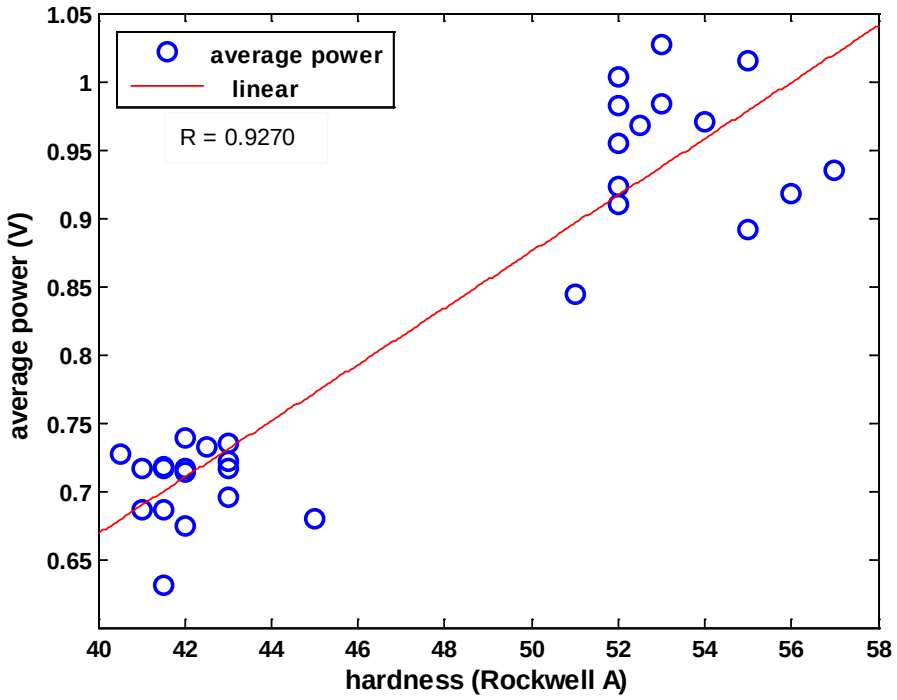

Figure 7-23. Hardness vs average cutting power (case single tool C-5)

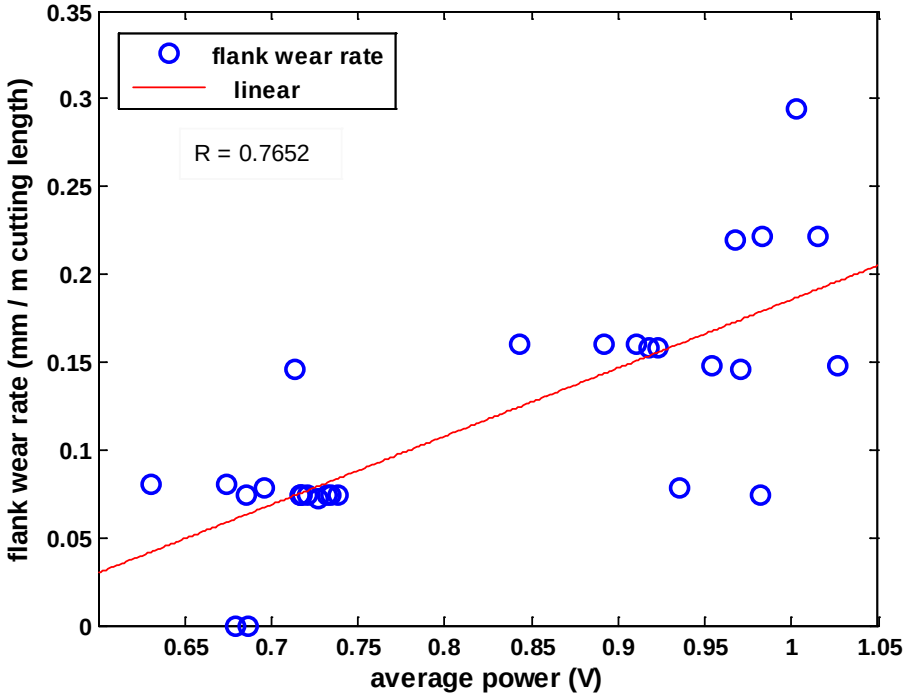

Figure 7-24. Average cutting power vs flank wear rate (case single tool C-5)

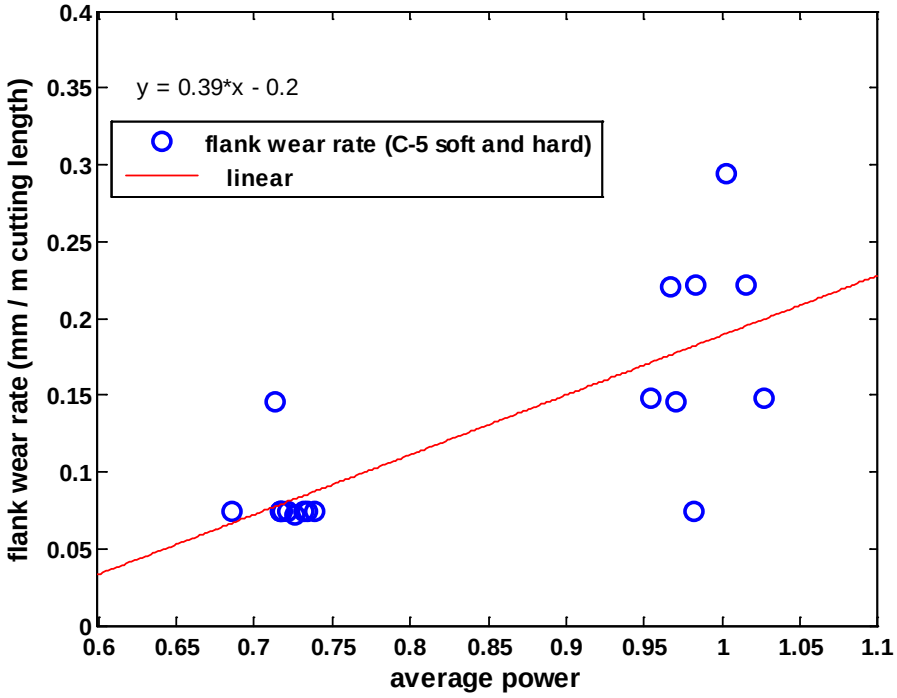

Figure 7-25. Flank wear model from C-5 case soft and hard

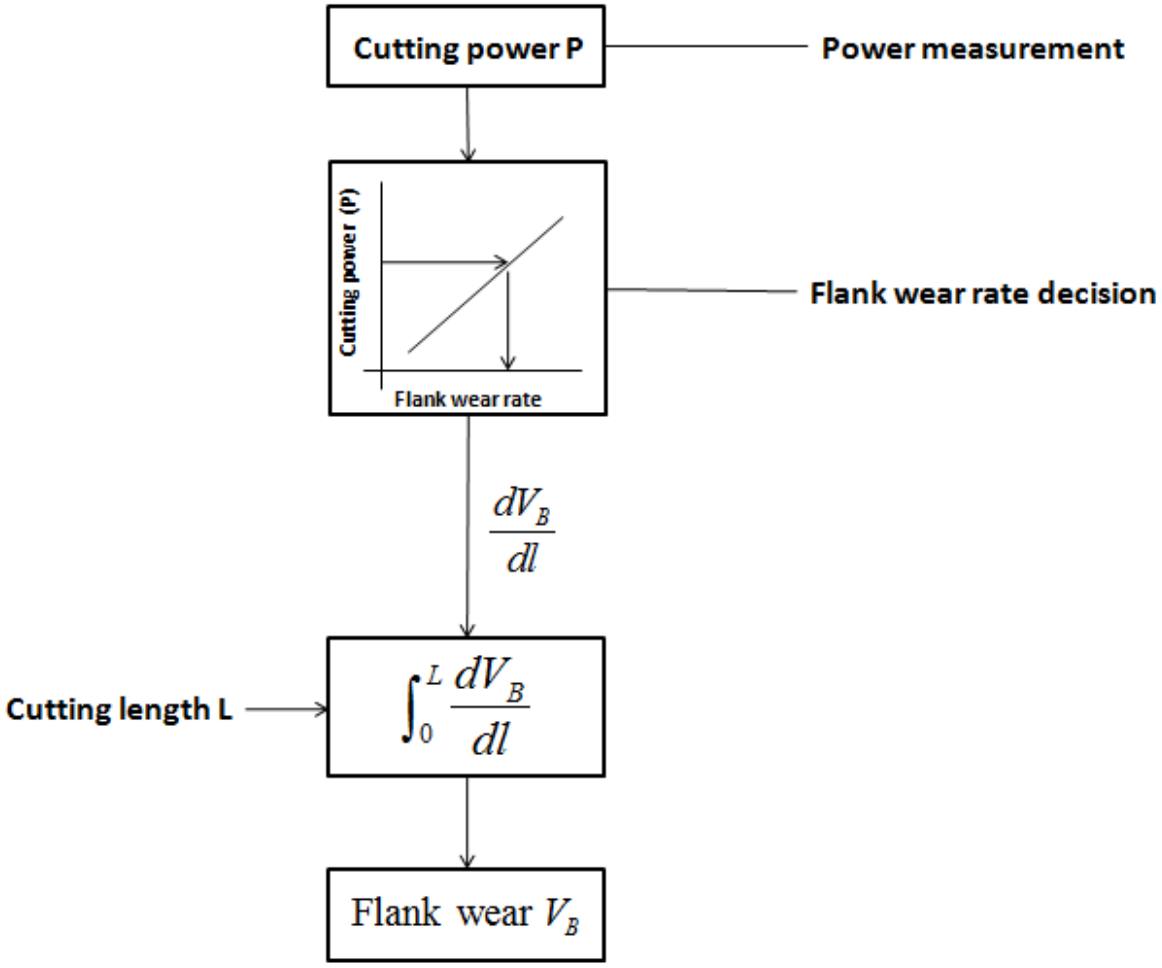

Figure 7-26. Real time flank wear estimation using power sensor

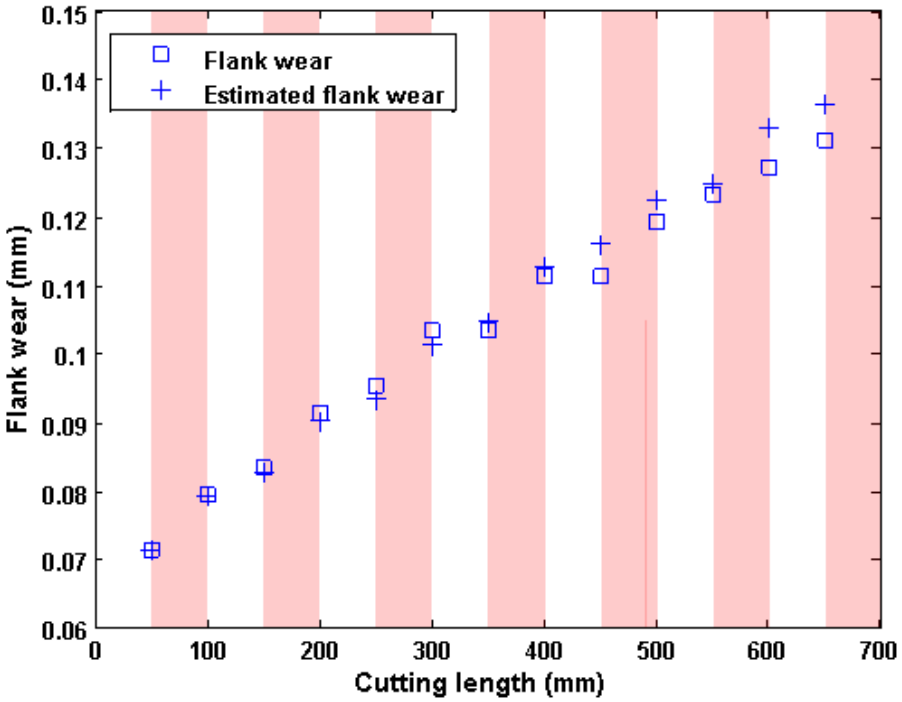

Figure 7-27. Difference between flank wear and estimated flank wear

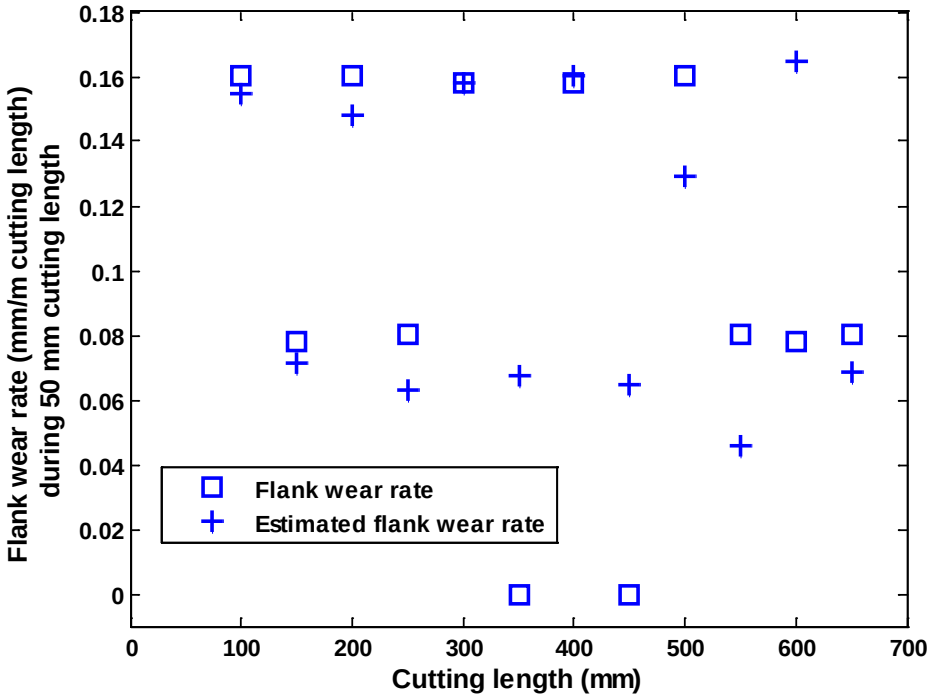

Figure 7-28. Flank wear rate (mm/m cutting length) during 50 mm cutting length

CHAPTER 8
CONCULSIONS AND FUTURE WORK

Tool condition monitoring is recognized as important in CNC processes since excessive wear or tool breakage has to be noticed immediately in an automated manufacturing system to maintain the quality and productivity. During metal cutting operations, unacceptable tool wear or breakage can damage the tool holder, the workpiece, or the machine elements. Also, the surface quality and the dimensional accuracy of the product degrade can be caused by tool failure. Moreover, operator safety, or problem in the manufacturing system can also be caused by tool breakage. Therefore, tools must be changed at the right time.

The cutting conditions in CNC machining such as cutting speed, feed per revolution, and depth of cut are conventionally based on prior experience. But, initial cutting conditions cannot anticipate in-process variations such as depth of cut or material hardness change. Increases in hardness and depth of cut raise cutting force and may cause faster tool wear, and loss of dimensions and surface finish. Therefore, workpiece material detection would be beneficial.

In chapter 4 and 5, three sensors (power sensor, ultimate thermometer, and dynamometer) were tested for the detection of material changes. It is confirmed that the power sensor is a cheap and non-contact way for detecting material changes. Theoretically, the spindle power required for turning operations in hard materials is higher than that required for soft materials. Both theory and experiments documented in this work show that a power sensor provides a means of detecting hardness changes in the work material without affecting the cutting process.

In this dissertation, flank wear was considered the main wear factor. Flank wear arises due to both adhesive and abrasive wear mechanisms from the intense rubbing action of the two surfaces in contact, i.e., the clearance face of the cutting tool and the newly formed surface of the workpiece. Its rate of increase at the beginning of the tool life is rapid, settling down to a steady state then accelerating rapidly again at the end of tool life. Flank wear leads to a deterioration of surface quality, increased contact area and, consequently, increased heat generation. Flank wear models have been developed for specific workpieces made of a single material in many studies. However, if workpiece material properties (such as hardness) are changed during operation, the existing flank wear models cannot be used, because general flank wear models cannot reflect the real-time workpiece material changes.

The work demonstrates a real-time flank wear model using a power sensor. At first, flank wear rates for multiple materials are determined by cutting tests. These flank wear rates are used for modeling the flank wear of workpieces of combined different materials by summation of the flank wear for each section. Each section of workpiece with different materials can be known by average power of measured spindle power. This proposed model estimates the flank wear for workpieces with varying material properties. In chapter 6 and 7, the flank wear rates for two materials were obtained and these two different rates can be used even if workpiece material is not one. However, case of low quality tool had some limitation. If tool and cutting conditions are exactly same, flank wear rate should be same. In case soft, the flank wear rate was different according to change of tool. Case hard also had different flank wear rates. The flank wear rates of soft material cutting and hard material cutting should be used for

workpiece of soft hard materials combined. However, known flank wear rates of soft and hard could not use for combined workpiece if tool was changed. However, one cutting edge maintained the same flank wear rate in the same material cutting section. From this result, consistency of tool is very important factor for wear model. Therefore, the study of tool consistency should be required in the future. The possible reason for different flank wear rates may be different hardness of tool or surface pattern. As shown in new tools surface, low quality tool flank surface patterns were different.

In this dissertation, the possibility of real time flank wear estimation was studied when workpiece combined with two different materials. It was confirmed that the flank wear rate of specific workpiece material can be used for cutting workpiece combined with different materials. And power sensor was used for detecting workpiece materials changes.

In the future, the advanced study about the sensor signal should be completed. The average of spindle power was used for detecting for workpiece change. To detect the tool breakage or other feature, different types of signal processing such as Wavelet transform should be required. As mentioned previous paragraph, the research about tool effect may be good topic. In high quality tool, consistency will be good. But low quality tool has no consistency. The technique proposed in this dissertation can be implemented with adaptive cutting condition rules to make decisions that reduce cutting cost and maintain product quality. To apply this to metal cutting industry, suitable test plan for obtaining flank wear rates should be developed according to the specific plant. If a manufacturing facility has consistent tools, experiments can be conducted to

establish the relationship between cutting power and tool wear rate. That relationship can be used in a real-time model to predict tool wear based upon the power sensor.

APPENDIX A
LINEAR POWER MODELING USING HASS-SL10 TEST DATA

In turning operations, the power can be modeled using $P = F_t \cdot \omega \cdot r + P_{non\ cutting}$, where F_t is the tangential cutting force, ω is the spindle speed, r is the part radius, and $P_{non\ cutting}$ is the non-cutting power. The non-cutting power is shown as a function of spindle speed in Fig. 5-4. The difference between the calculated power (based on the measured force) and experimental power for tests (using the aluminum-steel hybrid workpiece) is shown in Fig. A-1. It is seen that the power is over predicted using the traditional model. The cutting conditions are provided below. The average forces for 20 workpiece diameters are shown in Table A-1. Condition 1: depth of cut = 0.5 mm, feed per revolution = 0.2 mm/rev, spindle speed = 500 rpm. The averages tangential forces (measured separately using a cutting force dynamometer) were 155 N (Al) and 307 N (steel). Condition 2: depth of cut = 1 mm, feed per revolution = 0.2 mm/rev, spindle speed = 500 rpm. The average tangential forces were 265 N (Al) and 611 N (steel). Four alternative linear models were tested for describing the experimental power. The non-cutting power for driving the spindle at 500 rpm was taken to be 90 W (based on the Fig. 5-4 data).

The model 1 fitting form was $P = a \cdot F_t \cdot \omega \cdot r + P_{non\ \ cutting}$. Figure A-2 shows the total error between the experimental power and model 1 according to changes in the a value. When a is 0.83, the total error is smallest. The total error (over the 40 experimental data points shown in Table 1) for model 1 ($P = 0.83F_t \cdot \omega \cdot r + P_{non\ \ cutting}$) was

2135 W. This is smaller than the original model ($P = F_t \cdot \omega \cdot r + P_{non\ \ cutting}$) error of 4673 W. The difference between model 1 and the experimental power is shown in Fig. A-3.

The model 2 fitting form was $P = a \cdot F_t \cdot \omega \cdot r - b \cdot F_t + P_{non\ \ cutting}$. Figure A-4 shows the total error between the experimental power and model 2 according to changes in the a and b values. When a is 2.19 and b is 2.3, the total error is smallest. The total error (over 40 points) of model 2 ($P = 2.19F_t \cdot \omega \cdot r - 2.3F_t + P_{non\ cutting}$) was 1798 W. This is smaller than the original model ($P = F_t \cdot \omega \cdot r + P_{non\ \ cutting}$) error of 4673 W. The difference between model 2 and the experimental power is shown in Fig. A-5.

The model 3 fitting form was $P = a \cdot F_t \cdot \omega \cdot r - b \cdot (F_t + P_{non\ \ cutting})$. Figure A-6 shows the total error between the experimental power and model 3 power according to changes in the a and b values. When a is 1.26 and b is 0.43, the total error is smallest. The total error (over 40 points) of model 3 ($P = 1.26F_t \cdot \omega \cdot r + 0.43(F_t + P_{non\ \ cutting})$) is 891 W. This is smaller than the original model ($P = F_t \cdot \omega \cdot r + P_{non\ \ cutting}$) error of 4673 W. The difference between model 3 and the experimental power is shown in Fig. A-7.

The model 4 fitting form was $P = a \cdot F_t \cdot \omega \cdot r + b \cdot F_t$. Figure A-8 shows the total error between the experimental power and model 4 according to changes in the a and b values. When a is 1.905 and b is 1.58, the total error is smallest. The total error (over 40 points) of model 4 ($P = 1.905F_t \cdot \omega \cdot r + 1.58F_t$) is 563 W. This is smaller than the original model ($P = F_t \cdot \omega \cdot r + P_{non\ \ cutting}$) error of 4673 W. The difference between model 4 and the experimental power is shown in Fig. A-9.

Table A-2 shows the error $\left(\frac{1}{40} \sum_{i=1}^{40} \sqrt{\left(P_{fitting,i} - P_{\exp erimental,i} \right)^2} \right)$ over all 40 experimental data points. It is seen that model 4 yields an 8.5 times reduction in the error compared to the original model. The linear model will be useful to estimate the cutting force.

Table A-1. Measured cutting forces in the tangential direction

Workpiece diameter	Tangential force (N) (Condition 1)		Workpiece diameter	Tangential force (N) (Condition 2)	
	Al	Steel		Al	Steel
70	-151	-309	69.5	-261	-565
68.5	-153	-306	68	-264	-566
67	-146	-300	66.5	-258	-568
65.5	-153	-297	65	-263	-579
64	-153	-303	63.5	-251	-588
62.5	-157	-300	62	-267	-608
61	-156	-305	60.5	-252	-621
59.5	-156	-306	59	-284	-650
58	-165	-315	57.5	-271	-671
56.5	-160	-325	56	-279	-697
Average Tangential force	-155	-307	Average Tangential force	-265	-611

Table A-2. Total error for all power models

Model #	Model description	a	b	Total error: $\frac{1}{40}\sum_{i=1}^{40}\sqrt{\left(P_{fitting,i}-P_{experimental,i}\right)^2}$
	$P = F_t \cdot \omega \cdot r + P_{non\ cutting}$	--	--	117 W
1	$P = aF_t \cdot \omega \cdot r + P_{non\ cutting}$	0.83	--	53 W
2	$P = aF_t \cdot \omega \cdot r - bF_t + P_{non\ cutting}$	2.19	2.3	45 W
3	$P = aF_t \omega r - b(F_t + P_{non\ cutting})$	1.26	0.43	22 W
4	$P = aF_t \omega r - bF_t$	1.905	1.58	14 W

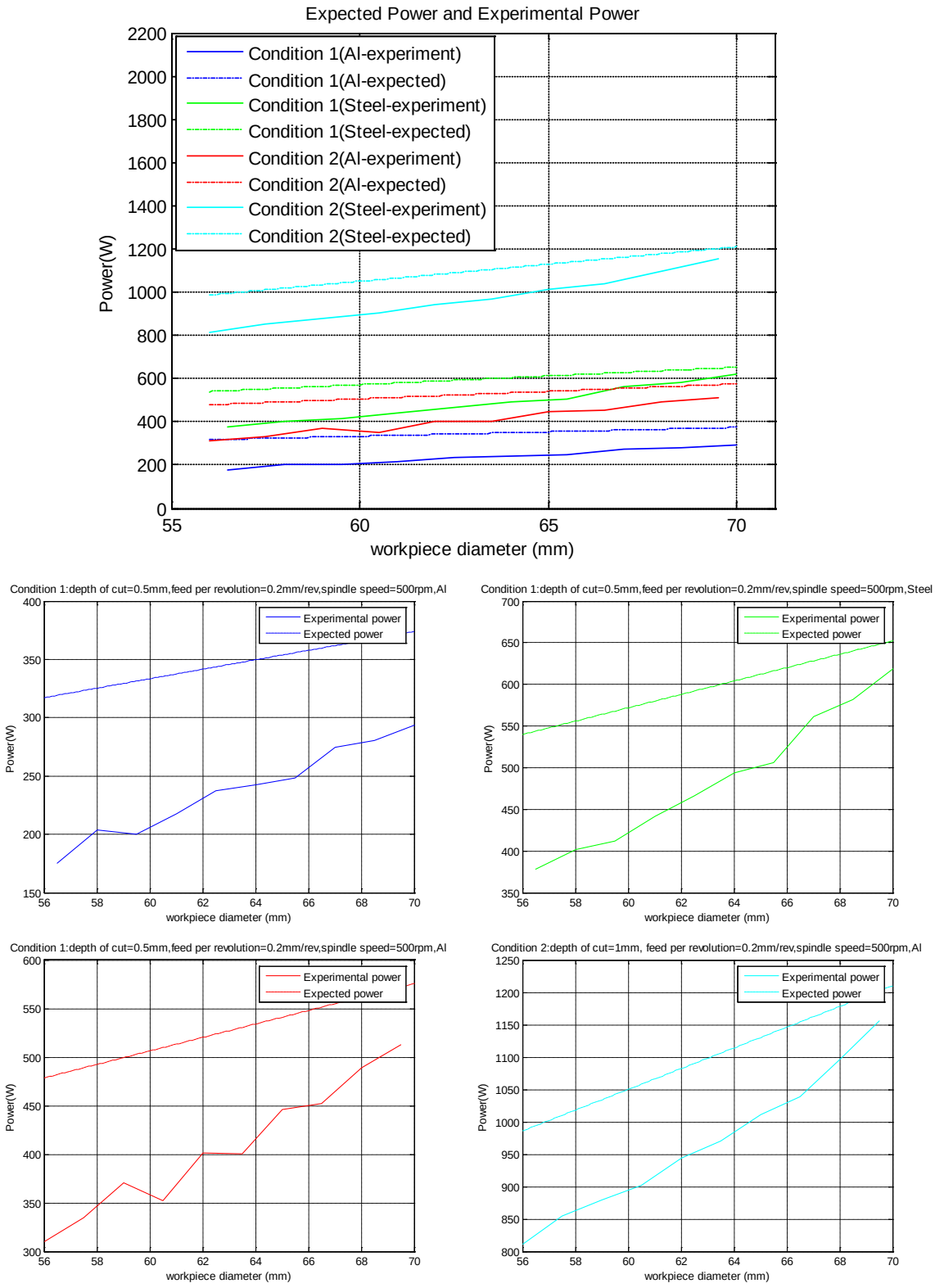

Figure A-1. Difference between experimental power and original power model

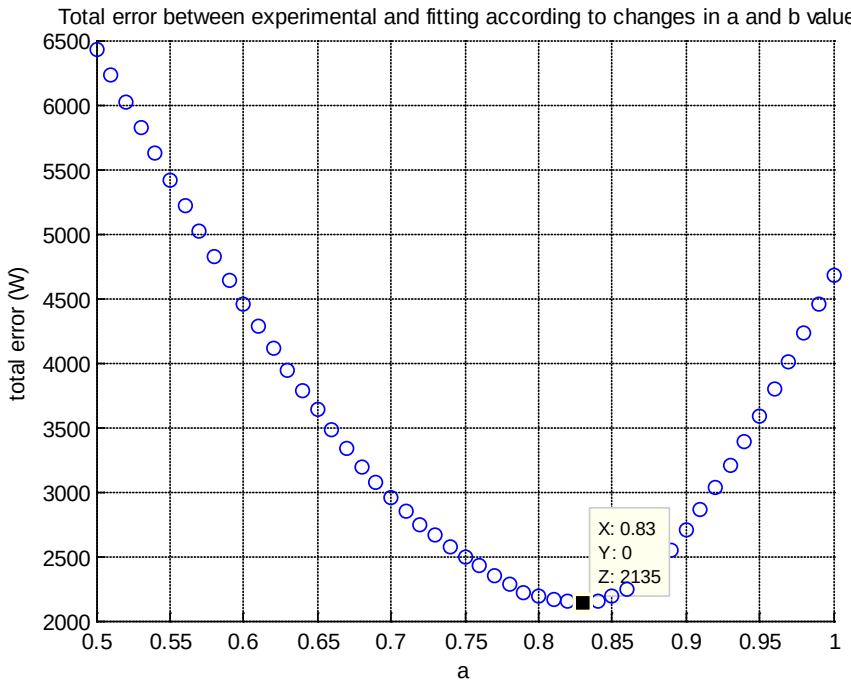

Figure A-2. Total error between experiment and model 1 according to changing *a* values

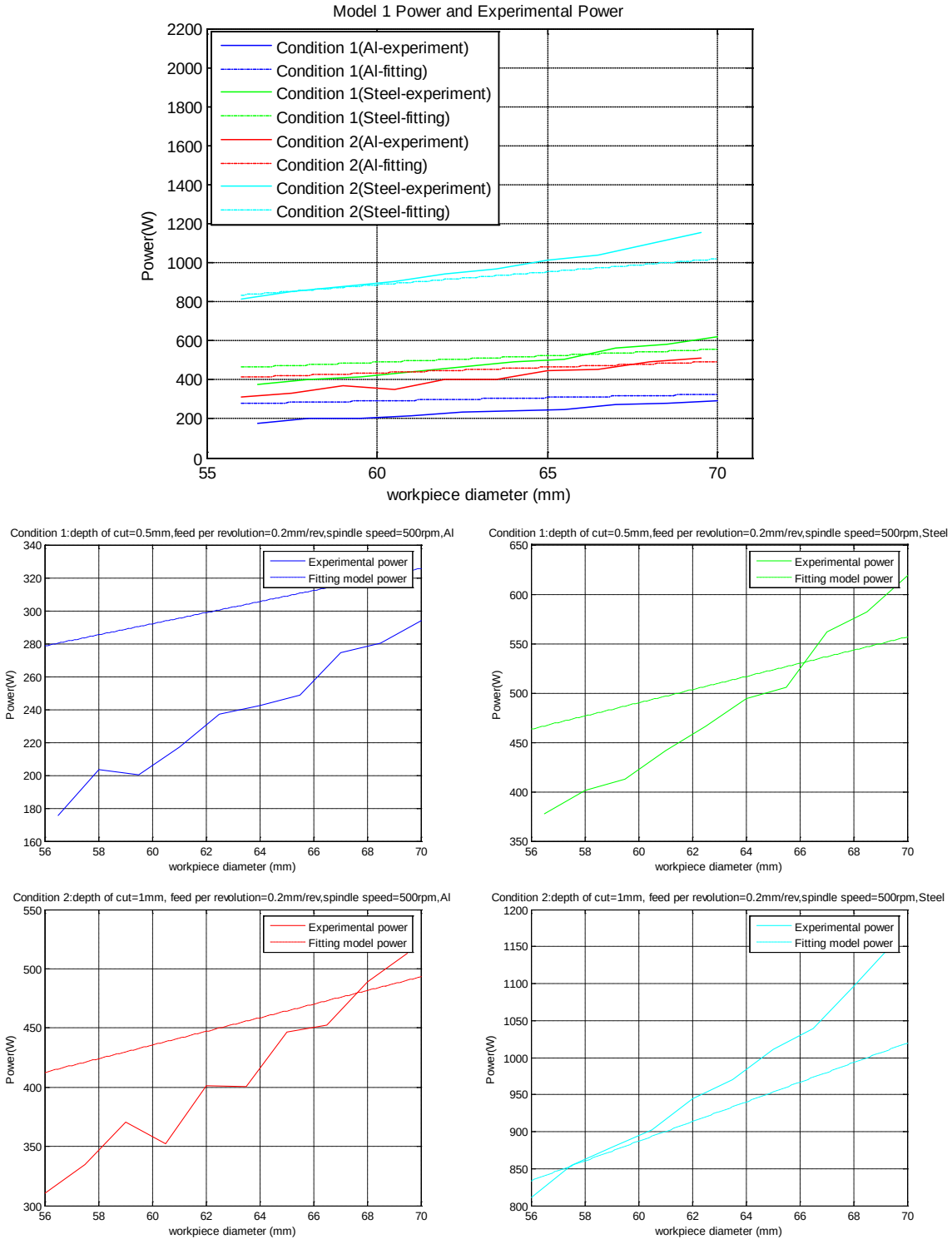

Figure A-3. Model 1 and experimental power

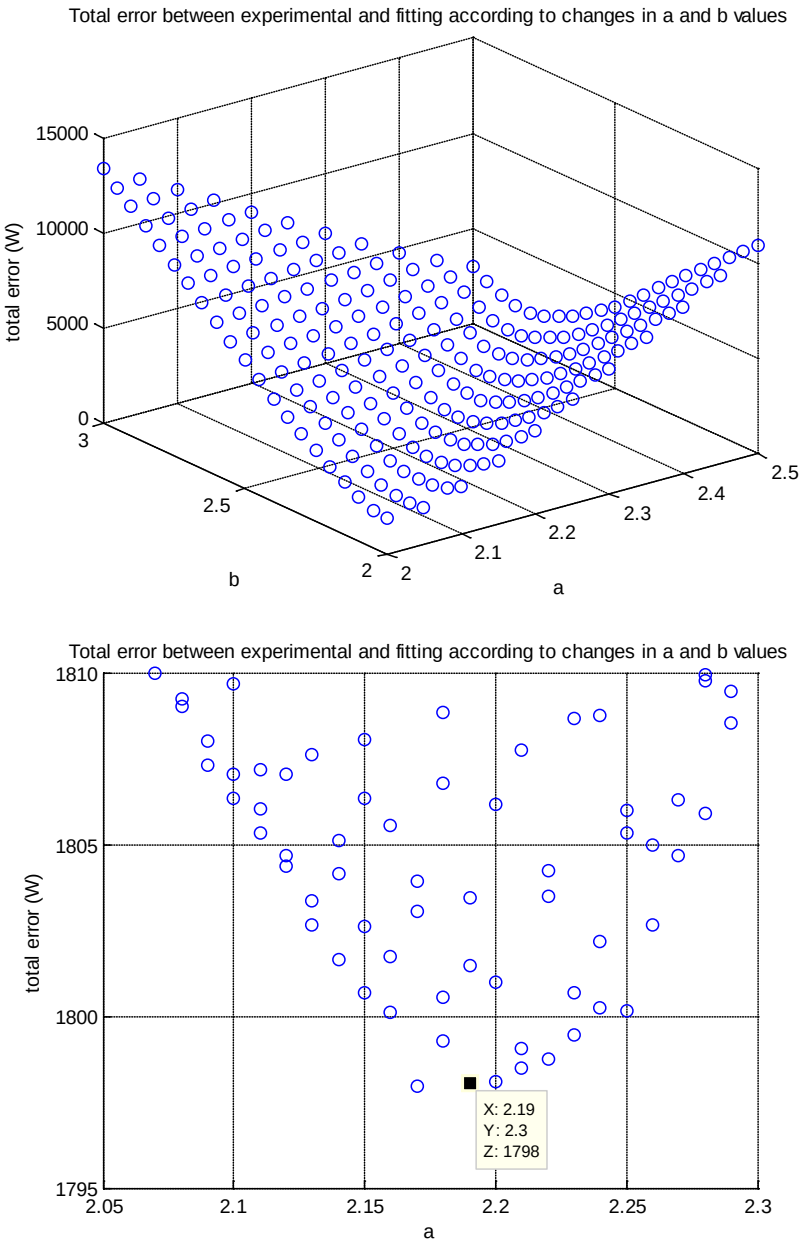

Figure A-4. Total error between experiment and model 2 according to changes in *a* and *b* values

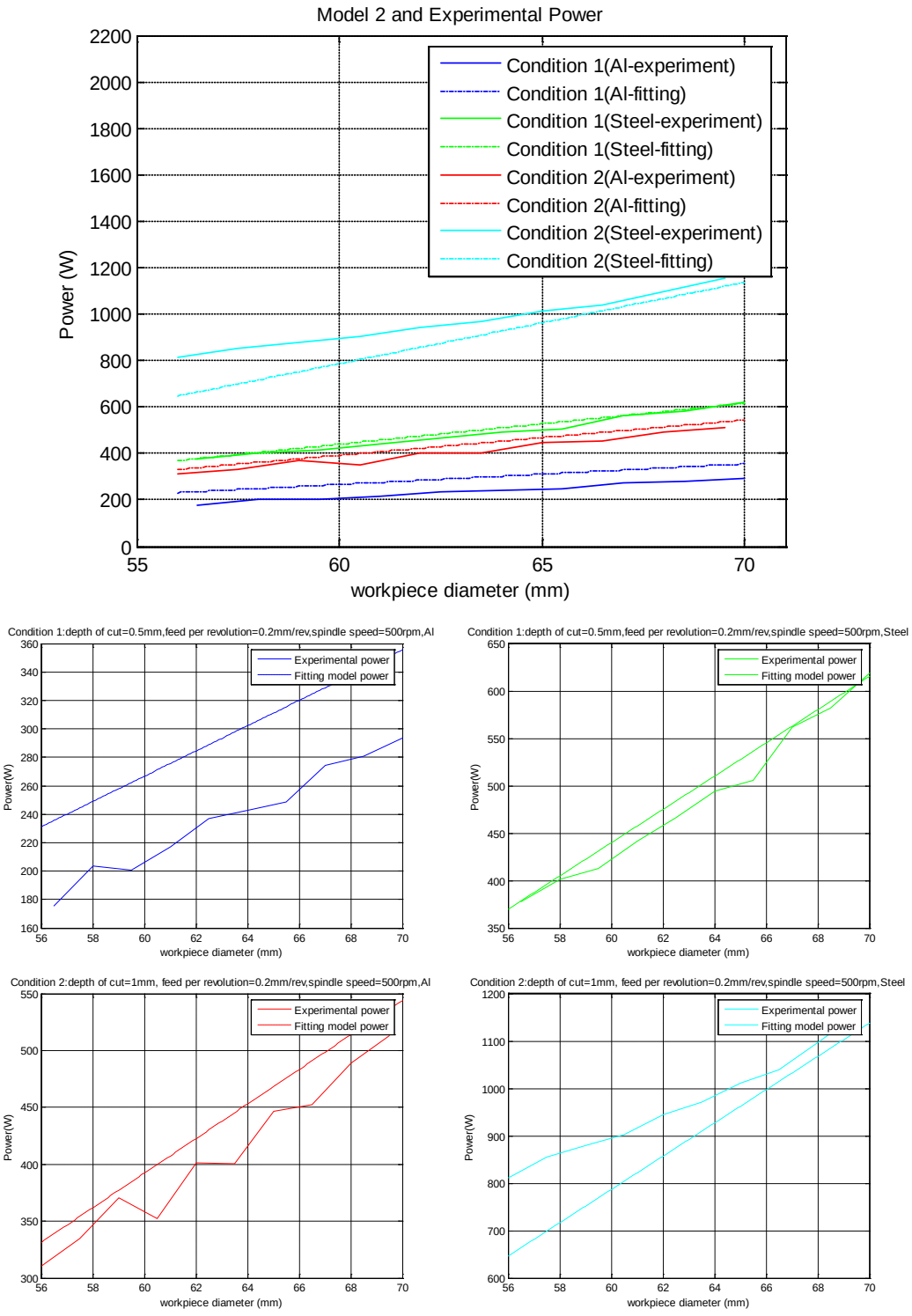

Figure A-5. Model 2 and experimental power

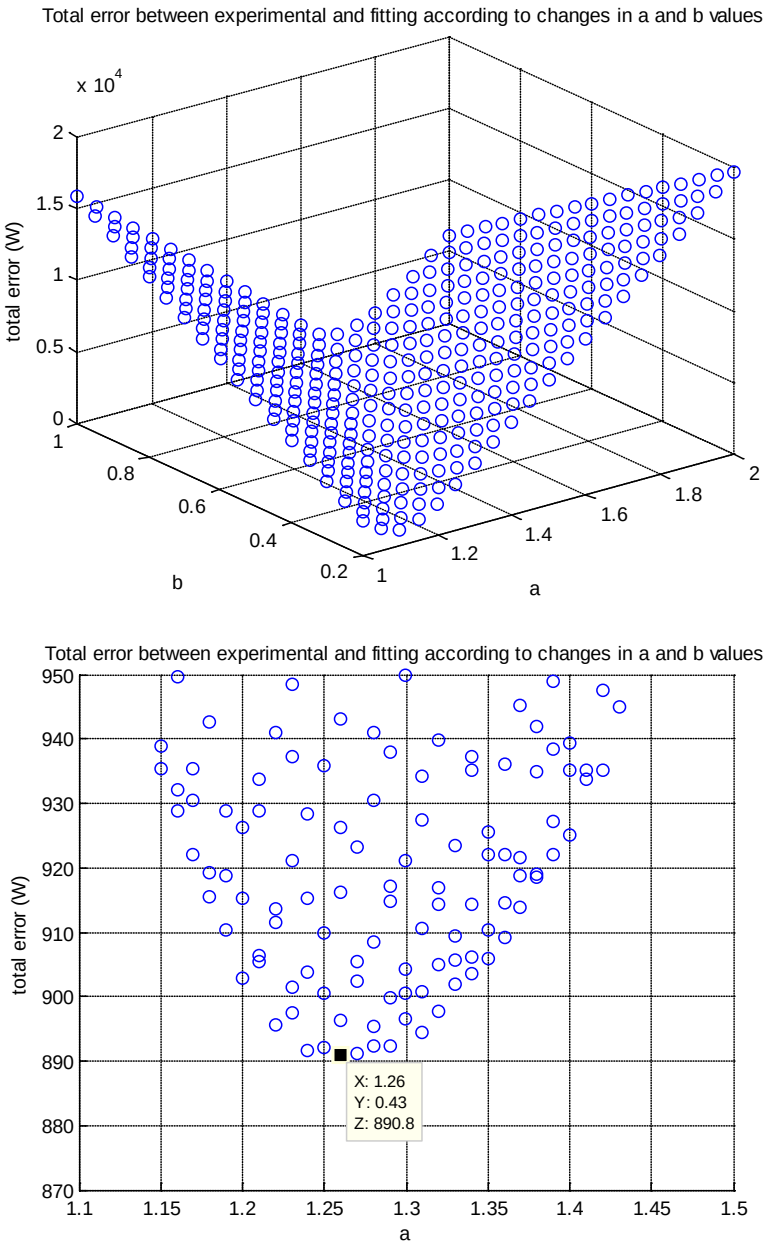

Figure A-6. Total error between experiment and model 3 according to changes in *a* and *b* values

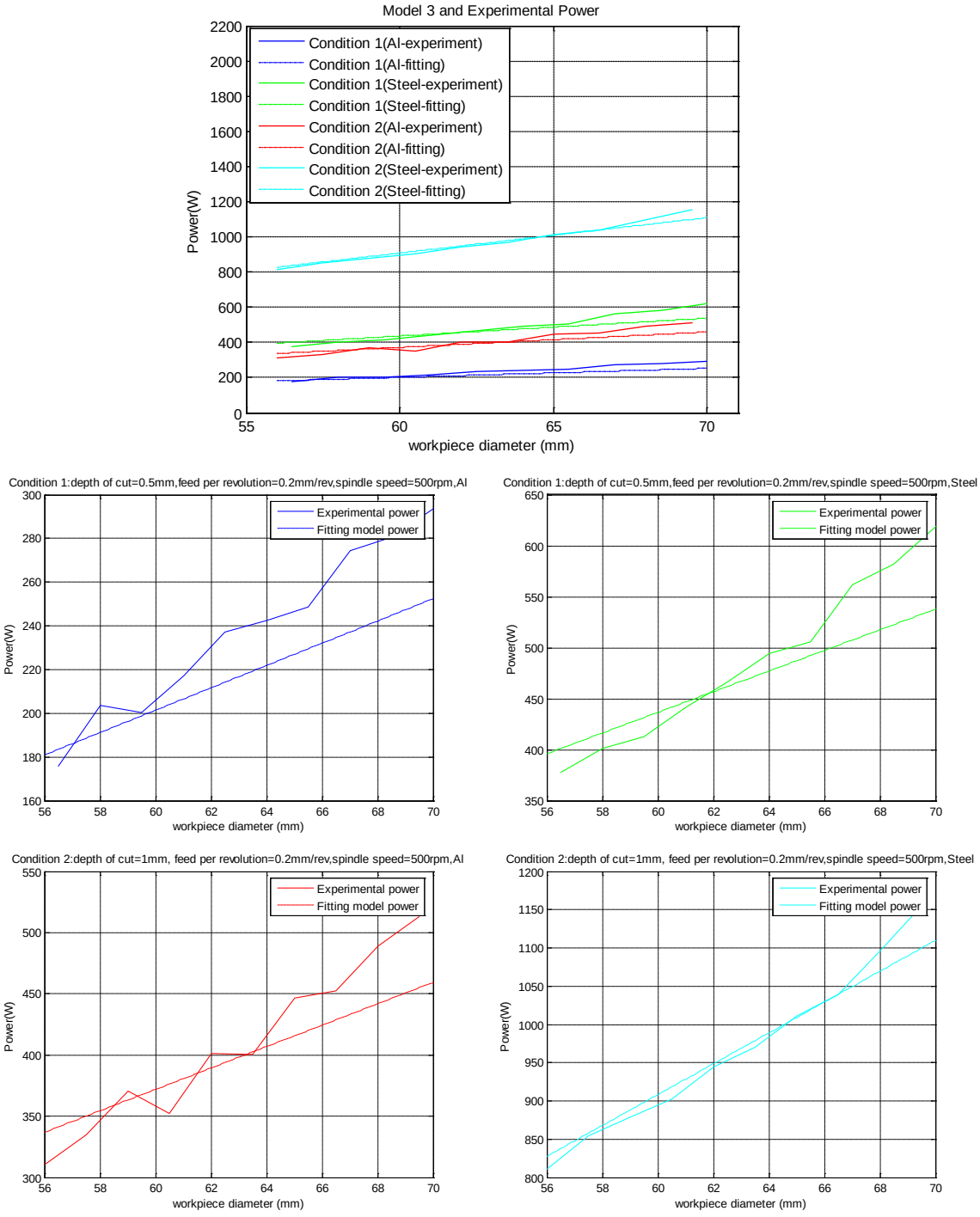

Figure A-7. Model 3 and experimental power

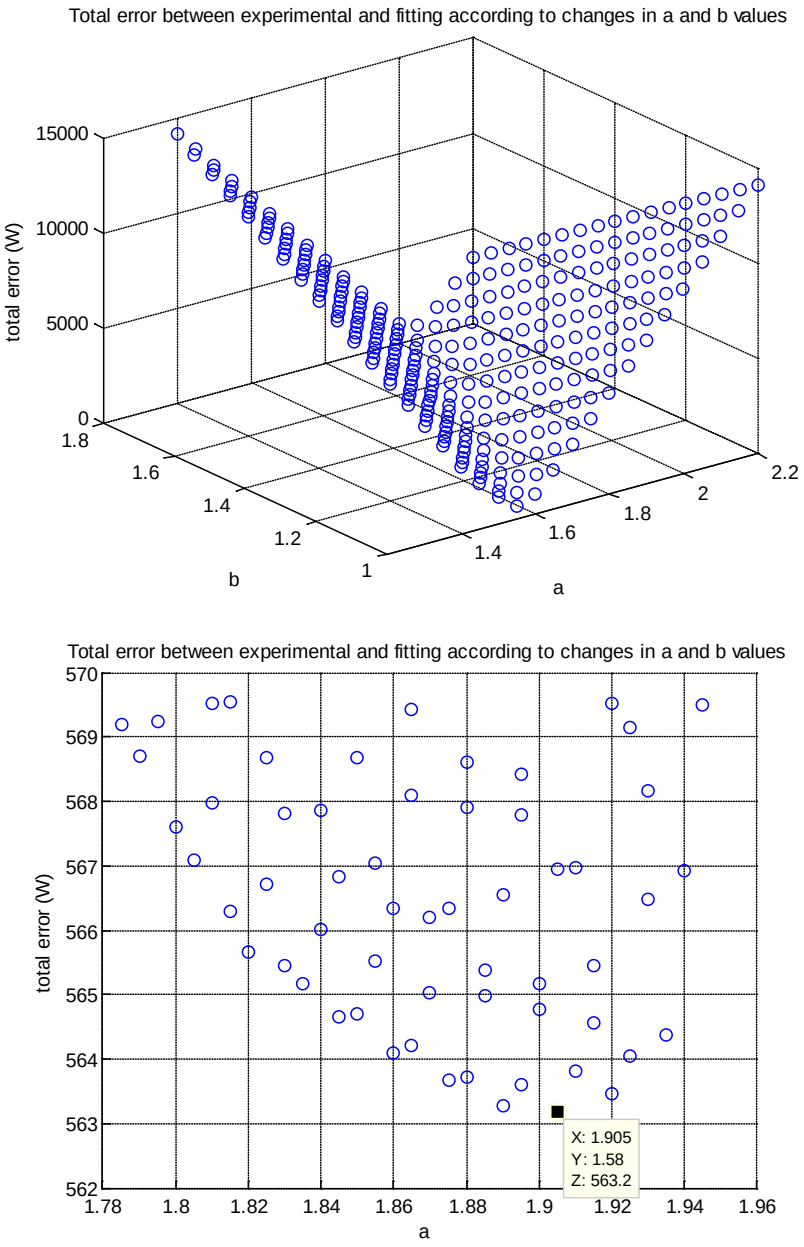

Figure A-8. Total error between experiment and model 4 according to changes in *a* and *b* values

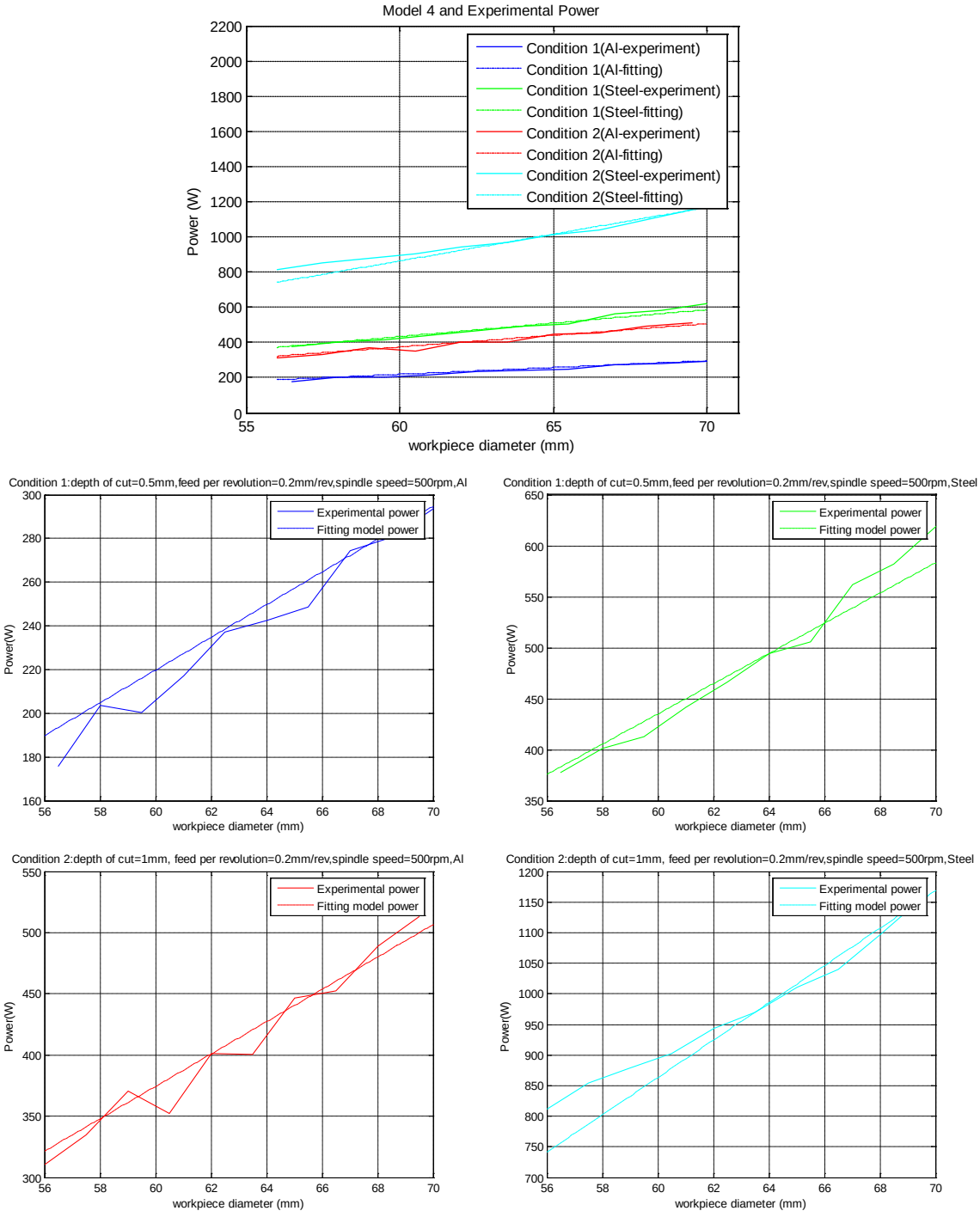

Figure A-9. Model 4 and experimental power

APPENDIX B
ANALYSIS OF OKUMA LC-40 POWER DATA (SECOND DAY SET)

The power measurement on Okuma LC-40 was performed during two days. The first day's measurements are in chapter 5.3. In this appendix, the second day's power measurement data is provided. (Table B-1 and Figures B-1~3)

Table B-1. Maximum values of facing operations, mean values and standard deviations of turning operations

Part #	facing Max.	facing Max.	OD-ID$_{mean}$	OD$_{mean}$	OD$_{mean}$	OD$_{mean}$	OD-ID$_{mean}$	OD-ID$_{SD}$	OD$_{SD}$	OD$_{SD}$	OD$_{SD}$	OD-ID$_{SD}$
1	2.954	3.776	3.0413	2.7194	2.5462	2.135	1.6379	0.2126	0.0255	0.021	0.02	0.0659
2	2.222	3.7398	3.0645	2.7288	3.0365	2.4559	1.6705	0.4232	0.3223	0.0282	0.024	0.192
3	3.176	3.786	3.0109	2.6946	2.515	2.0914	1.6172	0.1379	0.0561	0.0262	0.0276	0.049
4	2.388	3.785	2.9866	2.6994	2.5033	2.0892	1.6448	0.041	0.0244	0.0268	0.0245	0.0283
5	2.405	3.805	2.976	2.6858	2.5067	2.0745	1.6336	0.1614	0.0425	0.0225	0.0237	0.0411
6	2.365	3.222	2.5392	2.3414	2.1808	1.8331	1.4797	0.2561	0.0575	0.0218	0.0202	0.066
7	2.275	3.415	2.5535	2.3226	2.1813	1.8285	1.4697	0.1588	0.0268	0.0183	0.0182	0.0253
8	3.635	3.405	2.5631	2.335	2.179	1.8429	1.4626	0.1425	0.0271	0.022	0.0203	0.0307
9	2.284	3.826	2.9746	2.6887	2.4935	2.0718	1.625	0.0414	0.0303	0.0229	0.0235	0.0333
10	2.275	3.825	3.0042	2.6832	2.4985	2.0656	1.6195	0.1092	0.0235	0.0201	0.0212	0.026
11	1.735	3.866	3.0469	2.6989	2.5024	2.0796	1.6162	0.1898	0.0656	0.0291	0.0235	0.0617
12	2.163	3.857	3.0552	2.6937	2.5124	2.0742	1.6316	0.0527	0.0241	0.0235	0.0199	0.0243
13	2.592	3.895	2.9907	2.6866	2.4943	2.073	1.6138	0.1399	0.0344	0.022	0.0212	0.0412
14	3.435	3.918	2.9901	2.7037	2.5103	2.0758	1.6371	0.0988	0.0219	0.0214	0.0234	0.0265
15	2.775	3.903	2.9756	2.6937	2.5043	2.0745	1.6273	0.1308	0.0205	0.0205	0.0194	0.0311
16	2.418	3.852	2.9579	2.6918	2.4996	2.077	1.5966	0.1567	0.1586	0.0218	0.0202	0.119
17	1.615	3.946	3.0011	2.6958	2.4987	2.0873	1.6163	0.1389	0.0254	0.0225	0.022	0.0285
18	2.257	4.007	2.9942	2.6909	2.4935	2.0848	1.6012	0.0433	0.0334	0.0237	0.0219	0.0341
19	2.695	3.975	2.947	2.6787	2.4874	2.0938	1.6098	0.0839	0.0285	0.0215	0.0258	0.0324
20	2.161	4.008	2.9478	2.6877	2.4992	2.0829	1.6022	0.055	0.0178	0.0209	0.0196	0.0282
21	2.03	4.055	3.0238	2.6934	2.4999	2.0784	1.6058	0.1291	0.0463	0.0272	0.0231	0.0585
22	2.528	4.04	2.9856	2.6755	2.4963	2.0793	1.5913	0.1433	0.0458	0.0526	0.0205	0.0647
23	3.385	4.138	2.9453	2.6939	2.4883	2.0734	1.6063	0.214	0.1022	0.0438	0.0189	0.1097
24	2.278	4.268	2.9191	2.6426	2.4643	2.0427	1.6057	0.1884	0.0247	0.0203	0.0203	0.0318
25	4.099	4.356	2.9529	2.6389	2.4684	2.0407	1.5968	0.1639	0.0207	0.021	0.02	0.0346
26	2.555	4.097	2.9391	2.6308	2.4545	2.0396	1.6021	0.0627	0.0204	0.0207	0.0171	0.0272
27	3.345	4.298	2.9564	2.6414	2.4687	2.0534	1.5651	0.2032	0.0231	0.0192	0.0182	0.045
28	2.528	3.882	2.9357	2.6577	2.4815	2.0541	1.6208	0.1065	0.0189	0.0155	0.0188	0.0228
29	2.301	3.865	2.914	2.6492	2.4719	2.0509	1.611	0.0454	0.0252	0.0184	0.0193	0.03

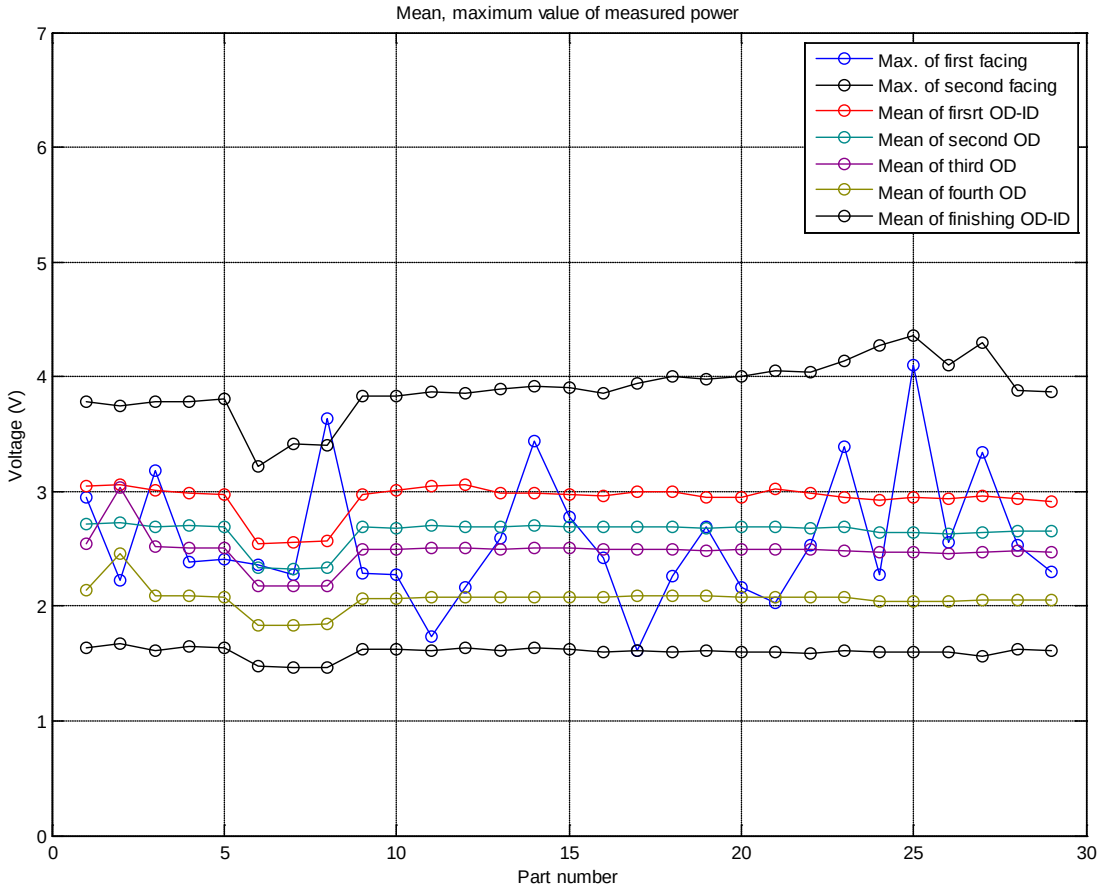

Figure B-1. Maximum values of facing operations, mean values of turning operations

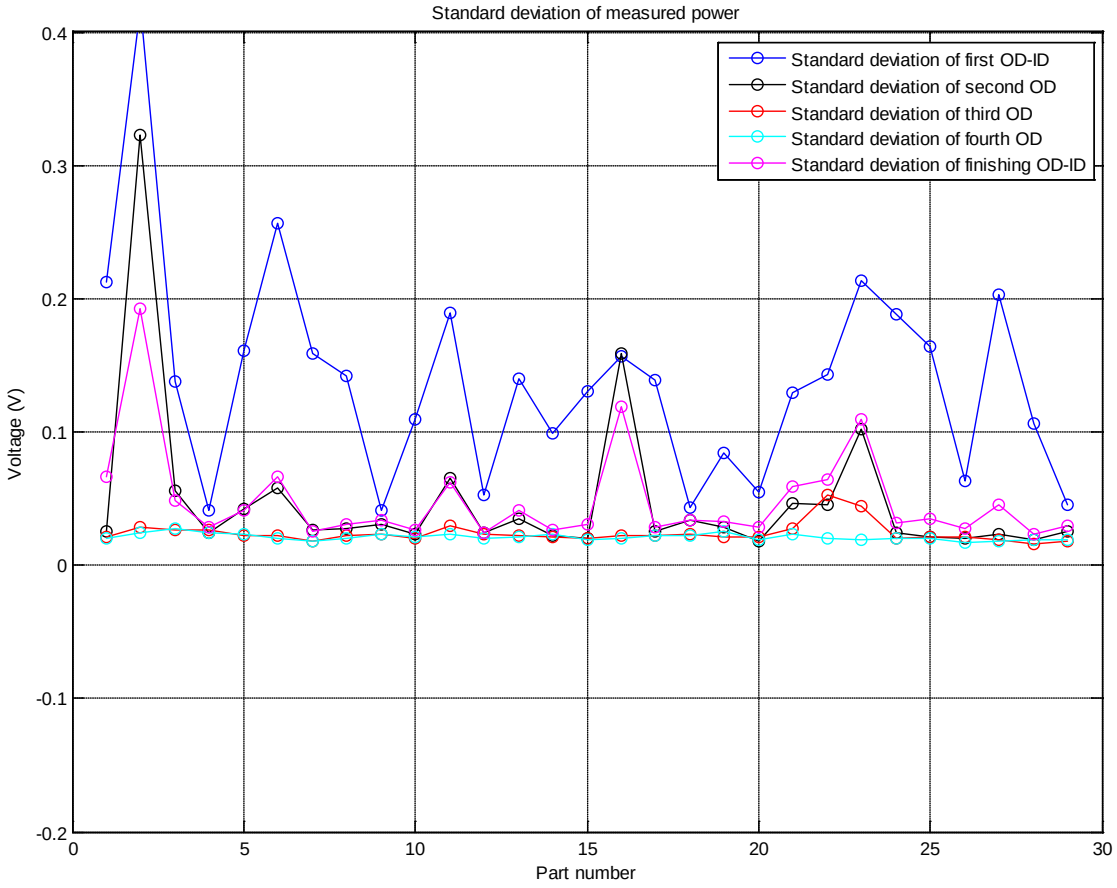

Figure B-2. Standard deviations of turning operations

A)

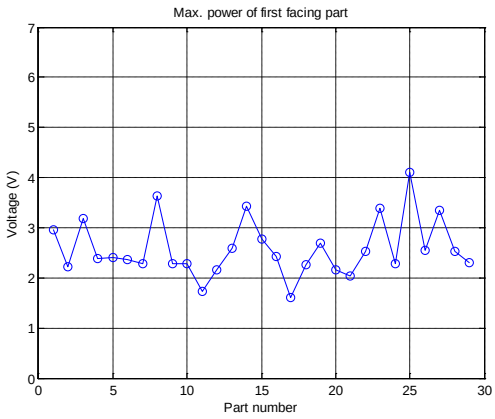
Max. power of first facing part
Voltage (V)
Part number

B)

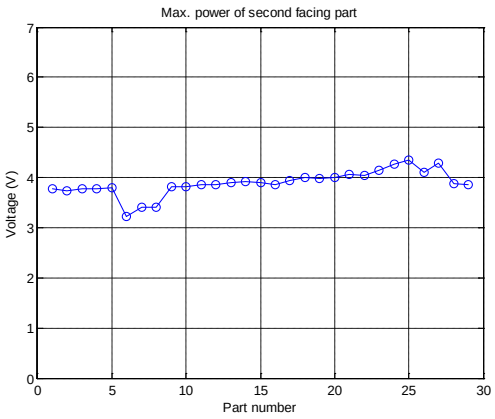
Max. power of second facing part
Voltage (V)
Part number

C)

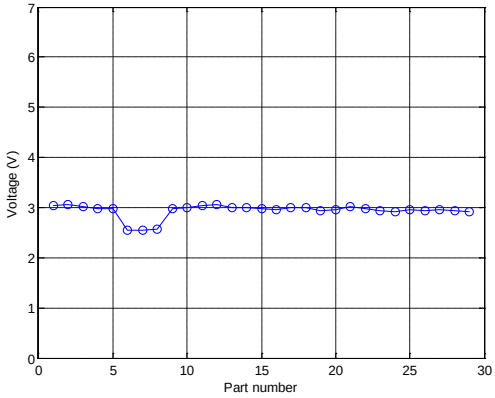
Mean power of first OD-ID
Voltage (V)
Part number

D)

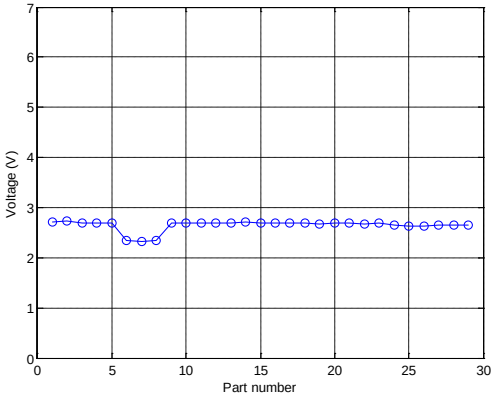
Mean power of second OD
Voltage (V)
Part number

E)

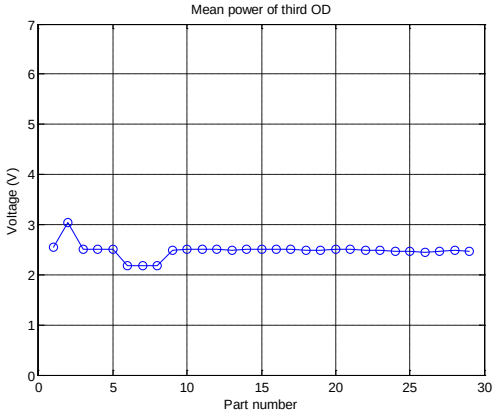
Mean power of third OD
Voltage (V)
Part number

F)

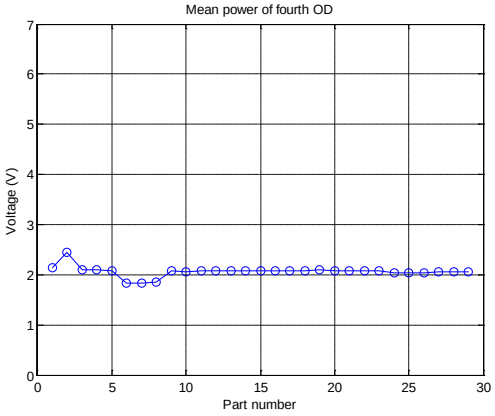
Mean power of fourth OD
Voltage (V)
Part number

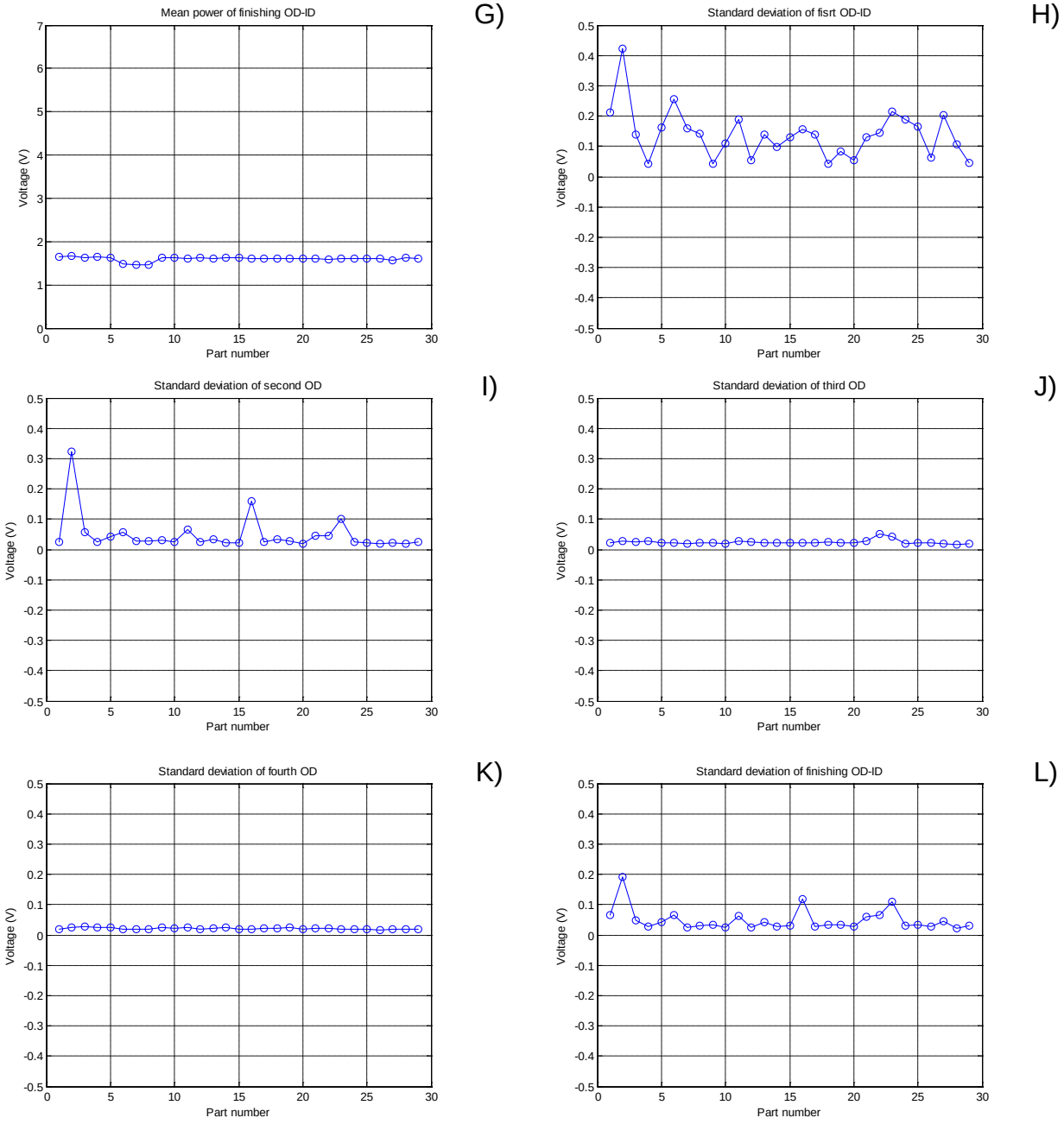

Figure B-3. A) Max value of first facing, B) Max value of second facing, C) Mean value of first turning (OD and ID are simultaneous cut), D) Mean value of third turning (OD cut), E) Mean value of second turning (OD cut), F) Mean value of fourth turning (OD cut), G) Mean value of finishing turning, H) Standard variation of second turning (OD cut), I) Standard variation of first turning (OD and ID are simultaneous cut), J) Standard variation of third turning (OD cut), K) Standard variation of fourth turning (OD cut), and L) Standard variation of finishing turning

APPENDIX C
SENSOR OUTPUT

To check the power sensor output, the current, voltage and sensor output were measured. The UPC power sensor from Load Controls Inc., was used to measure the DC power. Figure C-1 shows the connection of power sensor and DC motor, and also shows the turns (4 turns). Scaling for the analog output is the adjusted H.P. (1K ohm per H.P.) divided by the number of turns. For example, when H.P. scale is 5 K ohms and 4 turns, the full scale is 1.25 H.P. First test was performed under power sensor had 5 K Ohm and 1 turn as full scale. Figure C-2 shows the results. Second test was performed under power sensor had 20 K Ohm and 6 turns as full scale. Figure C-3 shows the result. As shown in Fig. C-2 and C-3, power sensor was good to measure the real power.

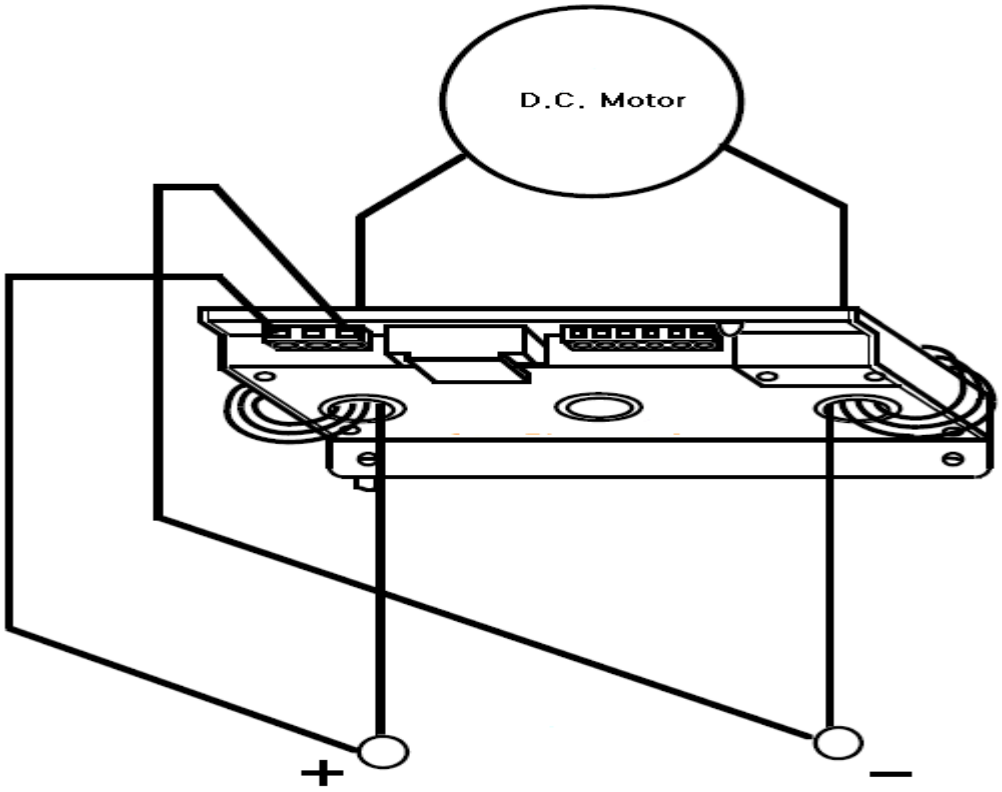

Figure C-1. Connection of UPC and D.C. motor, and turns (based on Load Controls Inc.)

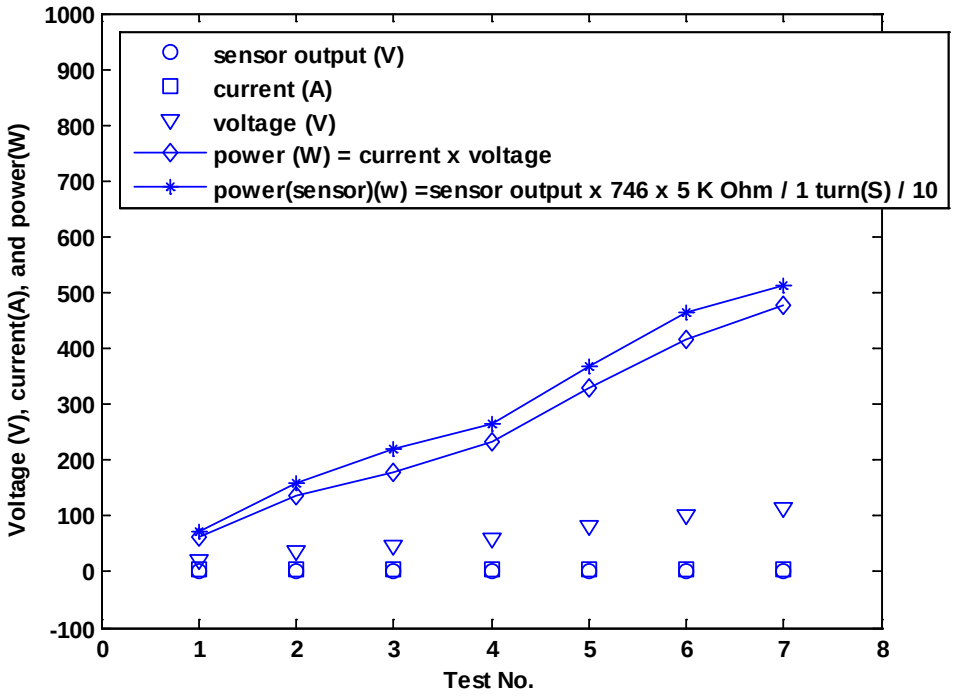

Figure C-2. Sensor output under 5 K Ohm and 1 turn of sensor set up

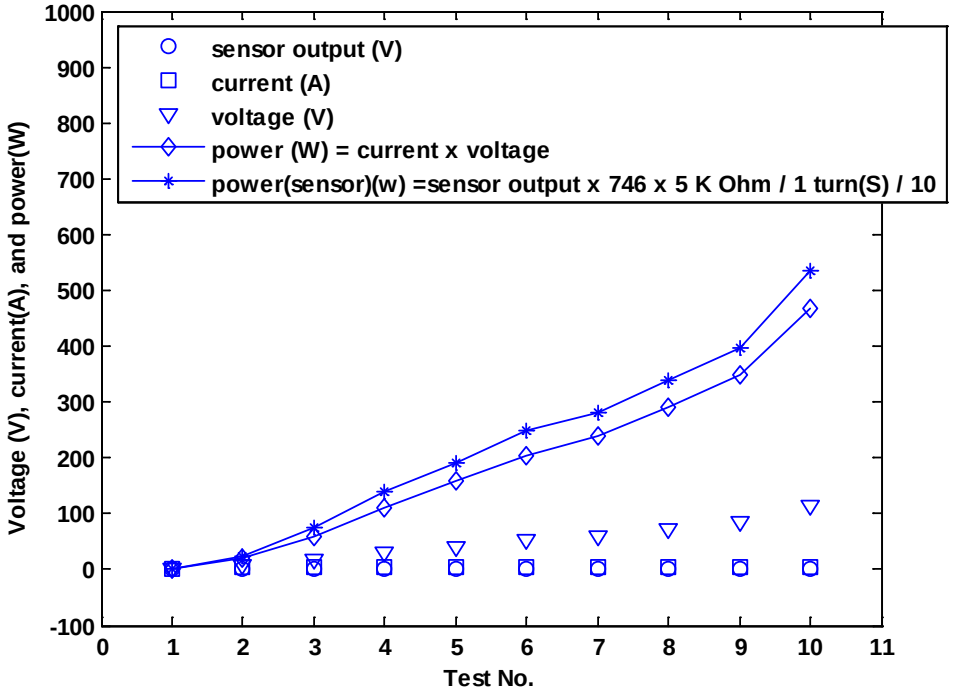

Figure C-3. Sensor output under 20 K Ohm and 6 turn of sensor set up

LIST OF REFERENCES

Abu-Zahra, N.H., and Nayfeh, T.H., 1997, “Calibrated method for ultrasonic on-line monitoring of gradual wear during turning operations,” International Journal of Machine Tools and Manufacture, Vol. 37, pp. 1475–1484.

Atli, A. V., Urhan, O., Ertürk, S., and Sönmez, M., 2006, “A computer vision-based fast approach to drilling tool condition monitoring,” IMechE Vol. 220 Part B: J. Engineering Manufacture pp1409-1415.

Azouzi, R., and Guillot, M., 1997, ‘‘On-Line prediction of surface finish and dimensional deviation in turning using neural network based sensor fusion,’’ Int. J. Mach. Tools Manuf., 37, pp. 1201–1217.

Bahr, B., Motavalli, S., and Arfi, T., 1997, ‘‘Sensor fusion for monitoring machine tool conditions,’’ International Journal Computer Integrated Manufacturing, 10, pp. 314–323.

Bayramoglu, M., and Düngel, Ü., 1998, “A systematic investigation on the use of force ratios in tool condition monitoring for turning operations,” Trans. Institute of Measurement and Control, Vol. 20 (2), pp. 92–97.

Blum, T., and Inasaki, I., 1990, “A study on acoustic emission from the orthogonal cutting process,” ASME Trans. Journal of Engineering for Industry, Vol. 112 (3), pp. 203–211.

Boothroyd, G., 1975, Fundamentals of Metal Machining and Machine Tools, McGraw-Hill, New York.

Burke, L.I., 1989, Automated identification of tool wear states in machining processes: an application of self-organising neural networks, Ph.D. thesis, Department of Industrial Engineering and Operations Research, UC at Berkeley, USA.

Byrne, G., Dornfeld, D., Inasaki , I., Ketteler, G., König, W., and Teti, R., 1995, “Tool condition monitoring (TCM)—the status of research and industrial application,” Annals of CIRP, Vol. 44 (2), pp. 541–567.

Chen X. and Li B., 2007, “Acoustic emission method for tool condition monitoring based on wavelet analysis,” Int J Adv Manuf Technol 33, pp968-976.

Cho, S., Binsaeid, S., and Asfour, S., 2009, “Design of multisensor fusion-based tool condition monitoring system in end milling,” Int J Adv Manuf Technol.

Choi, G.S., Wang, Z.X., Dornfeld, D.A., and Tsujino, K., 1990, “Development of an intelligent on-line tool wear monitoring system for turning operations,”, Proc. USA–Japan Symposium on Flexible Automation, A Pacific Rim Conference ISCIE Kyoto, pp. 683–690.

Choi, D., Kwon, W.T., and Chu, C.N., 1999, “Real-time monitoring of tool fracture in turning using sensor fusion,” International Journal of Advanced Manufacturing Technology, Vol. 15 (5), pp. 305–310.

Chow, J.G., and Wright, P.K., 1988, “On-line estimation of tool/chip interface temperatures for a turning operation,” ASME Trans. Journal of Engineering for Industry, Vol. 110, pp. 56–64.

Constantinides, N., and Bennett, S., 1987, “An investigation of methods for on-line estimation of tool wear,” International Journal of Machine Tools and Manufacture, Vol. 27 (2), pp. 225–237.

Cook, N. H., 1980, ‘‘Tool Wear Sensors,’’ Wear, 62, pp. 49–57.

Cuppini, D., D’Enrrico, G., and Rutelli, G., 1986, “Tool image processing with application to unmanned metal-cutting, a computer vision system for wear sensing and failure detection,” SPIE, Vol. 701, pp. 416–422.

Dan, L., and Mathew, J., 1990, “Tool wear and failure monitoring techniques for turning—a review,” International Journal of Machine Tools and Manufacture, Vol. 30 (4), pp. 579–598.

Dimla Snr. D.E., 1998, Multivariate tool condition monitoring in a metal cutting operation using neural networks, Ph.D. thesis, School of Engineering and the Built Environment, The University of Wolverhampton, UK.

Dimla Snr. D.E., 1999, “Tool wear monitoring using cutting force measurements,” 15th NCMR: Advances in Manufacturing Technology XIII, University of Bath, 6–8 September, pp. 33–37.

Dimla Snr. D.E., 2000, “Sensor signals for tool-wear monitoring in metal cutting operations - a review of methods,” International Journal of Machine Tools & Manufacture, , Vol. 40, pp. 1073–1098

Dimla Snr. D.E., and Lister, P.M., 2000, “On-line metal cutting tool condition monitoring—I: Force and vibration analyses,” International Journal of Machine Tools and Manufacture, Vol. 40 (5), pp. 739–768.

Dornfeld, D.A., 1990, “Neural network sensor fusion for tool condition monitoring,” Annals of the CIRP, Vol. 39 (1), pp. 101–105.

Dornfeld, D.A., 1992, “Application of acoustic emission techniques in manufacturing,” NDT and E International, Vol. 25 (6), pp. 259–269.

Dornfeld, D.A., 1994, “In process recognition of cutting states,” JSME International Journal, Series C: Dynamics Control, Vol. 37 (4), pp. 638–650.

Du, R., Zhang, B., Hungerford, W., and Pryor, T., 1993, ‘‘Tool condition monitoring and compensation in finish turning using optical sensor,’’ 1993 ASME WAM, Symposium of Mechatronics, DSC-Vol. 50/PED-Vol. 63, pp.245–253.

El Gomayel, J.I., and Bregger, K.D., 1986, “On-line tool wear sensing for turning operations,” ASME Trans. Journal of Engineering for Industry, Vol. 108, pp. 44–47.

Elanayar, S.V.T., Shin, Y.C., and Kumara, S., 1990, “Machining condition monitoring for automation using neural networks,” Monitoring and Control of Manufacturing Processes (Winter Annual Meeting of the ASME), PED, 44, pp. 85–100

El-Wardany, T.I., Gao, D., and Elbestawi M.A., 1996, “Tool condition monitoring in drilling using vibration signature analysis,” International Journal of Machine Tools and Manufacture, Vol. 36 (6), pp. 687–711.

Ertekin, Y. M., Kown, Y., and Tseng, T-L., 2003, ‘‘Identification of common sensory features for the control of CNC Milling operations under varying cutting conditions,’’ Int. J. Mach. Tools Manuf., 43, pp. 897–904.

Fan, Y. Y., and Du, R., 1996, ‘‘A laser diffraction method for rotating tool condition monitoring,’’ ASME J. Eng. Ind., 118, No. 4, pp. 664–667.

Finnie, I., and Shaw, M. C., 1956, “The friction process in metal cutting,” Trans. ASME, Vol. 78, p. 1649.

Gould, L., 1988, “Sensing tool and drive element conditions in machine tools,” Sensor, pp. 5–13.

Grabec, I., 1988, “Chaotic dynamics of the cutting process,” International Journal of Machine Tools and Manufacture, Vol. 28 (1), pp. 9–32.

Holmbom, P., Pedersen, O., Sandell, B., and Lauber, A., 1989, “Fusing sensor systems: promises and problems,” Sensor Reviews, Vol. 9 (3), pp. 143–152.

Huggins, L. F., 1975, “Analysis and interpretation,” American Society of Agricultural Engineering, First Edition, pp. 15-03~04

Jemielniak, K., and Otman, O., 1998, “Tool failure detection based on analysis of accoustic emission signals,” Journal of Material Processing Technology, Vol. 76, pp. 192–197.

Jetley, S.K., and Gollajesse, A., 1994, “Measuring tool wear using magnetism,” Proceedings: Japan–USA Symposium Flexible Automation, A Pacific Rim Conference, July 11–18, Kobe, Japan, pp. 345–347.

Jiang, C.Y., Zhang, Y.Z., and Xu, H.J., 1987, “In-process monitoring of tool wear stage by the frequency band-energy method,” Annals of the CIRP, Vol. 36 (1), pp. 45–48.

Kakade, S., Vijayaraghavan, L., and Krishnamurthy, R., 1994, “In-process tool wear and chip-form monitoring in face milling operation using acoustic emission,” Journal of Material Processing Technology, Vol. 44, pp. 207–214.

Karthik, A., Chandra, S., Ramamoorthy, B., and Das, S., 1997, ‘‘3D tool wear measurement and visualisation using stereo imaging,’’ Int. J. Mach. Tools Manuf., 37, pp. 1573–1581.

Khraisheh, M.K., Pezeshki, C., and Bayoumi, A.E., 1995, “Time series based analysis for primary chatter in metal cutting,” Journal of Sound and Vibration, Vol. 180 (1), pp. 67–87.

Kim, J.S., and Lee, B.H., 1991, “An analytical model of dynamic cutting forces in chatter vibration,” International Journal of Machine Tools and Manufacture, Vol. 31 (3), pp. 371–381.

Kim, J-D., and Choi, I-H., 1996, ‘‘Development of a tool failure detection system using multi-sensors,’’ Int. J. Mach. Tools Manuf., 36, pp. 861–870.

Kitagawa, T., Maekawa, K., Shirakashi, T., and Usui, E., 1988, “Analytical prediction of flank wear of carbide tools in turning plain carbon steels (Part 1),” Bull. Japan Soc. Precision Engineering, Vol. 22 (4), pp. 263–269.

Ko, T.J., and Cho, D.W., 1994, “Cutting state monitoring in milling by a neural network,” International Journal of Machine Tools and Manufacture, Vol. 34 (5), pp. 659–676.

König, W., Kutzner, K., and Schehl, U., 1992, “Tool monitoring of small drills with acoustic emission,” International Journal of Machine Tools and Manufacture, Vol. 32 (4), pp. 487–493.

Kurada, S., and Bradley, C., 1997, “A review of machine vision sensors for tool condition monitoring,” Computers in Industry, Vol. 34 (1), pp. 55–72.

Lee, G., Kim, K., and Jeon, D., 2002, “Tool condition monitoring based on wavelet transform”, International Conference on Control, Automation and System, Muju, Korea.

Lee, K.S., Lee, L.C., and Teo, S.C., 1992, “On-line tool wear monitoring using a PC,” Journal of Material Processing Technology, Vol. 29, pp. 3–13.

Lee, L.C., Lam, K.Y., and Liu, X.D., 1994, “Characterisation of tool wear and failure,” Journal of Materials Processing Technology, Vol. 40, pp. 143–153.

Lee, L.C., Lee, K.S., and Gan, C.S., 1989, “On the correlation between dynamic cutting force and tool wear,” International Journal of Machine Tools and Manufacture, Vol. 29 (3), pp. 295–303.

Lezanky, P., and Rafalowicz, J., 1993, ‘‘An intelligent monitoring system for cylindrical grinding,’’ CIRP Ann., 42, pp. 393–396.

Lin, J., 1995, “Inverse estimation of the tool-work interface temperature in end milling,” International Journal of Machine Tools and Manufacture, Vol. 35 (5), pp.751–760.

Lister, P.M., 1993, On-line measurement of tool wear. Ph.D. thesis, Manufacturing and Machine Tools Division, Department of Mechanical Engineering, UMIST, Manchester, UK.

Lister, P.M., and Barrow, G., 1986, “Tool condition monitoring systems,” Proceedings International 26th MATADOR Conference, Manchester, UK, pp. 271–288.

Lou, K-N., and Lin, C-J., 1996, ‘‘An intelligent sensor fusion system for tool monitoring on a machining center,’’ Proceeding of the 1996 IEEE/SICE/RSJ,International Conference on Multisensor Fusion and Integration for Intelligent Systems, pp. 208–214.

Marques, M.J.M., and Mesquita, R.M.D., 1991, “Monitoring the wear of sintered high-speed steel tools,” Journal of Material Processing Technology, Vol. 25, pp. 195–213.

Martin, K.F., 1994, “A review by discussion of condition monitoring and fault diagnosis in machine tools,” International Journal of Machine Tools and Manufacture, Vol. 34 (4), pp. 527–551.

Martin, K.F., Brandon, J.A., Grosvenor, R.I., and Owen, A., 1986, “A comparison of in-process tool wear measurement methods in turning,” Proceedings International 26th MATADOR Conference, Manchester, UK, pp. 289–296.

Matsumura, T., Obikawa, T., Shirakashi T., and Usui, E., 1993, “Automonus turning operation planning with predicting tool wear and surface roughness,” Transactions of the North American Manufacturing Institution of SME, Vol. 21, pp. 359-366.

Matsumura, T., Shirakashi, T., and Usui, E., 2008, “Identification of wear characteristics in tool wear model of cutting process,” International Journal of Material Forming, Vol. 1, pp. 555-558.

Moriwaki,T., and Tobito, M., 1990, “A new approach to automatic detection of life of coated tool based on acoustic emission measurement,” ASME Trans. Journal of Engineering for Industry, Vol. 112 (3), pp. 212–218.

Noori-Khajavi, A., and Komanduri, R., 1995, “Frequency and time domain analyses of sensor signals in drilling - I. Correlation with drill wear,” International Journal of Machine Tools and Manufacture, Vol. 35 (6), pp. 775–793.

Novak, A., and Wiklund, H., 1992, “Reliability of tool-wear monitoring,” Annals of the CIRP, Vol. 42 (1), pp. 63–66.

Oguamanam, D.C.D., Raafat, H., and Taboun, S.M., 1994, “A machine vision system for wear monitoring and breakage detection of single-point cutting tools,” Computers in Industrial Engineering, Vol. 26 (3), pp. 575–598.

Opitz, H. and König, W., 1967, “On the wear of cutting tools,” Adv. Mach. Tool Des. Res., Vol. 1, p. 173.

Oraby, S.E., and Hayhurst D.R., 1991, “Development of models for tool wear force relationships in metal cutting,” International Journal of Machine Tools and Manufacture, Vol. 33 (2), pp. 125–138.

P. Bhattacharyya, D. Sengupta, S. Mukhopadhyay and A. B. Chattopadhyay, 2008, “On-line tool condition monitoring in face milling using current and power signals,” International Journal of Production Research, Vol. 46, No. 4, pp 1187–1201.

Parra, L., Deco, G., and Miesbach, S., 1996, “Statistical independence and novelty detection with information preserving nonlinear maps,” Neural Computation, Vol. 8, pp. 260–269.

Patankar S. V., 1980, Numerical Heat Transfer and Fluid Flow, Hemisphere Publishing Corporation, Washington, DC.

Prickett, P.W., and Johns, C., 1999, “An overview of approaches to end milling tool monitoring,” International Journal of Machine Tools and Manufacture, Vol. 39 (1), pp. 105–122.

Purushothaman, S., and Srinivasa, Y.G., 1994, “A back-propagation algorithm applied to tool wear monitoring,” International Journal of Machine Tools and Manufacture, Vol. 34 (5), pp. 625–631.

Rabinowicz, E., Dunn, L. A., and P. G. Russell, 1961, “A study of abrasive wear under three-body conditions,” Wear, Vol. 4, pp. 345.

Radulescu, R., and Kapoor, S.G., 1994, “An analytical model for prediction of tool temperature fields during continuous and interrupted cutting,” ASME Trans. Journal of Engineering for Industry, Vol. 116 (2), pp. 135–143.

Raman, S., Shaikh, A., and Cohen, P.H., 1992, “A mathematical model for tool temperature sensing,” ASME Computational Methods in Materials Processing, PED 61, pp. 181–193.

Rangwala, S., 1988, Machining process characterisation and intelligent tool condition monitoring using acoustic emission signal analysis, Ph.D. thesis, Mechanical Engineering Department, UC at Berkeley, USA.

Rangwala, S., and Dornfeld, D., 1987, “Integration of sensors via neural networks for detection of tool wear states,” Winter Annual Meetings of the ASME, PED 25, pp. 109–120.

Rangwala, S., and Dornfeld, D., 1990, “Sensor integration using neural networks for intelligent tool condition monitoring,” ASME Trans. Journal of Engineering for Industry, Vol. 112 (3), pp. 219–228.

Ravindra, H.V., Srinivasa, Y.G., and Krishnamurthy, R., 1993, “Modelling of tool wear based on cutting forces in turning,” Wear, Vol. 169, pp. 25–32.

Roget, J., Souquet, P., and Gsib, N., 1988, “Application of acoustic emission to the automatic monitoring of tool condition during machining,” ASNDT Materials Evaluation, Vol. 46, pp. 225–229.

Rotberg, J., Braun, S., and Lenz, E., 1987, “Mechanical signature analysis in interrupted cutting,” Annals of the CIRP, Vol. 36 (1), pp.249–252.

Rotberg, J., Braun, S., and Lenz, E., 1989, “Vibration generation models for cutting tool monitoring,” Diagnostics, Vehicle Dynamics and Special Topics—ASME Design Engineering Division, Vol. 18 (5), pp. 1–6.

Sarwar, M., Li, J., Penlington, R., and Ahmed W., 1996, “Development of thermal imaging systems for metal cutting applications,” Proceedings Advanced Manufacturing Processes Systems and Technologies Conference (AMPST ’96), Bradford, UK, pp. 361–369.

Schey, J.A., 1987, Introduction to Manufacturing Processes (second Ed.), McGraw–Hill Book Company, London, Chapter 8.

Shaw, M. V., and Dirke, S. O., 1956, “On the wear of cutting tools,” Macrotecnic, Vol. 10(4), p. 187.

Shaw, M.C., 1954, Metal cutting principles, Massachusetts Institute of Technology Press, Cambridge, MA, p. 11-1.

Shaw, M.C., 1984, Metal Cutting Principles, Clarendon Press, Oxford, Chapter 3.

Shaw, M.C., 1988, “Temperature in cutting,” ASME Proceedings Symposium on Thermal Aspects in Manufacturing, Vol. 30, pp. 133–143.

Shi, T., and Ramalingam, S., 1990, “Real-time flank wear sensing,” Winter Annual Meeting of the ASME, PED 43, pp. 157–170.

Shiraishi, M., 1988, “Scope of in-process measurement, monitoring and control techniques in machining processes—Part 1: In-process techniques for tools,” Precision Engineering, Vol. 10 (4), pp. 179–189.

Silva, R. G., Wilcox, S., and Araujo, A. A.M.M., 2007, “Multi-sensor condition monitoring using spiking neuron networks,” IADIS International Conference Applied Computing.

Stephenson, D.A., and Ali A., 1990, “Tool temperatures in interrupted metal cutting,” Winter Annual Meeting of the ASME, PED 43, pp. 261–281.

Tanner, R., and Loh, N.K., 1994, “A taxonomy of multi-sensor fusion,” Journal of Manufacturing Systems, Vol. 11 (5), 314–325.

Tansel, I.N., and McLaughlin, C., 1991, “On-line monitoring of tool breakage with unsupervised neural network,” Trans. NAMRI/SME, pp. 364–370.

Tarng, Y.S., Hseih, Y.W., and Hwang, S.T., 1994, “Sensing tool breakage in face milling with a neural network,” International Journal of Machine Tools and Manufacture, Vol. 34 (3), pp. 341–350.

Teti, R., 1995, “A review of tool condition monitoring literature database,” Annals of the CIRP, Vol. 44 (2), pp. 659–666.

Tlusty, G., 2000, Manufacturing Processes and Equipment, Prentice Hall, Upper Saddle River, NJ, USA, Chapter 8.

Trent, E.M., 1977, Metal Cutting, Butterworths, London.

Trigger, K. J., and Chao, B. T., 1956, “The mechanism of crater wear of cemented carbide tools,” Trans. ASME, Vol. 78 (5), p. 1119.

Uehara, K., Takenshita, H., Nishina, K., and Sakurai, M., 1976, “On the generating mechanism of wear particles of carbide cutting tools,” Proc. 2nd Int. Conf. on Production Engineering, Tokyo, 1976, Japan Society of Precision Engineering, Tokyo, p. 203.

Usui, E., Shirakashi, S., and T. Kitagawa, 1984, “Analytical prediction of tool wear,” Wear, Vol. 100, pp.129-151.

Usui, E., Shirakashi, T., and T. Kitagawa, 1978, “Analytical prediction of three dimensional cutting process (Part 3),” Journal of Engineering for Industry, Transactions of ASME, Vol. 100, 236-243.

Warnecke, G., Jenewein, A., and Reinfelder, A., 1990, “Tool monitoring based on process identification, monitoring and control for manufacturing processes,” Winter Annual Meeting of the ASME, Dallas, TX, USA, pp. 43–55.

Weck, M., 1984, Metrological Analysis and Performance Tests, Handbook of Machine Tools (fourth ed.), Vol. 4, John Wiley and Sons, Chichester.

Wong, Y.S., Nee, A.Y.C., Li, X.Q., and Reisdorf, C., 1997, “Tool condition monitoring using laser scatter pattern,” Journal of Materials Processing Technology, Vol. 63, pp. 205–210.

Yan, D., El-Wardany, T.I., and Elbestawi, M.A., 1995, “A multi-sensor strategy for tool failure detection in milling,” International Journal of Machine Tools and Manufacture, Vol. 35 (3), pp. 383–398.

Yao, Y., and Fang, X.D., 1992, “Modelling of multivariate time series for tool wear estimation in finish-turning,” International Journal of Machine Tools and Manufacture, Vol. 32 (4), pp. 495–508.

Yao, Y., Fang, X.D., and Arndt, G., 1990, “Comprehensive tool wear estimation in finish-machining via multivariate time-series analysis of 3-D cutting forces,” Annals of the CIRP, Vol. 39 (1), pp. 57–60.

Yao, Y., Fang, X.D., and Arndt, G., 1991, “On-line estimation of groove wear in the minor cutting edge for finish machining,” Annals of the CIRP, Vol. 40 (1), pp. 41–44.

Zhang, D., Dai, S., Han, Y., and Chen, D., 1994, “On-line monitoring of tool breakage using spindle current in milling,” 1st Asia–Pacific and 2nd Japan–China International Conference Progress of Cutting and Grinding, Shanghai, China, pp. 270–276.

Zheng, S.X., McBride, R., Barton, J.S., Jones, J.D.C., Hale, K.F., and Jones, B.E., 1992, “Intrinsic optical fibre sensor for monitoring acoustic emission, Sensors and Actuators,”, Physical, Vol. 31, pp. 110–114.

Zhou, J.M., Andersson, M., and Ståhl, J.E., 1995, “A system for monitoring cutting tool spontaneous failure based on stress estimation,” Journal of Materials Processing Technology, Vol. 48, p. 231.

BIOGRAPHICAL SKETCH

Gun Lee was born in Pusan and raised in Seoul, Korea. He completed his Bachelor of Science degree in the mechanical engineering department and Bachelor of Arts in business administration at Sogang University in Seoul, Korea. He then finished Master of Science degree in the mechanical engineering department at Sogang University. After finishing his master's degree, Gun decided to continue his education towards a Ph.D. degree in the United States. He joined to his Ph.D. program at the Machine Tool Research Center (MTRC) in mechanical and aerospace engineering department. Gun has worked on tool wear monitoring research. After graduation, Gun will continue his career as an engineer in industry. His fields of interest include controls, image processing, and automation in manufacturing.